

THESIS

FACTORS AFFECTING LIGHTNING BEHAVIOR IN VARIOUS REGIONS OF THE
UNITED STATES

Submitted by

Brody Robert Fuchs

Department of Atmospheric Science

In partial fulfillment of the requirements

For the Degree of Master of Science

Colorado State University

Fort Collins, Colorado

Spring 2014

Master's Committee:

Advisor: Steven Rutledge

Timothy Lang
Susan van den Heever
Richard Eykholt

Copyright by Brody Fuchs 2014

All Rights Reserved

ABSTRACT

FACTORS AFFECTING LIGHTNING BEHAVIOR IN VARIOUS REGIONS OF THE UNITED STATES

Lightning activity varies greatly in different regions of the Earth. Global maps of total flash density show a strong tendency for lightning to favor continental areas over the open ocean, even in regions with similar thermodynamic instability. Previous studies have attributed the difference to thermodynamic and aerosol differences over continental regions, but the exact cause is still elusive. While this is not a global study, we attempt to characterize lightning activity in 4 different regions of the United States with high resolution Lightning Mapping Array (LMA) networks over one warm season. The regions of study are Washington, D.C. (DC), northern Alabama, central Oklahoma and northeast Colorado. A wide spectrum of environmental characteristics is afforded by these regions. Lightning characteristics include storm total flash rates, positive cloud-to-ground (+CG) strikes and intra-cloud (IC) to CG ratio (IC:CG). This is accomplished by using the CSU Lightning, Environmental, Aerosol and Radar (CLEAR) framework, first developed by Lang and Rutledge (2011), to objectively analyze large amounts of storm data. Lightning activity is provided by a new flash clustering algorithm, which produces total flash rates and IC flash rates when combined with NLDN CG data.

The results have shown that lightning behavior has high variability throughout the regions of study. Median total storm flash rates range from approximately 1 flash min^{-1} in Alabama and DC to near 8 flashes min^{-1} in Colorado. Positive CG flash fractions exhibit a similar relationship with 10% of all CG flashes being positive polarity in Alabama and DC and up to 45% in Colorado. The unusual nature of the Colorado region is evident in all lightning metrics. Colorado is also characterized by an environment with high cloud base storms and coincident shallow warm cloud

depths. Examination of all storms simultaneously has shown that relationships exist between total flash rate and environmental parameters. The similarity of these results to other studies on global scales is striking and provides evidence for the robustness of these relationships. Examination of relationships between radar and lightning intensity metrics are also performed. Similar behaviors between these intensity metrics are observed in all regions.

ACKNOWLEDGMENTS

I would first and foremost like to thank my adviser, Dr. Steven Rutledge, for all of the support and spirited discussion that we have had over the past couple years. Timothy Lang for his invaluable assistance with the framework and plethora of long scripts that I had to modify as well as helping me learn to think more like a scientist. I would also like to thank my committee members Drs. Sue van den Heever and Richard Eykholt for their valuable contributions to this thesis.

I would like to extend gratitude to Dr. Eric Bruning, currently at Texas Tech University for his development and collaboration with the flash counting algorithm used in this study. Valuable insight with LMA data and interpretation was provided by Paul Krehbiel, Bill Rison and Ron Thomas at New Mexico Technical University.

Special thanks are extended to Paul Hein for helping me with countless programming problems as well as the flexibility to help with other issues. The Rutledge research group, past and present: Brett Basarab, Nick Beavis, Angela Rowe, Tiffany Meyer, Doug Stolz, Nick Guy, Elizabeth Thompson, Weixin Xu, Alyssa Matthews and Brenda Dolan. Introduction and assistance with Python and Latex code was provided by Christopher Slocum. Friends and family deserve a large debt of gratitude for their support throughout this whole process, I wouldnt be in this position without them.

LMA data for various regions were provided by Drs. Don MacGorman, Rich Blakeslee, and Paul Krehbiel, Bill Rison and Ron Thomas. Missing environmental data was supplied by Dan Lindsey, currently of CIRA. This work was supported by NSF Grant No. AGS1010657.

TABLE OF CONTENTS

Abstract	ii
Acknowledgments	iv
List of Tables	vii
List of Figures	viii
Chapter 1. Introduction	1
1.1. Lightning Production	1
1.2. Lightning activity in thunderstorms	3
1.3. CG Lightning Polarity	7
1.4. Storm Electrification and Inverted Storms	9
1.5. Approach of this Study	13
Chapter 2. Data and Methodology	22
2.1. CLEAR Framework	22
2.2. Radar	22
2.3. National Lightning Detection Network (NLDN)	25
2.4. Lightning Mapping Array (LMA)	25
2.5. Flash Clustering Algorithm	25
2.6. Environmental Hourly Isobaric Analysis	27
2.7. Aerosols	28
Chapter 3. Results	33
3.1. Overview	33
3.2. Alabama	34

3.3. Washington, D.C. (DC)	42
3.4. Oklahoma	48
3.5. Colorado	63
3.6. Lightning Behavior and Environment in All Regions	76
3.7. Sensitivity Studies	86
Chapter 4. Summary	144
References	150
Appendix A. LMA Detection and Flash Counting Performance	160

LIST OF TABLES

3.1 Flash rate and echo top height fit parameters 138

3.2 Storm and environmental variables in severe and non-severe storms in Alabama 139

3.3 Storm and environmental variables in severe and non-severe storms in DC 140

3.4 Storm and environmental variables in severe and non-severe storms in Oklahoma 141

3.5 Storm and environmental variables in severe and non-severe storms in Colorado 142

3.6 Comparison of storm autocorrelation in Alabama 142

3.7 Comparison of storm autocorrelation in DC 143

3.8 Comparison of storm autocorrelation in Oklahoma 143

3.9 Comparison of storm autocorrelation in Colorado 143

LIST OF FIGURES

1.1 LIS and OTD flash rate density for (some time frame) from Boccippio et al. (2000). Note that the LIS instrument only captures flashes from ± 35 degrees latitude.	15
1.2 Fraction of total CG flashes that are positive polarity from Boccippio et al. (2001).	16
1.3 Relative rates of IC flashes to CG flashes, otherwise known as IC:CG ratio from Boccippio et al. (2001). Note that the large values near the west coast and New England areas are likely NLDN detection efficiency artifacts.	17
1.4 Sign acquired by graupel upon rebounding collisions with ice crystals as a function of cloud temperature and liquid water content from Takahashi (1978). The dark region represents negative graupel charging and the light region represents positive charging. Note the log scale on the vertical axis.	18
1.5 Schematic diagrams of normal polarity (left) and inverted polarity (right) storms. Approximate location of charge regions are indicated by the plus and minus signs. The green lines indicate general vertical VHF LMA source distributions. Approximate temperatures follow the middle red scale.	19
1.6 Depiction of the graupel charge sign along a parcel trajectory in a storm from Bruning et al. (2012). The dotted lines represent different parcel trajectories through this phase space. Different trajectories are manifestations of different liquid water depletion rates. The top and left portions of the figure represent positive charge to graupel. The bottom and right portion of the figure represents negative charge to graupel.	20
1.7 Map of approximate regions and seasons of study with notable cities included for reference. The radii of the circles represent the selected LMA radius criterion for sample	

inclusion. Note that the colors representing each region are consistent throughout the study..... 21

2.1 Flow chart depiction of CLEAR framework. Parallel arrows indicate that not every module is required to produce statistics or case studies. Cell tracking is a required step to attribute data to cells. 30

2.2 Example of XLMA style plot used to subjectively analyze performance of flash clustering algorithm. The top panel shows the time-height source plot with points colored by time (throughout the whole figure) and identified flashes denoted by a black 'x'..... 31

2.3 Image of an LMA station. Each LMA network is comprised of multiple stations. VHF radiation produced by lightning channel propagation is detected by multiple stations that relayed via cell phone modems to a central processing facility. 32

3.1 Probability Distribution Function (PDF) of storm total flash rates in isolated Alabama convective cells. Colors here will remain consistent throughout the study. Note the log scale on the vertical axis. 88

3.2 Cumulative distribution function (CDF) of +CG rate (red) and CG rate (blue) for all storms in the Alabama region. Note that the vertical axis starts at 0.5 because many storms did not produce any CG lightning. 89

3.3 8 panel plot of storm variables and flash rates for the Alabama region. Each point represents the median flash rate for all storms within a particular bin. Error bars indicate the median absolute deviation of the flash rate distribution for each bin. Points are colored by the relative population of the horizontal variable following the bottom

	colorbar. R^2 value represents the goodness of fit to a linear function. ρ value represents the how well the relationship can be represented by a monotonic function.	90
3.4	Log of total flash rate versus log of CG fraction for Alabama storms. The best fit line parameters are displayed in the title along with the linear correlation coefficient	91
3.5	8 panel plot of environmental variables and flash rates for the Alabama region. Each point represents the median flash rate for all storms within a particular bin. Error bars indicate the median absolute deviation of the flash rate distribution for each bin. Points are colored by the relative population of the horizontal variable following the bottom colorbar. R^2 value represents the goodness of fit to a linear function. ρ value represents the how well the relationship can be represented by a monotonic function.	92
3.6	Probability Distribution Function (PDF) of storm total flash rates in isolated DC convective cells. Colors here will remain consistent throughout the study. Note the log scale on the vertical axis.	93
3.7	Cumulative distribution function (CDF) of +CG rate (red) and CG rate (blue) for all storms in the DC region. Note that the vertical axis starts at 0.5 because many storms did not produce any CG lightning.	94
3.8	8 panel plot of storm variables and flash rates for the DC region. Each point represents the median flash rate for all storms within a particular bin. Error bars indicate the median absolute deviation of the flash rate distribution for each bin. Points are colored by the relative population of the horizontal variable following the bottom colorbar. R^2 value represents the goodness of fit to a linear function. ρ value represents the how well the relationship can be represented by a monotonic function.	95

3.9 Log of total flash rate versus log of CG fraction for storm in DC. The best fit line parameters are displayed in the title along with the linear correlation coefficient 96

3.10 8 panel plot of environmental variables and flash rates for the Alabama region. Each point represents the median flash rate for all storms within a particular bin. Error bars indicate the median absolute deviation of the flash rate distribution for each bin. Points are colored by the relative population of the horizontal variable following the bottom colorbar. R^2 value represents the goodness of fit to a linear function. ρ value represents the how well the relationship can be represented by a monotonic function. 97

3.11 Probability Distribution Function (PDF) of storm total flash rates in isolated Oklahoma convective cells. Colors here will remain consistent throughout the study. Note the log scale on the vertical axis. 98

3.12 Cumulative distribution function (CDF) of +CG rate (red) and CG rate (blue) for all storms in the Oklahoma region. Note that the vertical axis starts at 0.5 because many storms did not produce any CG lightning. 99

3.13 8 panel plot of storm variables and flash rates for the Oklahoma region. Each point represents the median flash rate for all storms within a particular bin. Error bars indicate the median absolute deviation of the flash rate distribution for each bin. Points are colored by the relative population of the horizontal variable following the bottom colorbar. R^2 value represents the goodness of fit to a linear function. ρ value represents the how well the relationship can be represented by a monotonic function. 100

3.14 Log of total flash rate versus log of CG fraction for storms in Oklahoma. The best fit line parameters are displayed in the title along with the linear correlation coefficient 101

- 3.15 8 panel plot of environmental variables and flash rates for the Oklahoma region. Each point represents the median flash rate for all storms within a particular bin. Error bars indicate the median absolute deviation of the flash rate distribution for each bin. Points are colored by the relative population of the horizontal variable following the bottom colorbar. R^2 value represents the goodness of fit to a linear function. ρ value represents the how well the relationship can be represented by a monotonic function. 102
- 3.16 8 panel plot of environmental variables and LMA mode temperature for the Oklahoma region. Each point represents the median LMA mode temperature for all storms within a particular bin. Error bars indicate the median absolute deviation of the LMA mode temperature distribution for each bin. Points are colored by the relative population of the horizontal variable following the bottom colorbar. R^2 value represents the goodness of fit to a linear function. ρ value represents the how well the relationship can be represented by a monotonic function. 103
- 3.17 Total flash rate density normalized by storm 30 dBZ composite area and LMA mode temperature for Oklahoma storms. The vertical line represents the 90th percentile of flash rate density for all storms in the region. The horizontal lines represent the LMA mode temperature criteria. Storms in that box are considered inverted by this method. . . 104
- 3.18 Synoptic setup and composite radar reflectivity for Oklahoma inverted case study. Reflectivity follows colorbar on the right, surface temperature follows the bottom colorbar. Other contours indicated in title. Unique cell identification number is indicated near cell. 105
- 3.19 Radar and LMA source density structure of Oklahoma case study. Black contours indicate 2D LMA source density. Barbs on left are wind profile from inflow sounding

point. Upper-right panel is a plan view of composite reflectivity with a 2D height integrated source density and the black line indicates the latitude choice of cross section. Temperature is indicated in red text. Total number of flashes and sources are located on the top of the right panel. 106

3.20 4 panel plot comparing storm variables between positive (red) and negative (blue) storms in the Oklahoma region. The red number represents the median quantity of the positive storms and the blue number is the median quantity of the negative storms. The black number is the 2-sided p-value of the Wilcoxon rank-sum test. 107

3.21 4 panel plot comparing environmental variables between positive (red) and negative (blue) storms in the Oklahoma region. The red number represents the median quantity of the positive storms and the blue number is the median quantity of the negative storms. The black number is the 2-sided p-value of the Wilcoxon rank-sum test. 108

3.22 Probability Distribution Function (PDF) of storm total flash rates in isolated Colorado convective cells. Colors here will remain consistent throughout the study. Note the log scale on the vertical axis. 109

3.23 Cumulative distribution function (CDF) of +CG rate (red) and CG rate (blue) for all storms in the Oklahoma region. Note that the vertical axis starts at 0.5 because many storms did not produce any CG lightning. 110

3.24 8 panel plot of storm variables and flash rates for the Oklahoma region. Each point represents the median flash rate for all storms within a particular bin. Error bars indicate the median absolute deviation of the flash rate distribution for each bin. Points are colored by the relative population of the horizontal variable following the bottom

colorbar. R^2 value represents the goodness of fit to a linear function. ρ value represents the how well the relationship can be represented by a monotonic function. 111

3.25 Log of total flash rate versus log of CG fraction for storms in Oklahoma. The best fit line parameters are displayed in the title along with the linear correlation coefficient. . . . 112

3.26 8 panel plot of environmental variables and flash rates for the Oklahoma region. Each point represents the median flash rate for all storms within a particular bin. Error bars indicate the median absolute deviation of the flash rate distribution for each bin. Points are colored by the relative population of the horizontal variable following the bottom colorbar. R^2 value represents the goodness of fit to a linear function. ρ value represents the how well the relationship can be represented by a monotonic function. 113

3.27 8 panel plot of environmental variables and LMA mode temperature for the Colorado region. Each point represents the median LMA mode temperature for all storms within a particular bin. Error bars indicate the median absolute deviation of the LMA mode temperature distribution for each bin. Points are colored by the relative population of the horizontal variable following the bottom colorbar. R^2 value represents the goodness of fit to a linear function. ρ value represents the how well the relationship can be represented by a monotonic function. 114

3.28 6 panel plot similar to previous plot but shows relationships between environmental parameters and LMA mode temperatures in Colorado. Points, colors and bars all follow previous figures. 115

3.29 Total flash rate density normalized by storm 30 dBZ composite area and LMA mode temperature for Oklahoma storms. The vertical line represents the 90th percentile of

flash rate density for all storms in the region. The horizontal lines represent the LMA mode temperature criteria. Storms in that box are considered inverted by this method. . . 116

3.30 Synoptic setup and composite radar reflectivity for Oklahoma inverted case study. Reflectivity follows colorbar on the right, surface temperature follows the bottom colorbar. Other contours indicated in title. Unique cell identification number is indicated near cell. 117

3.31 Radar and LMA source density structure of Oklahoma case study. Black contours indicate 2D LMA source density. Barbs on left are wind profile from inflow sounding point. Upper-right panel is a plan view of composite reflectivity with a 2D height integrated source density and the black line indicates the latitude choice of cross section. Temperature is indicated in red text. Total number of flashes and sources are located on the top of the right panel. 118

3.32 4 panel plot comparing storm variables between positive (red) and negative (blue) storms in the Oklahoma region. The red number represents the median quantity of the positive storms and the blue number is the median quantity of the negative storms. The black number is the 2-sided p-value of the Wilcoxon rank-sum test. 119

3.33 4 panel plot comparing environmental variables between positive (red) and negative (blue) storms in the Oklahoma region. The red number represents the median quantity of the positive storms and the blue number is the median quantity of the negative storms. The black number is the 2-sided p-value of the Wilcoxon rank-sum test. 120

3.34 CDF of storm total flash rates for each region. Colors are indicated in the legend. 121

3.35 Log flash rate and LCL heights for all storms in all regions of study. Points denote the median flash rates for each LCL bin. Bottom error bar denotes the 25th percentile of

the flash rate distribution for each LCL bin. Top bar denotes the 75th percentile of flash rate distribution for each LCL bin. Color of point indicates relative population of LCL heights following the colorbar.	122
3.36 Figure 1 from Williams et al. (2005), showing log of total flash rate measured by the TRMM LIS instrument and maximum dry bulb temperature approximately 1700 storms less than 35 degrees latitude. Figure included for comparison purposes.	123
3.37 CDFs of LCL heights for each region. Colors follow each region and are indicated in the legend.	124
3.38 Log flash rate and dry bulb temperatures for all storms in all regions of study. Points denote the median flash rates for each dry bulb temperature bin. Bottom error bar denotes the 25th percentile of the flash rate distribution for each dry bulb temperature bin. Top bar denotes the 75th percentile of flash rate distribution for each dry bulb temperature bin. Color of point indicates relative population of dry bulb temperatures following the colorbar.	125
3.39 Figure 2 from Williams et al. (2005), showing log of total flash rate measured by the TRMM LIS instrument and maximum dry bulb temperature approximately 1700 storms less than 35 degrees latitude. Figure included for comparison purposes.	126
3.40 Log flash rate and WCD values for all storms in all regions of study. Points denote the median flash rates for each WCD bin. Bottom error bar denotes the 25th percentile of the flash rate distribution for each WCD bin. Top bar denotes the 75th percentile of flash rate distribution for each LCL bin. Color of point indicates relative population of WCD values following the colorbar.	127

3.41 CDFs of WCDs for each region. Colors follow each region and are indicated in the legend.	128
3.42 Log flash rate and CAPE values for all storms in all regions of study. Points denote the median flash rates for each CAPE bin. Bottom error bar denotes the 25th percentile of the flash rate distribution for each CAPE bin. Top bar denotes the 75th percentile of flash rate distribution for each CAPE bin. Color of point indicates relative population of CAPE values following the colorbar.....	129
3.43 CDFs of CAPE values for each region. Colors follow each region and are indicated in the legend.	130
3.44 Flash rates as a function of LCL height and CAPE for all storms of study. Median flash rate for each 2D bin is colored following the colorbar. The white numbers denote the number of storm observations in the bin.	131
3.45 Same as previous figure, but for CAPE and WCD.	132
3.46 Same as previous figure, but for WCD and LCL.....	133
3.47 Same as previous figure, but for surface temperature and surface dew point temperature.	134
3.48 Figure 3 from Williams et al. (2005). Sizes of the circles indicate log of total flash rate for all storms in a particular bin. Effects of surface dry bulb temperature and dew point temperature are shown for 1700 storms less than 35 degrees latitude. Figure included for comparison purposes.	135
3.49 Same as previous figure, but for maximum flash altitude and LMA mode temperature..	136
3.50 Median flash rate dependence on echo top heights for 0 to 50 dBZ in each region. Bars represent the median absolute deviation for the flash rate distribution for each height bin.	137

3.51 Relationship between storm total flash rate and percentage of CG flashes that are positive polarity. Same binning and median analysis as previous plots. Points are colored by relative population of flash rates. 138

A.1 2D frequency of flash altitude and distance from LMA center for the Alabama LMA network. Other networks have similar behaviors. 165

A.2 2D plan view of source density for the Alabama LMA network for the 3 months of study. 166

A.3 Sensitivity plots of various storm lightning and radar quantities for storms in the Alabama region. Points denote the median quantity for each bin following the horizontal axis. Error bars indicate the median absolute deviation of flash rates for each bin. 167

A.4 Same as previous plot for DC. 168

A.5 Same as previous plot for Oklahoma. 169

A.6 Same as previous plot for Colorado. 170

CHAPTER 1

INTRODUCTION

1.1. LIGHTNING PRODUCTION

Thunderstorms are by definition clouds that produce lightning and thunder. Thunderstorms are the most intense form of moist convection and represent a small fraction of all moist convective clouds. Yet, lightning is of great interest to researchers from many different disciplines. Lightning can pose a threat to human lives, causing 1000 deaths per year in the United States (Curran et al. 2000). Lightning can also cause billions of dollars in damages and affect Earth's climate indirectly, for example through wildfires (Price and Rind 1994; Rorig and Ferguson 1999). The physics of lightning are still largely unknown. Moreover, the controls on lightning activity and global lightning distributions still remain a mystery, which is the focus of this thesis. Lightning is caused by the breakdown of air, which is a loss of its insulating properties, when it is subjected to strong electric fields (MacGorman et al. 2001). These electric fields are caused by transfer of charge upon collisions between ice particles and the subsequent separation of those particles by virtue of differential sedimentation in the presence of convective air motions (Williams 1985).

Lightning can be used to study thunderstorms and Earth's atmosphere as a whole. For example, global lightning activity has been argued to be used as a proxy for global climate change (e.g. Williams 1992, 1994; Reeve and Toumi 1999; Williams 2005). Lightning is an interesting and fruitful subject to study but is also a very difficult phenomenon to study for many reasons. One complication is that the scales at which thunderstorms transfer charge are very small. While laboratory simulations (e.g. Takahashi 1978; Jayaratne et al. 1983; Saunders and Peck 1998) provide very useful insights into the intricate charging mechanisms of thunderstorms, they may not be representative of actual storm environments. However, field studies detailed by Dye et al. (1989) and

French et al. (1996) have shown that these simulations are somewhat reasonable representations of thunderstorm environments. The strong vertical motions in thunderstorms and the presence of hail make it difficult to obtain *in situ* observations of actual storm characteristics such as the microphysics, vertical motions and the magnitude of electrical quantities such as charge density or electric fields. Such measurements would provide valuable insight into the conditions within a thunderstorm and can validate laboratory charging results.

Many theories have been offered to explain the buildup of charge in a thunderstorm. These theories are reviewed in Saunders (2008), but the currently accepted theory involves the non-inductive (NI) charging mechanism. First discovered by Workman and Reynolds (1950) and Reynolds et al. (1957), the non-inductive charging theory states that charge is transferred upon rebounding collisions between ice particles in the presence of supercooled liquid water. Specifically, these particles are often ice crystals and soft hail (graupel), although hail can be and is often involved as well. Since these particles have very different fall speeds by virtue of their different masses and shapes, collisions occur permitting the transfer of charge. Takahashi (1978) and Saunders et al. (1991) found that graupel and ice crystals can exchange significant amounts of charge per collision, accounting for large macroscopic electric fields capable of producing lightning observed in thunderstorms. Studies such as Baker et al. (1987), Baker and Dash (1989), Dong and Hallett (1992) and Dash et al. (2001) postulated that the polar nature of water and the molecular interactions in ice are fundamental to charge transfer upon rebounding collisions. Dash et al. (2001) claimed that rapid growth of an ice particle from vapor diffusion results in disordered growth and ionic defects at the ice surface. The surface charge produced by this effect is dependent on the diffusional growth rate of the particle, meaning that ice particles growing rapidly by vapor diffusion will possess high amounts of charge near the surface of the particle (Baker et al. 1987; Saunders et al. 1991, 2006).

By virtue of the differential ion mobility, the positive ions are able to diffuse from the ice surface, leaving it with a net negative charge. When collisions occur between ice particles, the particle growing faster by deposition will lose more mass at the surface which leaves it with net positive charge (Baker and Dash 1989). The mechanism for the mass (and charge) transfer is a microscopic liquid layer that exists at the solid-gas interface, estimated to be a few molecular diameters thick. The particle growing more rapidly by vapor deposition has a thick quasi-liquid layer (QLL) and will transfer mass to the particle with a thin QLL via pressure and chemical potential differences. The difference between QLL thicknesses helps determine the magnitude of charge transferred by each collision (Baker and Dash 1989). It has been found that supercooled liquid water is a necessary condition to produce appreciable charge transfer rates within thunderstorms. First, the presence of supercooled liquid water is indicative of water supersaturation conditions producing rapid diffusional growth rates. Also, the accretion of supercooled liquid water influences the temperature of the rimed particle by latent heat release upon freezing (Saunders et al. 2006). This will be detailed more in the next section.

1.2. LIGHTNING ACTIVITY IN THUNDERSTORMS

Lightning activity in thunderstorms is a main focus investigated in this study, therefore it is necessary to explicitly define lightning activity in the context of this study. For the purposes of this study lightning activity is defined by (1) the total lightning flash rate, (2) the dominant cloud-to-ground (CG) lightning polarity, and (3) the ratio of intra-cloud flashes to CG flashes (IC:CG). These three quantities have all been studied individually in previous studies, however not coincidentally or in the specific regions outlined in this study.

Investigation into global lightning activity was first attempted by Wilson (1916, 1920) in an attempt to explain fair-weather electric fields oriented toward the ground at a nearly constant value

of 120 V m^{-1} . It was from these measurements that he postulated thunderstorms were the drivers of the global circuit by constantly supplying the surface of the Earth with negative charge and the ionosphere with positive charge. This led to the discovery of the electrical thunderstorm dipole, with positive charge residing above negative charge within the thunderstorm (Wilson 1920). Readily following from this typical charge distribution in thunderstorms, the negative charge transferred to the Earth's surface was via negative CG (-CG) flashes along with charged precipitation (Williams and Heckman 1993). Although a nearly constant potential exists between the Earth and the ionosphere, fluctuations were also present, occurring at regular intervals (Whipple 1929; Price 1993; Williams and Heckman 1993). This was later attributed to the lightning activity of the prominent tropical chimneys in the West Pacific Warm Pool, Africa and South America via Schumann resonance studies (e. g. Williams 1992; Heckman et al. 1998; Williams 2009). With the more recent advent of lightning detectors aboard satellites (Christian et al. 1999, 2003) it is now clear that lightning favors continents by roughly an order of magnitude over oceanic regions. This is illustrated in Fig. 1.1 from Boccippio et al. (2000). However, this behavior is not coincident with the rainfall distribution over the same domain. This raises the question: what causes lightning to favor land when rainfall does not necessarily follow the same pattern? Many studies have documented this result (e.g. Zipser 1994; Boccippio et al. 2000; Williams and Stanfill 2002; Christian et al. 2003; Zipser et al. 2006) but the exact cause remains elusive.

Williams (1985) has shown that lightning flash rates are directly linked to vertical air motions. Storms with stronger updrafts produce more lightning. There are numerous reasons for this. Recall that microscopic collisions (in the presence of supercooled liquid) and subsequent separation of small particles are responsible for thunderstorm electrification. Stronger updrafts are able to

move air parcels through the warm-rain zone of the cloud faster, thereby suppressing collision-coalescence and supplying the mixed phase region with larger amounts of liquid water. Stronger updrafts are also more able to support the weight of any condensate that forms upon ascent of the parcel, either leading to larger amounts of liquid water supplied to the mixed-phase region or a greater amount of riming particles upon freezing of the droplets. These frozen droplets can become graupel and hail, via riming processes, necessary to facilitate electrification processes.

Strong updrafts can also modify the drop size distribution by creating large supersaturations, thereby activating more cloud condensation nuclei (CCN) than modest supersaturations (Williams et al. 2005). An increase in activated CCN results in greater competition for liquid water, therefore decreasing the average droplet size. Smaller drops are less likely to undergo collision-coalescence processes and fall out as warm rain, resulting in a greater supply of liquid water to the mixed-phase region (0 °C to -40 °C). Larger amounts of liquid water boost electrification because the magnitude of collisional charge transfer is dependent on available supercooled liquid water content (Takahashi 1978; Saunders et al. 1991). Stronger updrafts also produce a greater number of collisions, which leads to greater charge separation. It logically follows for these reasons that strong updrafts produce highly electrically active thunderstorms.

Multiple studies have found that characteristic updraft speeds are larger over land than over oceanic regions (Kyle et al. 1976; LeMone and Zipser 1980; Williams and Stanfill 2002). These stronger updrafts have also been found to be coincident with characteristically broader updrafts, therefore sparking interest in the relationship between these quantities. A manifestation of the link between lightning and updraft strength was found by a number of studies (Goodman et al. 1988; Price and Rind 1992; Deierling and Petersen 2008) and is summarized by Williams (1985) in which a consistent relationship was found in multiple regions of the United States. Lightning

was found to be proportional to the fifth power of cloud top height, although these results came from continental regions and may not be applicable to tropical convection. These relationships are broadly consistent with the scaling relationships of Vonnegut (1963). That study also postulated that vertical velocities are proportional to cloud scales, meaning that broader updrafts would also have to be stronger in order to produce the required electrical power in a thunderstorm. This was based on an electrical argument with no microphysical or dynamical evidence used to support this claim.

If updrafts over continental regions are stronger and broader than oceanic regions, there must be environmental factors explaining the characteristic differences in the updrafts. Current studies find that these differences are caused thermodynamically or by aerosol interactions. Thermodynamic arguments state that since land heats up more than adjacent ocean regions during periods of solar insolation due to different heat capacities and radiative properties, the warmer surfaces produce greater instabilities resulting in stronger updrafts by simple parcel theory (Williams and Stanfill 2002; Williams et al. 2005). However, Williams and Renno (1993) found that no significant instability differences exist between tropical oceans and land masses on global scales. Williams et al. (2005) argue that any differences in values of convective available potential energy (CAPE) do not explain the magnitude of flash rate difference between land and ocean. Instead they argue that deviations from simple parcel theory are necessary to explain lightning differences. They found that the cloud base height (CBH), a function of surface dew point depression, was well correlated with the log of total flash rate despite considerable scatter characteristic of their framework. In other words, storm total flash rate is a quasi-exponential function of CBH. A similar relationship was observed between total flash and surface dry bulb temperature. Moreover, the highest overall flash

rates were found to correspond with high surface dry bulb temperatures and modest dew point temperatures rather than high dew point temperatures. Williams et al. (2005) and Williams and Stanfill (2002) argue that storms in warm and dry environments produce higher overall flash rates because of broad updrafts due to high CBHs. They offer the fixed angle hypothesis (Morton et al. 1956) as a possibility, which states that storms with higher cloud bases will be broader because thermal plumes expand as they rise. Broader updrafts are less prone to entrainment of drier ambient air and therefore can transport a larger portion of the adiabatic water content to the mixed-phase region where it can assist in superlative electrification.

Aerosol arguments are based on observations that land regions are typically characterized by higher aerosol concentrations by virtue of surface characteristics and anthropogenic emissions. Higher aerosol concentrations result in a greater number of CCN competing for the same amount of liquid water, therefore sharing the available liquid water amongst a larger number of particles. These droplets will be on average smaller and more numerous than in a clean environment and thus modify the drop size distribution. A greater number of small particles will then suppress collision-coalescence processes, permitting more liquid water to survive to the mixed-phase region (Williams et al. 2002). Freezing of larger amounts of supercooled liquid water releases more latent heat to the updraft, which in turn makes the updraft more buoyant. This is known as the aerosol invigoration of convection (Lyons et al. 1998; Williams et al. 2002; Andreae et al. 2004; Koren et al. 2005; van den Heever et al. 2006; Rosenfeld et al. 2008; Altaratz et al. 2010; Yuan et al. 2011). These effects due to aerosol concentrations are similar to the previously mentioned thermodynamic effect of stronger updrafts. The debate of the more prominent effect on global lightning distributions is still ongoing. Decoupling the two effects is very difficult because often times they occur simultaneously (e.g. Lang and Rutledge 2006).

1.3. CG LIGHTNING POLARITY

The large majority of cloud-to-ground (CG) lightning strikes in the United States are of negative polarity, meaning that negative charge is lowered from cloud to ground (Williams 1992; Orville 1994; Orville and Silver 1997; Orville and Huffines 2001). Zajac and Rutledge (2001) estimate that nearly 10% of all CG flashes in the continental United States (CONUS) lower positive charge to ground. It has been well established however, that there exist many different types of thunderstorms exhibiting various electrical characteristics throughout the United States (Reap and MacGorman 1989; Branick and Doswell 1992; Curran and Rust 1992; Stolzenburg 1994; Carey and Rutledge 1998; Lang et al. 2000; Williams 2001; Lang et al. 2004b; Wiens et al. 2005; Tessendorf et al. 2007; Lang and Rutledge 2011). Among others, Boccippio et al. (2001) showed a region of enhanced positive CG (+CG) production east of the Rocky Mountains in the upper Great Plains as high as 20% of total CG flashes. This is illustrated in Fig. 1.2 taken from Boccippio et al. (2001). This percentage generally decreases toward the east with a minimum in +CG production of 4% of total CG flashes east of the Appalachian Mountains. For example storms in Alabama and Florida very rarely produce large amounts of +CGs regardless of storm intensity and the environments in which they exist (Williams et al. 1999; Zajac and Rutledge 2001).

These regional differences in +CG lightning are likely caused by several factors. The mature stages of strong and severe thunderstorms can exhibit periods of high +CG lightning production via inverted charge structures (Seimon 1993; Smith et al. 2000; Carey and Rutledge 2003; Carey et al. 2003) discussed later. Other theories have been put forth to explain elevated rates of +CG flashes in other types of storms. Large stratiform regions of mesoscale convective systems (MCSs) can produce copious amounts of +CG flashes (Orville et al. 1988; Rutledge and MacGorman 1988; Rutledge et al. 1990). Storms during the cold season tend to produce relatively large fractions of

+CG lightning, likely due to the tilted dipole mechanism (Brook et al. 1982). Dissipating stages of ordinary and weak convection have also been shown to produce +CG lightning at increased rates (Fuquay 1982). This can be the result of precipitation unshielding (Williams 2001; Carey and Rutledge 1998) or a systematic lowering of all charge regions via gravitational sedimentation, also known as an end of storm oscillations (EOSO; Moore and Vonnegut 1977; Livingston and Krider 1978; Pawar and Kamra 2007). Storms undergoing these processes are not particularly important in the scope of this study because +CG production is not studied in detail in regions where this process is a main producer of +CGs. These storms are also in the weak tail of the distribution and are therefore excluded from the bulk analysis described later.

These factors help explain why large amounts of positive lightning are produced in the lee of the Rocky Mountains. Storms that initiate off of the Rockies have a tendency to grow upscale into nocturnal MCSs that produce positive lightning (Rutledge and MacGorman 1988; Rutledge et al. 1990). Climatological cloud-base heights (CBHs) in this region are also relatively high compared to other regions east of the Rockies which is postulated to have a relationship with total lightning and +CG lightning production (Williams et al. 2005). Zajac and Rutledge (2001) showed that the +CG lightning maximum in the upper Great Plains region temporally leads the maximum in CG lightning. This suggests that in this region, lightning is being produced by strong convection that produces +CGs before -CGs, however this is not necessarily the case in other regions of the CONUS. We will only investigate the strong convection and dissipating stages of ordinary convection because our period of study is the warm season isolated convection.

Similar to the production of +CGs, the relative production of intra-cloud (IC) flashes to CG flashes (IC:CG ratio; Williams et al. 1989) has a strong regional dependence. Boccippio et al. (2001) used both satellite and ground-based measurements to estimate the IC:CG ratio over the

CONUS and found a very similar spatial pattern to the fractions of +CG production. Fig. 1.3 shows the variation in IC:CG ratio in the CONUS, taken from Boccippio et al. (2001). A IC:CG maximum of approximately 6-9 was found in the upper Great Plains region east of the Rocky Mountains coincident with the highest proportions of +CG flashes. The minimum +CG flash rates in the southeastern US was coincident with low IC:CG ratios of 1-2. This suggests a relationship between greater production of IC flashes and +CG flashes.

1.4. STORM ELECTRIFICATION AND INVERTED STORMS

Laboratory studies first conducted by Reynolds et al. (1957) and Takahashi (1978) showed that charge transfer occurred when rimed ice particles (graupel) collided with ice crystals in the presence of supercooled liquid water. The polarity of charge acquired on the rimer depends on both the temperature and liquid water content (LWC) of the environment, which is illustrated in Fig. 1.4 from Takahashi (1978). Later studies including Jayaratne et al. (1983) and Saunders et al. (1991) conducted similar experiments and arrived at generally similar results. A later study by Saunders et al. (2006) reviewed the different methods of these previous studies while conducting sensitivity studies of different variables and slightly modified the charge-sign reversal lines but the general conclusion remained the same: warmer and wetter environments tend to promote positive charging of the rimed particles. Portions of the cloud with higher temperatures and LWCs will have a preference to charge the rimed particle positive whereas portions of the cloud with less liquid water or lower temperatures will charge the rimed particle negative.

It is of interest to investigate the controls on cloud LWC because the sign of charged particles depends on temperature and LWC. Many studies have postulated that the environment in which a storm forms affects its dynamics and thermodynamics. This in turn affects its electrical characteristics and therefore the storm's lightning behavior (Lyons et al. 1998; Smith et al. 2000; Gilmore

and Wicker 2002; Williams et al. 2005; Carey and Buffalo 2007; Lang and Rutledge 2011). After studying several storms in Oklahoma in 2002, Carey and Buffalo (2007) postulated that dominant CG polarity is controlled by warm cloud depth (dependent on CBH) along with instability and shear. Their results showed that storms producing high fractions of +CGs had higher cloud bases and formed in regions with larger amounts of instability and shear. These environments are more conducive to the formation of severe storms with stronger updrafts. Shallower warm cloud depths should result in a shorter residence times for parcels below the freezing level, thus allowing more liquid water to survive into the mixed-phase region (0 °C to -40 °C). This increases the amount of supercooled liquid water and the likelihood of producing positively charged graupel. Considerations should be made for the fact that this study only examined one region in the CONUS and may not necessarily be indicative of all regions. Lang and Rutledge (2011) probed storms that occurred during the Severe Thunderstorm Electrification and Precipitation Study (STEPS), which took place near the Colorado/ Kansas border during the warm season of 2000 (Lang et al. 2004b). While their results showed storms producing large fractions of +CGs formed in regions of higher shear and instability, positive CG storms did not have significantly higher cloud bases or shallower warm cloud depths.

Many studies have investigated vertical charge structures of thunderstorms throughout the CONUS and have found a so-called normal tripole charge structure, characterized by a layer of negative charge at mid-levels (-10°C to -30 °C) situated between upper and lower positive charge regions (Williams 1989). In this model, most flashes that initiate between the upper dipole (upper positive and mid-level negative) result in IC flashes while some flashes that initiate between the lower dipole (mid-level negative and lower positive) may result in CG flashes (Williams 1985; Krehbiel 1986; Williams 1989). This is the reason why most CG flashes are negative polarity

(Krehbiel 1986), consistent with the early observations of Wilson (1920). However, it has been found that a group of storms exist that produce more +CGs than CGs (e.g. Brook et al. 1982; Reap and MacGorman 1989; Branick and Doswell 1992; MacGorman and Burgess 1994; Carey and Rutledge 1998; Lang and Rutledge 2002; Lang et al. 2004b; Wiens et al. 2005; Tessendorf et al. 2007; Lang and Rutledge 2011). These storms are thought to have an inverted charge structure with mid-level positive charge situated between layers of negative charge (Lang et al. 2004b; Rust et al. 2005; Wiens et al. 2005; MacGorman et al. 2008), although there is evidence that the lower negative region does not necessarily exist (Lang et al. 2004b; Bruning et al. 2012). Storms lacking a lower charge region have a difficult time producing CG flashes due to the weak electric fields near the base of the storm. Inverted storms are found to produce higher fractions of +CG flashes in the High Plains region of the United States and are largely responsible for the maximum in +CG percentage (e.g. Zajac and Rutledge 2001). Inverted storms have been observed to be stronger and more severe in general than normal charge structures (e. g. Lang et al. 2000), although this appears to be regionally dependent.

With the use of three-dimensional (3D) LMA data, it is now possible to infer charge regions in thunderstorms through the use of LMA VHF source densities. A simple model of a normal tripole thunderstorm with negative charge at mid-levels sandwiched by positive charge will manifest as a relative minimum in source density between two maxima at upper (approximately 10 km) and lower (approximately 5 km) levels, as depicted in Fig. 1.5. This is due to greater VHF radiation production by negative breakdown into regions of positive charge than positive breakdown into regions of negative charge (Rison et al. 1999). Conversely, a storm with an inverted charge structure would exhibit a single maximum in source density corresponding to mid-level positive charge (near 8 km).

Assuming a simple two-dimensional (2D) representation of a storm, it should be possible to identify the vertical charge structure from the distribution of VHF sources (Tessendorf et al. 2007; Lang and Rutledge 2008, 2011). This knowledge, paired with National Lightning Detection Network (NLDN) CG and model analysis environmental data will allow us to determine the charge structure of storms producing predominantly +CGs and examine the environmental controls on storms exhibiting mid-level positive charge structures, such is the focus of this thesis. This is of course ignoring any horizontal variability and complicated charge structures previously discussed, which can be common in larger and severe storms, especially supercells (Bruning et al. 2010). However, severe storms with associated complicated charge structures are a small percentage of the total storm observations ($\leq 4\%$) and therefore influence is mitigated in the results shown in this study by virtue of the analysis methods detailed in the results section.

An alternate view to the storm charge structures classified as normal and inverted (e.g. Tessendorf et al. 2007) has been provided by Bruning et al. (2012). The normal polarity tripole model states that precipitation particles are a fundamental ingredient in the charge separation process (Williams 1989). Collisions between graupel and ice crystals in the presence of supercooled liquid water deposit negative charge on the graupel while the ice crystals acquire positive charge. Macroscopic convective air motions carry the ice crystals to the upper portions of the cloud while leaving the larger graupel particles behind in the mid-levels of the storm. As graupel grows by accretion of supercooled liquid water, they descend and acquire positive charge as they fall into warmer temperatures and collide with ice crystals. The relative strengths of these charging mechanisms may dictate the charge densities of the layers and affect the lightning behavior in different thunderstorms. Baker et al. (1987) concluded that the relative growth rate of the two ice hydrometeors from the vapor phase controls the charging sign of the rimed particle. This effect is enhanced as

supercooled liquid water amounts increase. These processes are happening continuously throughout storms and are consistent from storm to storm. Fig. 1.6 taken from Bruning et al. (2012) depicts multiple trajectories of hypothetical parcels as they ascend through the storm. As parcels ascend, both temperature and LWC decrease. The important consideration is the LWC loss rate as the parcel decreases in temperature. Some parcels undergo faster liquid water depletion due to warm-rain processes (e.g. collision-coalescence), which is more characteristic of maritime convection. Conversely, we expect slow depletion rates from storms with strong updrafts or high cloud bases where warm-rain processes are suppressed (Williams et al. 2002; Williams and Stanfill 2002), permitting the survival of large amounts of liquid water into the mixed-phase region. Parcels slowly losing liquid water will follow a trajectory similar to the top curve on Fig. 1.6, leading to a deep layer of positive graupel charging and possibly contributing to an inverted charge structure. Note that graupel is charged negative at lower temperatures and is charged positive at warmer temperatures, making it difficult for storms to possess an inverted lower negative charge without the assistance of another process. If this does not occur, then only a negative-over-positive upper dipole is present and no lower charge exists to help initiate breakdown to connect with the ground (Livingston and Krider 1978). Many processes can contribute to the loss of a parcel's liquid water besides riming by supercooled liquid water. Detrainment of cloud liquid water can occur to the surrounding drier ambient air, resulting in a loss of supercooled liquid water via evaporation. Wet growth of hail will scavenge liquid water from the parcel while possibly shutting down the electrification process by preventing the rebounding collisions and charge transfer (Bruning et al. 2012). It is possible then that one storm may have different parcel trajectories through this parameter space depending on location in the storm. The normal/inverted terminology is problematic for this continuous and varying behavior because the same processes are continuously occurring in all storms, regardless

of charge structure or lightning behavior. It is for this reason that this study is concerned only with isolated storms as this will minimize the complicating effects of entrainment of modified air or advection from other cells (i.e. in an organized system).

It appears that similar storm dynamics and microphysical processes within a storm tend to cause storms to become anomalously electrified, both from a total flash rate and CG polarity perspective. These microphysical processes are produced by a variety of factors. Stronger updrafts are able to supply the mixed-phase region with superlative amounts of liquid water. These storms will produce stronger overall charge separation and are more likely to support anomalous charging of graupel by virtue of graupel and ice crystal microphysics. It stands to reason that regions conducive to high flash rate storms should also be supportive of anomalous charging and inverted storms. This claim will be investigated in this thesis.

1.5. APPROACH OF THIS STUDY

The variations in lightning activity throughout the United States and the globe spark interest on the effects of local environments on storm radar and lightning characteristics. This is investigated by extending the Lang and Rutledge (2011) study, which developed the Colorado State University (CSU) Lightning, Environmental, Aerosol and Radar (CLEAR) framework as a tool to take advantage of various datasets currently available. CLEAR objectively analyzes large amounts and varieties of data to compile statistics on storms with specific properties (e.g. dominant CG polarity or total flash rate) in an effort to understand the factors that control or are related to lightning behavior. This study utilizes the 3D mosaic radar data combined with CG lightning data from the NLDN and total lightning information from Lightning Mapping Array (LMA) networks, model reanalysis environmental data and ground aerosol data to formulate a comprehensive study. The regions of study include northern Alabama, central Oklahoma, northeast Colorado and the greater

Washington, D.C. area. These regions were chosen for the availability of LMA networks in order to provide detailed investigations of storm lightning behavior. All periods of study were during the 2011 warm season with the exception of Colorado since installation of its LMA occurred in the spring of 2012. The year 2011 was chosen because this study began in the fall of 2011. Fig. 1.7 shows a map of the approximate regions and season of study.

This study utilizes total flash rates calculated by a novel flash clustering algorithm to understand the link between storm intensity from both radar and lightning perspectives in each region. The distinct lightning behaviors in each region are also documented, and an attempt to establish relationships between storm intensity and environmental parameters are performed in each region of study. If evidence suggests that anomalous electrification (i.e. inverted storms) are present within a particular region, further investigation of those storms was carried out. Finally, all storms from each region will be investigated simultaneously in an attempt to determine the causes of the different lightning behaviors observed in each region. These results will be compared to other global studies to examine the robustness of the relationships.

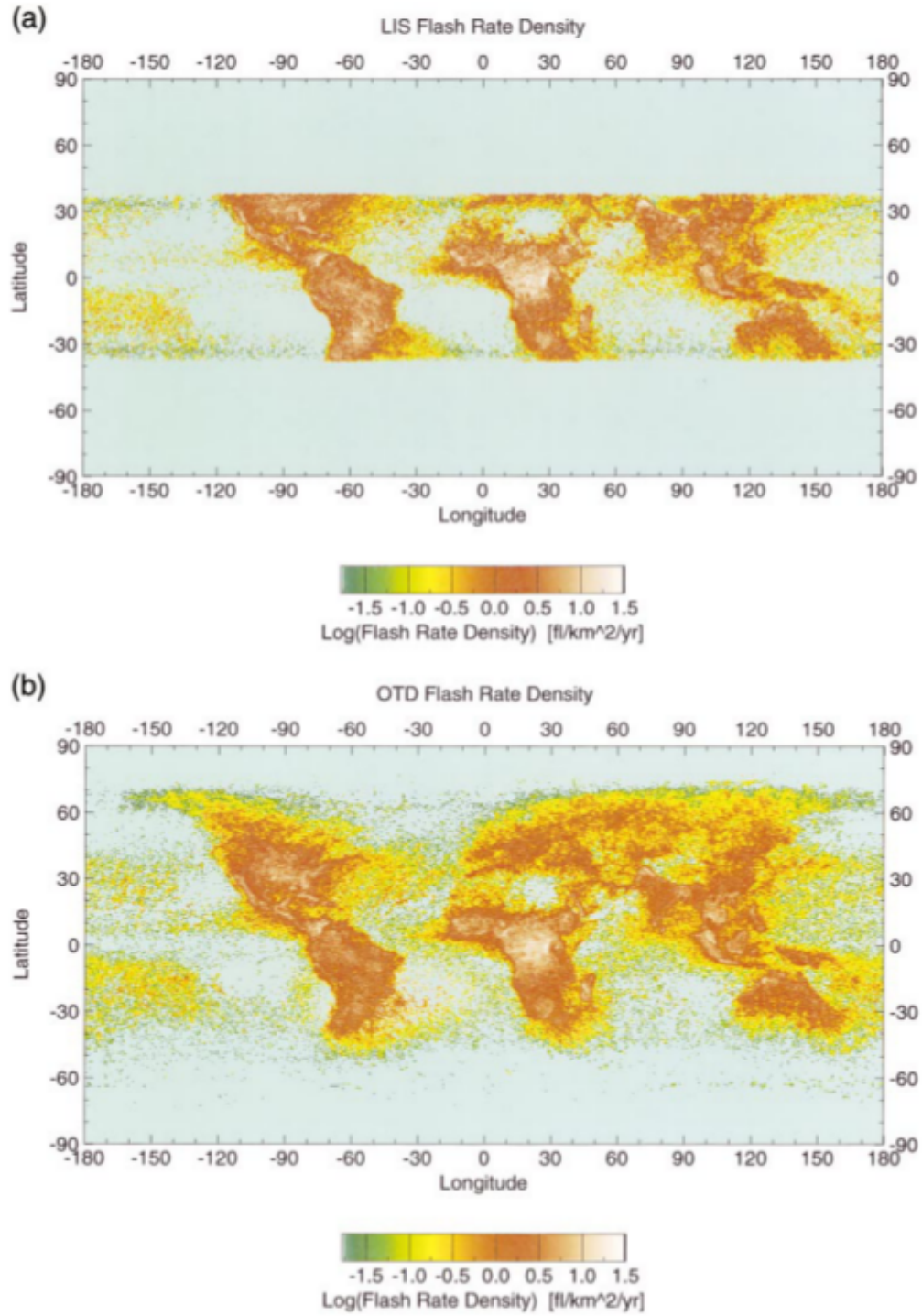


FIG. 1.1. LIS and OTD flash rate density for (some time frame) from Boccippio et al. (2000). Note that the LIS instrument only captures flashes from ± 35 degrees latitude.

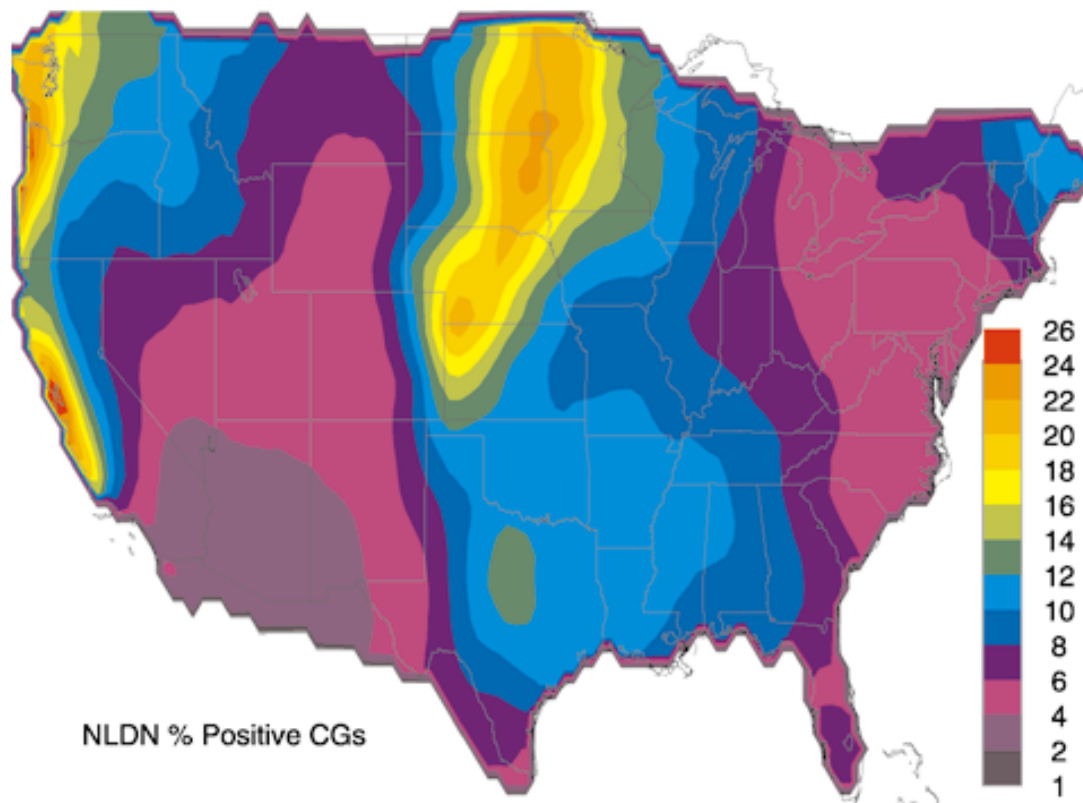


FIG. 1.2. Fraction of total CG flashes that are positive polarity from Boccippio et al. (2001).

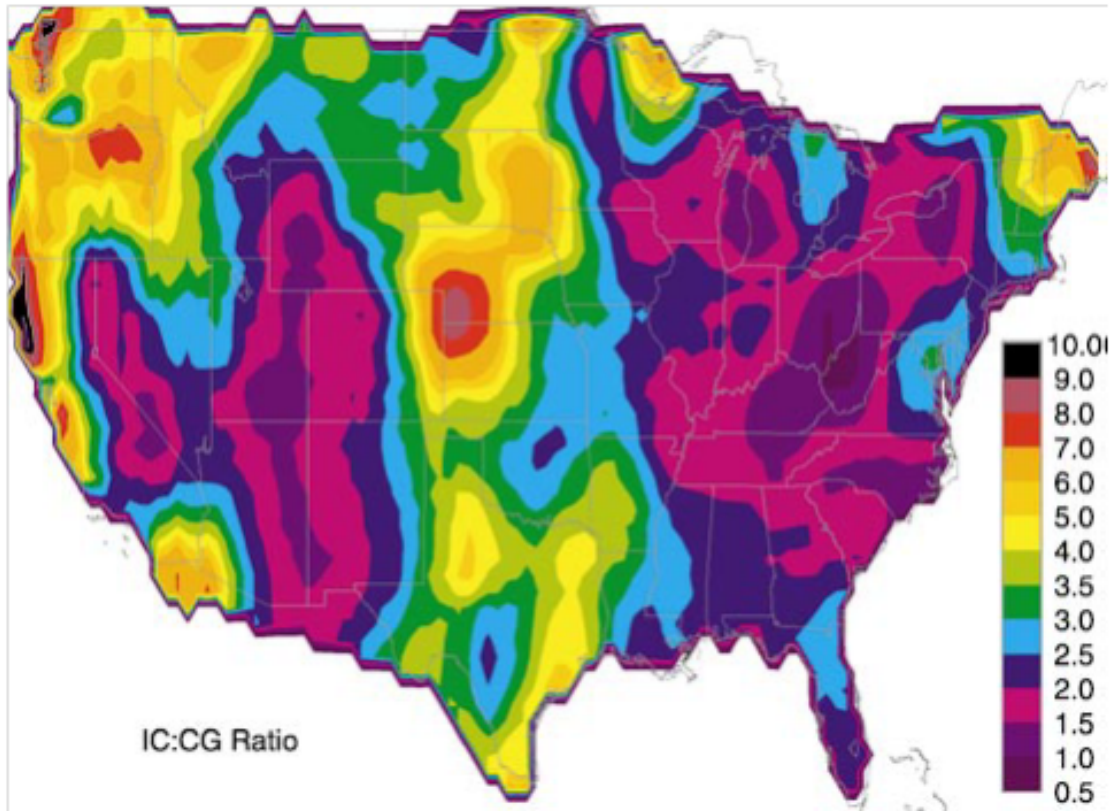


FIG. 1.3. Relative rates of IC flashes to CG flashes, otherwise known as IC:CG ratio from Boccippio et al. (2001). Note that the large values near the west coast and New England areas are likely NLDN detection efficiency artifacts.

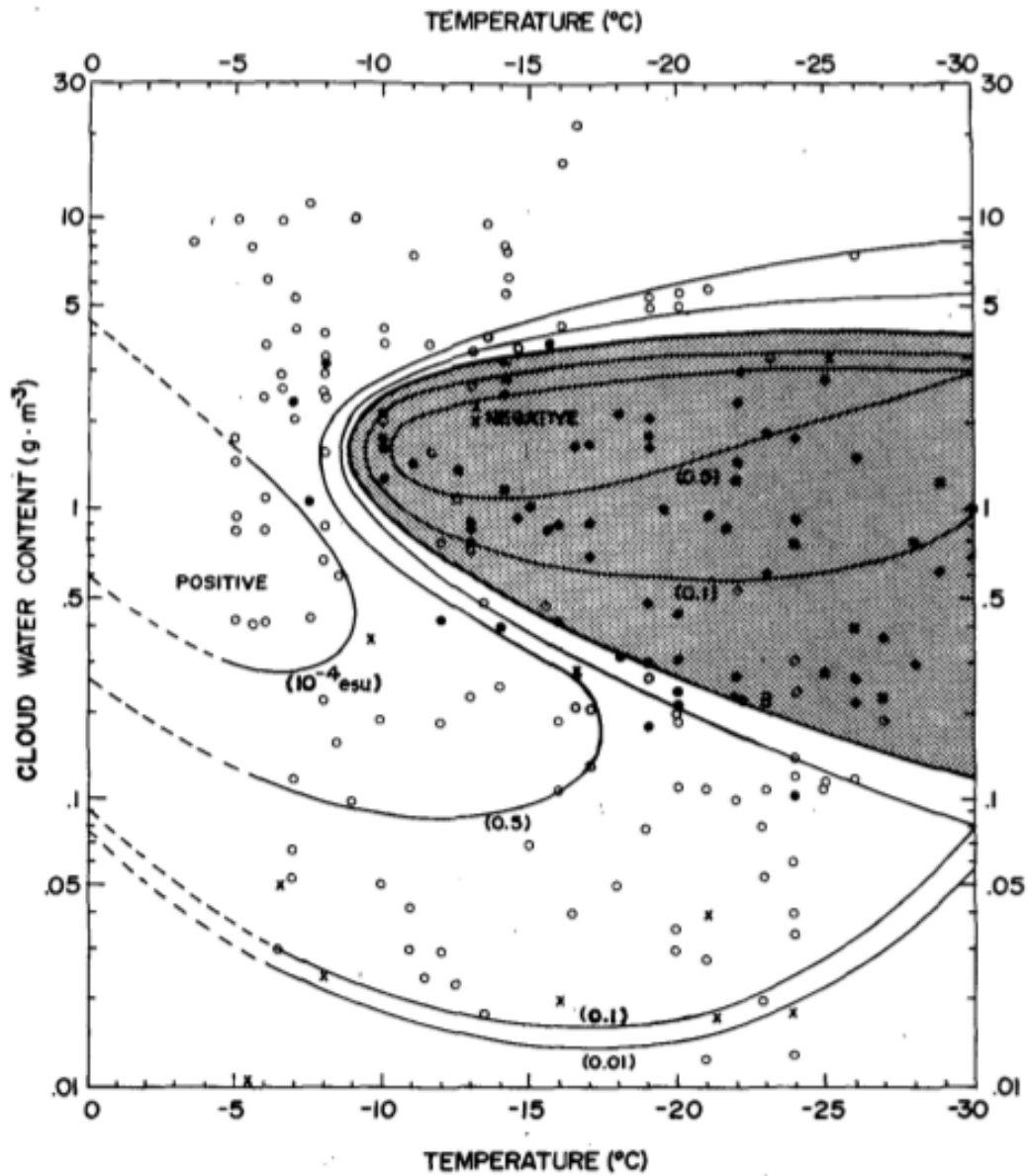


FIG. 1.4. Sign acquired by graupel upon rebounding collisions with ice crystals as a function of cloud temperature and liquid water content from Takahashi (1978). The dark region represents negative graupel charging and the light region represents positive charging. Note the log scale on the vertical axis.

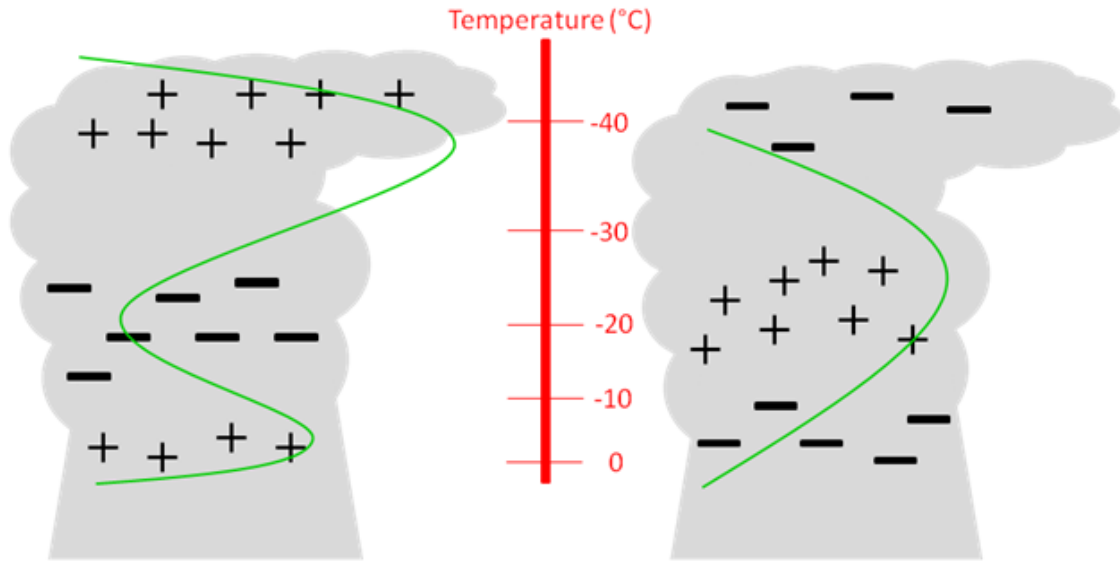


FIG. 1.5. Schematic diagrams of normal polarity (left) and inverted polarity (right) storms. Approximate location of charge regions are indicated by the plus and minus signs. The green lines indicate general vertical VHF LMA source distributions. Approximate temperatures follow the middle red scale.

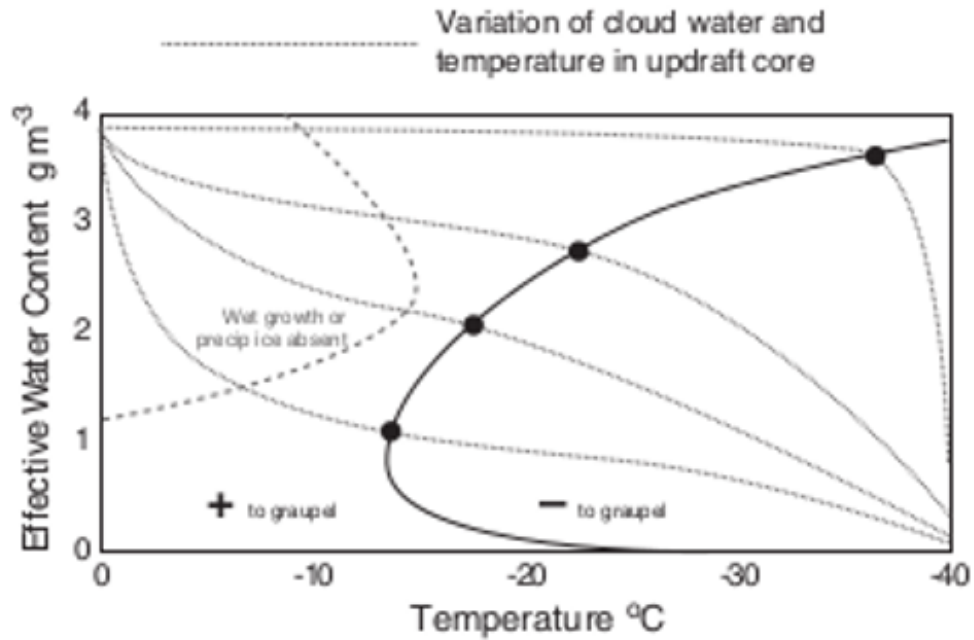


FIG. 1.6. Depiction of the graupel charge sign along a parcel trajectory in a storm from Bruning et al. (2012). The dotted lines represent different parcel trajectories through this phase space. Different trajectories are manifestations of different liquid water depletion rates. The top and left portions of the figure represent positive charge to graupel. The bottom and right portion of the figure represents negative charge to graupel.

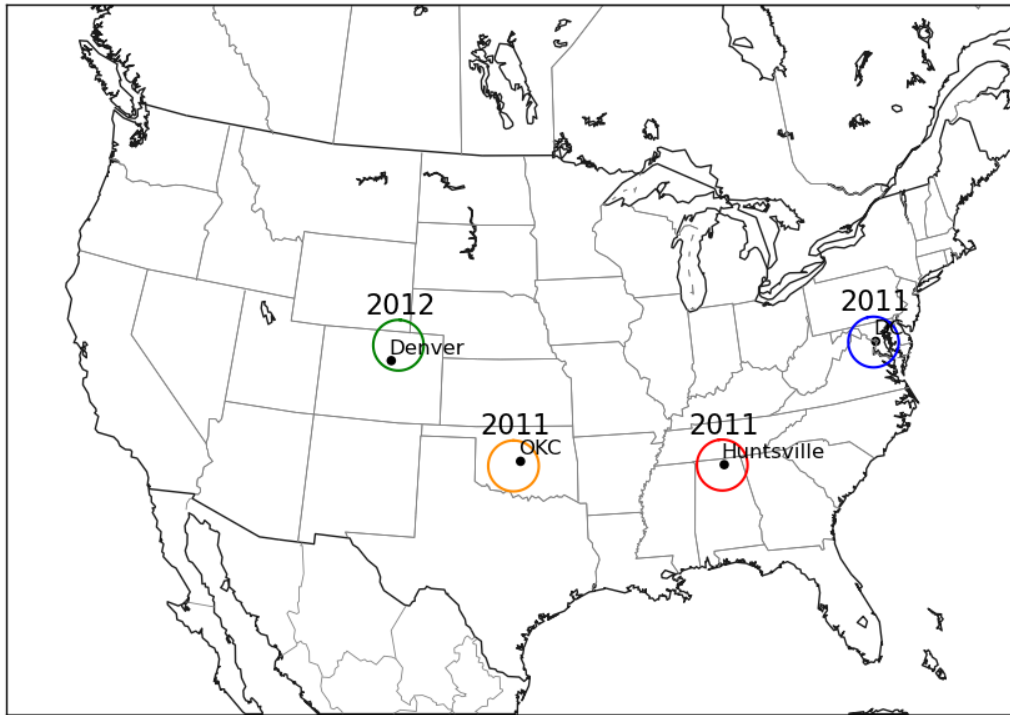


FIG. 1.7. Map of approximate regions and seasons of study with notable cities included for reference. The radii of the circles represent the selected LMA radius criterion for sample inclusion. Note that the colors representing each region are consistent throughout the study.

CHAPTER 2

DATA AND METHODOLOGY

2.1. CLEAR FRAMEWORK

The CLEAR analysis framework was developed by Lang and Rutledge (2011) in an effort to automate the analysis of large amounts of thunderstorm data from a variety of sources. The work discussed here improved upon elements of the CLEAR framework to provide a more robust method to analyze storms. The framework is a fully modular collection of programs designed to merge a multitude of data and link these data to storms. Once data are attributed to identified cells, analysis can be performed and statistics and can be compiled in an efficient and automated manner.

The value of CLEAR is in its flexibility. The framework was used in this study as a way to compile statistics for a large set of storms with many different types of data, but can also be used to look at specific case studies. Case studies can be investigated through CLEAR's cell-tracking explained in a later section. Tracks of storms can be probed for a wide range of storm characteristics to investigate time evolution of storm parameters. All data used in this study are in Network Common Data Form (NetCDF) files. These file types are advantageous to this framework because of ease and commonality of use with these files. Appending the ancillary data to the radar files only results in about a 20% increase in overall file size, keeping the processing efficient (Lang and Rutledge 2011). A simple schematic of the CLEAR algorithm is included in Fig. 2.1.

2.2. RADAR

The radar data used in this study are from the National Mosaic and Multi-Sensor Quantitative Precipitation Estimates (NMQ) mosaic 3D radar data (Zhang et al. 2011). NMQ mosaic data are arranged in latitude/ longitude coordinates with $0.1^\circ \times 0.1^\circ$ horizontal resolution with a variable

stretched vertical grid from 500 m to 18 km above mean sea level (MSL). Vertical resolutions vary from 500 m near the surface to 2 km at the highest levels. These mosaics cover the entire CONUS and neighboring regions near the Atlantic and Pacific coasts and are currently produced every 5 minutes. Since these files come from Next-Generation Radar Weather Surveillance Radar (NEXRAD-WSR88D) radars and are gridded to constant altitude levels, artifacts are introduced that may manifest themselves in some of the data. Methods for managing these artifacts are discussed below. Polarimetric and single radar data are able to be used with CLEAR but are not used in this study.

To objectively identify convective cells in the different regions, a cell-tracking algorithm similar to Rowe et al. (2011) and Lang and Rutledge (2011) was used. This algorithm is a variant of the Thunderstorm Identification, Tracking, Analysis and Nowcasting (TITAN) tracking methodology (Dixon and Weiner 1993), and uses a composite reflectivity field to locate individual cells or convective elements within a larger organized convective system. The main advantage of this type of identification is computational efficiency with isolated cells. As discussed before, isolated cells are the focus of this study in order to avoid the complicating effects of interacting storms in organized convection.

CLEAR cell tracking is a centroid-based algorithm that identifies cells based on a 2D composite reflectivity field. The software uses a two-threshold system to identify cells. The reflectivity thresholds are tunable along with the minimum area associated with each reflectivity. Reflectivity regions that do not meet the requisite size were thrown out and were not included in the study. For this study, reflectivity thresholds of 30 and 40 dBZ with minimum areas of roughly 20 km² and 13 km² respectively were imposed. A large requisite cell size with high reflectivities was mandated because electrified cells are of interest in this study. These thresholds are larger than

similar tracking algorithms by a factor of approximately 50-100% (Johnson et al. 1998; Rowe et al. 2011; Gauthier et al. 2010; Lang and Rutledge 2011). This resulted in fewer identified cells and kept processing more efficient. This large requisite cell size also eliminated ground clutter and any artifacts that result from gridding NEXRAD radar data to constant altitude levels because those errors were spatially limited.

Since the focus of this study was isolated convection, a method for objectively identifying isolated cells was implemented. A novel approach was employed based on the convective-stratiform partitioning put forth by Yuter and Houze (1998). In addition to cells being identified by the methods described above, convective regions were also identified with the Yuter and Houze (1998) algorithm. A search was then performed on each convective region to count the number of identified cells located within each convective region. If multiple cells were identified in a convective region then those cells were classified as organized, but if only one cell occupied a convective region then the cell was classified as isolated. Since multiple convective (and reflectivity) cores may exist in one storm, these cores may be incorrectly identified as separate cells, and hence incorrectly classified as organized. A solution to this problem was to apply a bi-linear smoothing to the linear reflectivity field before feature identification was performed. This smoothing resulted in fewer identified cells that are larger on average.

Attribution of Storm Prediction Center (SPC; Corfidi 1999) storm reports was added to the cell-tracking algorithm. These reports were attributed to the closest cell in time if the location of the report fell within the region of an identified cell. This lends itself to streamlined studies of storm and environmental characteristics of severe weather along with possible lightning jump (e.g. McCaul et al. 2009; Gatlin and Goodman 2010) and nowcasting studies. Simple storm and environmental comparisons between isolated severe and non-severe convective cells were performed

in this study to display severe weather attribution proof-of-concept within this framework. The results of this simple investigation show promising and realistic results.

2.3. NATIONAL LIGHTNING DETECTION NETWORK (NLDN)

This study used 1-ms resolution NLDN flash-level data. Detection efficiencies in all regions of study are at or above 90% (Cummins et al. 1998; Cummins and Murphy 2009). Per the recommendations of Cummins and Murphy (2009), any CG peak currents under 10 kA were reclassified as IC flashes and any IC flashes with peak currents over 25 kA were reclassified as CG flashes of appropriate polarity. Any detected IC flashes were discarded and only appropriate CG flashes were included. Appropriate flashes were those either within an identified cell or within 10 km of an identified cell. These flashes were attributed for processing.

2.4. LIGHTNING MAPPING ARRAY (LMA)

There are currently multiple LMA networks in operation in the United States. This study made use of 4 of them located in northern Alabama Goodman et al. (2005), Washington, D.C. (Krehbiel 2008), central Oklahoma (Krehbiel et al. 2000) and northeast Colorado. LMAs use time-of-arrival (TOA) techniques from multiple detection stations, like the one shown in Fig. 2.3, to locate VHF radiation sources produced by the propagation of a breakdown channel or flash (Rison et al. 1999; Thomas et al. 2004). A single flash may produce tens to thousands of VHF sources depending on many factors including total channel length and network detection efficiency. Detection of many points along breakdown channels of flashes affords highly accurate 3D mapping of both IC and CG flashes. By virtue of the different installation times and locations, different LMAs have different technologies employed which leads to variations in detection performance

and sensitivities. Because of this, comparisons of VHF source rates are only valid within a region and not between regions.

2.5. FLASH CLUSTERING ALGORITHM

A flash clustering algorithm based on spatial and temporal clustering of VHF sources has been developed by Prof. Eric Bruning (personal communication) and has been implemented into this framework. This algorithm produces total flash rates that can be used to calculate IC flash rates when used in concert with NLDN CG observations. While LMAs are not currently available throughout the entire CONUS, storms in the LMA regions can be studied with great detail and accuracy when paired with flash counting. This study is the first implementation of an automated and open source flash counting algorithm. This required some performance testing of the flash counting ability. Testing was performed by visual inspection of random cells in each region along with comparisons between flash counts produced by the XLMA program (Rison et al. 1999; Lang et al. 2004a), considered to be the gold-standard in flash counting analysis. Fig. 2.2 shows an example of the visual plots used to subjectively evaluate this flash counting algorithm. The top panel shows a time-height plot that is the most effective way to identify flashes, which are denoted by a black x. Under that panel is a longitude-height cross section and a vertical histogram of LMA sources in blue and flashes in red. The large panel in the lower left is a plan view of the sources associated with the particular cell of interest. The bottom right panel is a latitude-height cross section. This multi-panel plot is an effective way to inspect the sources associated with a particular cell. This plot was designed to emulate XLMA plots and was used as a comparison to those plots.

The flash counting algorithm is implemented within the Python programming language using the Density-based spatial clustering of applications with noise (DBSCAN) clustering algorithm

(Ester et al. 1996). This algorithm clusters objects (LMA sources in this case) based on specified space and time criteria. The DBSCAN function has two tunable parameters: ϵ , the maximum distance between two objects to be considered within the same neighborhood, and the number of minimum points in a neighborhood to be considered as a valid neighborhood (or flash in this case). The ϵ parameter is normalized to the maximum specified distance and time separation such that larger values permit larger flashes, but also has a tendency to group two adjacent flashes together. Alternatively, an epsilon value that is too small may break up a large flash into multiple smaller flashes. This typically results in less accurate flash rates for highly electrically active storms. However, this effect is observed with other flash clustering algorithms as well (Bruning 2013). Typical threshold values that are used are a distance maximum of 3 km and a time maximum of 0.15 seconds (MacGorman et al. 2008). This study uses those same values for the Colorado and Oklahoma networks. McCaul et al. (2009) found that increasing the maximum distance threshold to 6 km resulted in fewer flashes being broken up due to the decreased sensitivity of the Alabama network. This study uses this maximum distance value for both the Alabama and DC networks because of the similar detection efficiencies of both networks. The commonly accepted value of a 10 point minimum per identified flash is used in Colorado and Oklahoma but a 2 point minimum must be used in Alabama and DC (McCaul et al. 2009). Due to the decreased sensitivity of those networks, many smaller flashes have fewer than 10 detectible sources which would result in artificially low flash rates, particularly in high flash rate storms which have appreciable amounts of small flashes (Bruning and MacGorman 2013). The flash counting algorithm is tuned such that approximate flash counts can be achieved for these types of storms because weaker storms tend to have larger

flashes that are easily captured regardless of clustering settings. This shows evidence that the algorithm is producing reasonable flash rates. Flash counts in Oklahoma and Colorado are also within 10% of XLMA values with criteria.

2.6. ENVIRONMENTAL HOURLY ISOBARIC ANALYSIS

This study used hourly analysis from both the Rapid Update Cycle (RUC; Benjamin et al. 2004) until May 1, 2012 and Rapid Refresh (RAP; Benjamin et al. 2006) model afterwards. All model data were characterized by 13 km horizontal resolution and 37 vertical levels of varying resolution based on mandatory pressure levels. These hourly model data included a number of 2D variables such as convective available potential energy (CAPE) and storm-relative helicity (SRH) along with 3D variables such as temperature and geopotential height. With the given variables from the model, other variables such as vertical wind shear and CBH (Bradbury 2000) were calculated following Lang and Rutledge (2011).

In an effort to obtain the most representative measure of storm inflow, the environmental variables were first interpolated to the radar scan time in an effort to capture any temporal evolution of the environment. The closest environmental grid point to a particular storm was then identified and the interpolated storm motion vector was calculated. Using the storm motion vector, the forecast position of the storm was calculated and the nearest grid point from that position was determined. Once the forecast grid point was determined, an average of low-level wind vectors was taken to determine the most appropriate upwind grid point, similar to Thompson et al. (2003). This grid point was usually around 40 km from the storm's forecast position. This grid point was taken as the upwind sounding location and the environmental variables at this point were associated with the appropriate radar feature. By virtue of avoiding the nearest grid point from the forecast position, the inflow sounding is located near the so-called Goldilocks Zone (Potvin et al. 2010) that is

not too close to the storm so as to be influenced by convection, but not so far away that it is not representative of the storm environment.

2.7. AEROSOLS

The inclusion of aerosol observations is a new addition to the CLEAR framework. Satellite and ground-based aerosol optical depth (AOD) data were used in this study. The satellite data were provided by the Moderate Resolution Imaging Spectrometer (MODIS) instrument aboard both the Aqua and Terra satellites (e. g. King et al. 1999; Remer et al. 2008). Along with the satellite data, Aerosol Robotic Network (AERONET; Holben et al. 1998) fixed ground observations are also used. While the ground stations do not give spatially or vertically varying data, they do output relatively frequent observations (approximately 10 per day). Use of AERONET data complemented the MODIS data. MODIS observations give potentially important spatially varying data but may be limited by the cloud mask (e. g. King et al. 2003; Ackerman et al. 2010). While AERONET observations are subject to the same limitation, fixed stations are capable of more frequent observations whenever possible.

Since most aerosol observations were not concurrent with radar observations of storms, special considerations had to be made when temporally matching aerosol observations to radar features. MODIS observations are infrequent (1-3 per day over a particular region) so it was optimal to take the nearest observation in time. The nearest pass in time over a region was found and an inflow region was determined for each storm present in a radar volume. This inflow region consisted of a semicircle of 100 km radius whose orientation was calculated by an average upwind vector from the surface to 500 mb. This inflow region was inspected for number of footprints that were valid. If the number of valid footprints was greater than a set threshold of 5, then that swath was used and an average inflow region AOD was taken as the representative MODIS AOD for the cell. If

the number of valid footprints did not meet the threshold then the next temporally valid swath was investigated and this process was repeated until the prescribed criteria were met. Once the criteria were met, the time difference between the aerosol and radar observations along with the number of valid points were saved for later filtering.

A temporal interpolation between the nearest AERONET observations before and after the radar observation time was used to give the representative AOD at 500 nm for all cells in the region for that particular radar scan time. Both AERONET and MODIS observations can be used in tandem to investigate aerosol effects on storms but the majority of MODIS observations were deemed unrepresentative due to large gaps between MODIS and radar observation times. The AERONET stations used in this study were: UA-Huntsville (AL), UMBC (DC), NEON CVALLA (CO) and Cart Site (OK). Any storms deemed to have unrepresentative aerosol observations were flagged and sensitivity studies on their inclusion were performed.

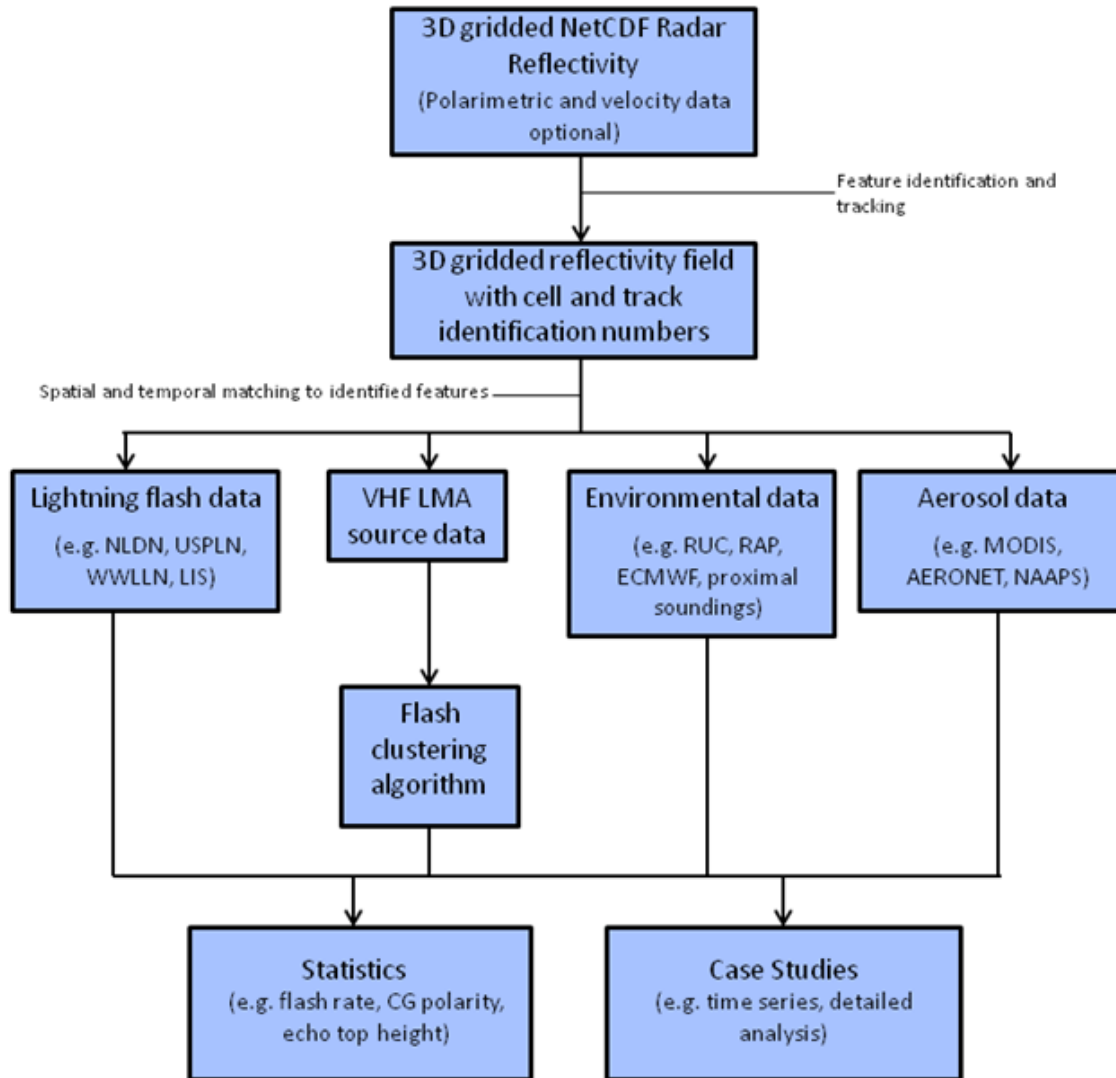


FIG. 2.1. Flow chart depiction of CLEAR framework. Parallel arrows indicate that not every module is required to produce statistics or case studies. Cell tracking is a required step to attribute data to cells.

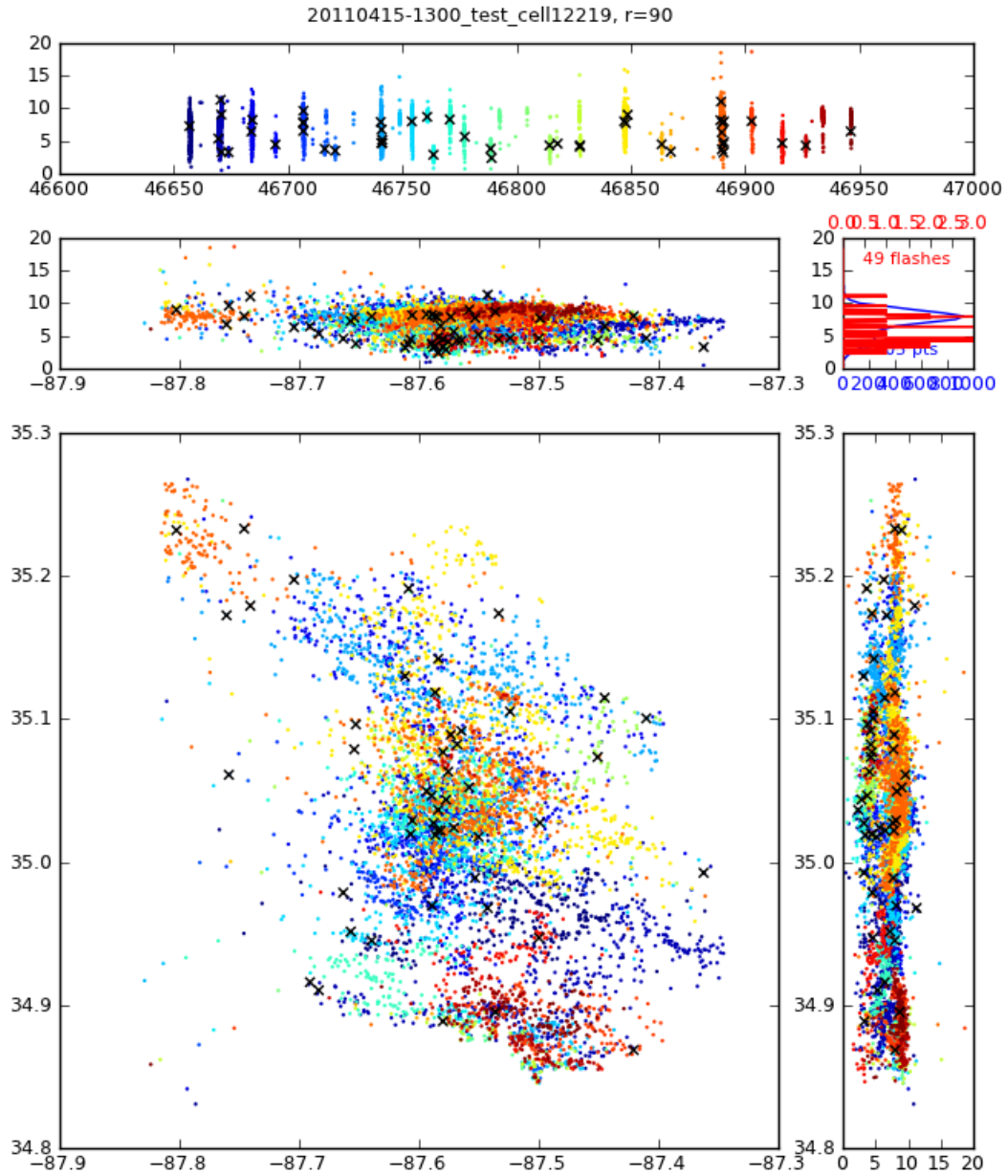


FIG. 2.2. Example of XLMA style plot used to subjectively analyze performance of flash clustering algorithm. The top panel shows the time-height source plot with points colored by time (throughout the whole figure) and identified flashes denoted by a black 'x'.



FIG. 2.3. Image of an LMA station. Each LMA network is comprised of multiple stations. VHF radiation produced by lightning channel propagation is detected by multiple stations that relayed via cell phone modems to a central processing facility.

CHAPTER 3

RESULTS

3.1. OVERVIEW

The total number of convective cells observed ranged from approximately 4500 in the Colorado domain to 16000 in the Alabama domain during the 3 months of study. Due to the strict isolated classification scheme, the number of cell observations included in each region of the study was less than 1500 for each region as less than 20% of all cells in each region were classified as isolated. The number of cells included in this study is about 10% of the total number of cells analyzed in Lang and Rutledge (2011) due to the isolated classification scheme and the larger requisite cell size. This sample size would obviously increase with the inclusion of another year of data.

The following sections will detail how isolated convective storms differ in the 4 regions of study. First the electrical characteristics such as total flash rate, IC:CG ratio and +CG flash rates in each region will be detailed. Then radar characteristics such as echo top heights and reflectivity volumes will be explored for each region. The environments of each region will be examined using variables such as CAPE, deep-layer shear and CBH. The electrical and radar characteristics will be put in the context of the environments in which they exist in an attempt to shed light on the factors that control the electrical characteristics of isolated convection in each region. Finally, all storms included in the study will be investigated simultaneously to identify any systematic behaviors that elucidate differences in electrical activity observed in the study. The bifurcation of cells in this study is different than the Lang and Rutledge (2011) classification scheme which is based on the dominant polarity of CG flashes in a storm and is similar to other studies (e.g. Carey and Buffalo 2007). This classification scheme is appropriate for those studies because those regions produce intense storms with high characteristic +CG rates, justifying that classification scheme. As detailed

below, storms in Alabama and DC never produce large +CG rates observed in previous studies, therefore a similar classification and direct comparisons of positive storms between regions would be misleading.

The majority of the analysis presented in forthcoming sections attempts to exclude outliers by using medians such that the storms in the tails of the distribution are ignored. This is in an attempt to characterize representative storms to get an overall sense of thunderstorm behaviors in each region. Some outliers will be investigated by their superlative electrical characteristics in a case study format.

3.2. ALABAMA

3.2.1. OVERVIEW

The number of identified cell observations in the region totaled over 16000 during the entire period of study. A majority of these observations were associated with organized convection. As a result, only about 1300 cell observations were included for detailed analysis. Overall, 81% of all remaining cell observations were electrically active, meaning they produced at least one flash within the observing period. Cells that produced at least one CG flash were 55% of the total. Consequently, 26% of cells produced only IC flashes during an observation period. Of all the CG flashes within the study, only 10% of them were positive polarity. The Alabama region is characterized by two different types of climate regimes. During the month of April, the majority of storms are produced by synoptic events. This is typically when severe weather occurs and provides the majority of storms with superlative electrification in this region. May and June are usually characterized by tropical or maritime airmass thunderstorms with little synoptic forcing and weak shear (Williams et al. 1999). These storms are much more frequent but are not as strong and are not as electrically active as the synoptically forced storms. The year of 2011 was particularly

violent as multiple large tornado outbreaks occurred, including April 27 which was one of the largest tornado outbreaks in recorded history. However, the majority of analysis presented here will not include storms from these types of events because of the exclusion of outliers by median analysis.

3.2.2. LIGHTNING CHARACTERISTICS

Fig. 3.1 shows the probability distribution function (PDF) of storm total flash rates produced by the flash counting algorithm for all included storms in the Alabama region. A large majority of storms (90%) in Alabama produce flash rates fewer than 10 flashes min^{-1} . These flash rates are typical of summertime airmass thunderstorms often observed in this region (Williams et al. 1999). Note however that a very small portion of storms produce copious flash rates, as a handful of storms produce greater than 100 flashes min^{-1} . The largest flash rates observed in this region are near 300 min^{-1} , consistent with Williams et al. (1999) and Goodman et al. (2005). These storms are associated with severe weather such as hail and tornadoes.

The overwhelming majority of CG flashes in Alabama storms in this study were of negative polarity. Fig. 3.2 displays the CDF of CG rates of both polarities for all storms included in the study. Note that the vertical axis begins at 0.5 because the majority of cells in this region did not produce any CG flashes during an observation period. The disparity between CG polarity is striking, the CG flash rates are significantly larger than +CG flash rates. The maximum +CG flash rate in any storm was around 1 flash min^{-1} while nearly 10% of all cells produced CG flash rates greater than 10 flashes min^{-1} . This result is reasonable in the context of studies that have shown a very low fraction of CG flashes in this region to be positive polarity (Boccippio et al. 2001; Orville and Silver 1997).

3.2.3. STORM PARAMETERS

Next, we will investigate the dependence of total flash rates on storm parameters determined by radar and LMA data. Fig. 3.3 shows multiple plots, all of which have total flash rate on the vertical axis. Note that the magnitudes of the axes on each plot may be different. This is an artifact of binning the different variables on the horizontal axis and different flash rate dependence on these various quantities. These plots are created by binning cell observations, then calculating the median flash rates of all storms in a particular bin to provide the flash rates plotted. The color of the points is determined by the number of cell observations in each bin, and follows the colorbar on the bottom of the figure. The bars on each point signify the median absolute deviation of the flash rate distribution for each bin. The median absolute deviation is the median analog to the standard deviation. Median analyses are used in this study because we want to avoid outliers. Quantification of the behaviors presented here are located next to the label on each horizontal axis. The square of the Pearson correlation coefficient (denoted by R^2) measures the linearity of the relationship and the Spearman rank correlation coefficient (denoted by ρ) gives an indication as to whether the relationship between two variables is monotonic. Positive values near one indicate that the relationship is monotonic and positively correlated. Values near -1 indicated that the relationship is monotonic and negatively correlated. Values near zero indicate that the relationship is scattered and not monotonic. Fig. 3.3a shows the flash rate dependence on the echo top height of the 30 dBZ surface, chosen as an indication of storm intensity (Lang and Rutledge 2002). Flash rates are low and nearly constant for 30 dBZ heights less than 12 km but rapidly increase for heights above 12 km. For 30 dBZ heights near 16 km, the median flash rate is double the flash rate for any other height. Also note that the largest fractions of storms have 30 dBZ tops around 10 km as indicated by the color of those points, and the smallest fraction of storms have tops either less than 8 km

or greater than 14 km. For the highest echo top heights, the effects of radar gridding and coarse vertical resolution of 3D mosaic data cast doubt upon the magnitude of the values. Trends of values are more believable for these data. The qualitative result is similar in Fig. 3.3b for 40 dBZ echo top heights. A near constant median flash rate is observed for heights less than 10 km, then flash rates increase for storms with higher echo tops while much larger flash rates are observed for 40 dBZ echo tops above 14 km. These flash rates dwarf flash rates of other heights and the large bars indicate that the highest flash rate storms tend to possess tall echo top heights. Inspection of these panels indicates that these relationships are clearly non-linear so the linear correlation value is meaningless. However, the Spearman coefficient is very nearly 1 which means that these relationships are monotonic. The relationships between flash rates and tall echo tops heights is not a surprising one, given that the same updrafts capable of lofting large particles to great heights are also capable of producing significant charge separation (e.g. Williams 1985). Strong updrafts also loft graupel to significant altitudes in the storm and provide ingredients for non-inductive charging. This large separation of charge rapidly produces immense electric fields and high total flash rates. The total flash rates are fairly well correlated with reflectivity volumes above the freezing level, as shown in Figs. 3.3c and 3.3d. With the exception of the largest volumes, the flash rates are approximately linear with 30 dBZ volume above the freezing level. This volume can be thought of as the non-inductive charging factory and larger volumes should produce more charge separation and larger flash rates. The largest volumes are also associated with the largest spread of flash rates, indicating that large flash rate storms are located in those volume bins. Note that the largest fractions of storms in this region have the smallest volumes, which is expected of weak airmass thunderstorms. Moving to lightning statistics, Fig. 3.3e shows the relationship between total flash rate and the maximum flash altitude computed by the flash clustering algorithm. A slow increase

in flash rate is observed for an increase in maximum flash altitude. Then finally a much larger flash rate is observed for storms with very high flash altitudes. This comes as no surprise because storms with high altitude flashes should be those supported by strong updrafts that are capable of producing large flash rates. Note that the largest percentage of storms have maximum flash altitudes around 8-10 km, while the highest flash altitudes are rare, consistent with the overall electrical behavior of storms in this region. The last data point makes it difficult to conclude the functional form of this relationship but it is safe to say that the relationship is monotonic, given the large rho value. The total CG rates from the NLDN data are displayed in Fig. 3.3f. The relationship between total CG rate and total flash rate is approximately linear, suggesting that the IC:CG ratio is similar in a large majority of storms in this region.

Fig. 3.3g shows similar information as the previous panel but in a more instructive manner. The relationship between total percentage of IC flashes are strongly related to total flash rate, especially as IC fractions approach 100%. The flash rate increase is very high as IC percentage becomes greater than 80%. Note that this plot only includes storms producing flashes as IC percentage has little meaning for a storm with no flashes. Perhaps the most interesting information is in Fig. 3.3h, which shows the temperature of the LMA mode height (a proxy for strongest positive charge location) relationship with total flash rate. This illustrates that the total flash rates are lowest for the warmest positive charge regions while the largest flash rates are associated with very cold (high) positive charge regions. We can infer from this that storms with very high and cold positive charge regions are caused by strong updrafts lofting positively charged ice crystals to great heights causing large amounts of charge separation. With the positive charge located at or near the top of the storm, these storms are likely strong versions of normal polarity tripole charge structures described in Williams et al. (1989). It is possible that some of these storms have elevated dipole

charge structures, but it is very difficult to know based strictly on LMA source data since charge regions can only be inferred from these data. Note that these storms are relatively rare but do have a large spread indicating that higher flash rates exist in storms with these positive charge temperatures.

While total flash rate is commonly used as a metric for electrical activity or storm intensity, additional information may be provided by investigating the IC:CG ratio, or CG fraction. Studies such as Seimon (1993), MacGorman et al. (2008) and Williams et al. (1989) have shown that intense storms with high flash rates have a propensity to produce IC flashes over CG flashes. They have also found that storms undergoing intensification can be associated with a rapid increase in IC flashes and total flashes, sometimes called a lightning jump (Gatlin and Goodman 2010). CG fraction is linked to IC:CG ratio but is used in this study to avoid infinite ratios in storms with no CG flashes during a period of observation. Fig. 3.4 shows LMA total flash rate and CG fraction on a log-log plot. The plot shows a general trend for storms that produce high flash rates to be associated with low CG fractions. In other words, storms that produce large flash rates are favoring production of IC flashes to CG flashes. Note the modest linear correlation coefficient value as this is not a very strong correlation. This correlation is better in the weaker storms with lower flash rates, as the stronger storms with larger flash rates have similar CG fractions. The modest correlation value indicates that simple CG flash rate analysis may not give the whole story of a storm's electrical activity. It appears that storms in this region are not capable of producing CG fractions less than 1%, or an IC:CG ratio of approximately 100. The average IC:CG ratio of all storms in this region is near 3, a low number consistent with Boccippio et al. (2001).

3.2.4. STORM ENVIRONMENT

The environment in which a storm forms affects the thermodynamics, microphysics and dynamics of a particular storm. These factors influence the electrical characteristics so it follows that a storm's environment should also have impacts on its electrical activity. We now investigate Alabama's environment and its relationships with storm intensity. Fig. 3.5 shows the relationship between storm total flash rate and common environmental variables. Fig. 3.5a shows the relationship between flash rate and environmental CAPE, a general increase in flash rates is observed with increasing CAPE. Parcel theory states that larger values of CAPE promote stronger updrafts, which in turn should produce larger flash rates. The largest median flash rates are associated with large CAPE values near 4000 J kg^{-1} . This is also the location of the largest spread, indicating that higher flash rate storms are present in those bins. A larger sample size is desired to increase the robustness of this result. Note that a large fraction of storms are in a region of zero CAPE, which was found to be most common in nocturnal convection. In agreement with other studies, warm cloud depth (WCD) is negatively correlated with total flash rate in Alabama. A shallower WCD is associated with a shorter parcel residence time in the warm rain zone of the storm. The flash rate dependence on AOD in this region is dubious. Although the largest flash rates are associated with higher AODs, the lack of cell observations with large AODs is not to be trusted until more observations are obtained. A goal of future work is to incorporate a different aerosol dataset, such as IMPROVE, in an effort to provide more consistent observations which will be more representative of storm environments. No obvious relationships are observed between total flash rate and environmental shear, although the highest flash rates are associated with the smallest 0-3 km shear values in Fig. 3.5e. The relationship between total flash rate and CBH (represented here by LCL, calculated following Bradbury 2000) is approximately linear and monotonic. Higher cloud

bases tend to be associated with larger flash rates. This is somewhat tied to WCD because higher cloud bases will lead to shallower WCD values, assuming a nearly constant freezing height. The generally increasing flash rate with increasing surface dry bulb temperature is expected because a warmer surface will increase instability and also increase LCL heights, both factors thought to increase flash rates. This result is in line with Williams et al. (2005), where an increase in flash rate was observed for increasing surface dry bulb temperature in the tropics.

3.2.5. SEVERE WEATHER

A discussion of lightning activity would not be complete without an investigation into lightning in severe storms. Using the new ability of the CLEAR cell tracking algorithm to attribute SPC severe weather reports to cells based on space and time criteria, a comparison of isolated severe weather producing cells to all other cells is possible. Table 3.2 shows various median comparisons of storm parameters and environmental parameters between severe and non-severe storms in the Alabama region accompanied by the p-value from the Wilcoxon rank-sum significance test (Wilcoxon and Wilcox 1964; Wilks 2006). Given the severe nature of the 2011 season, the 2% occurrence of severe weather is surprisingly low. Although severe weather in Alabama is usually associated with synoptic events and strong forcing, many of the severe storms were classified as organized by the strict classification employed here and were not included in this study. A possible future study would be to include all storms regardless of isolation to get a more comprehensive study of severe weather behavior. Even with the small sample size the p-values in Table 3.2 show that all parameters are significantly different with the exception of LCL height, freezing height and warm cloud depth. Severe storms are clearly much stronger electrically as determined by total flash rate, CG flash rate and maximum flash altitude. They are also stronger storms from a radar

structure perspective. All radar areas, heights and volumes are much larger in severe storms than non-severe storms.

3.2.6. SUMMARY

The environment in Alabama is characterized by a tropical-like regime in the summer (Rutledge et al. 1992) with a much more synoptic influence during a large portion of April, when severe weather occurs there. In accordance with the generally weak forcing, a large majority of isolated convective storms in Alabama produce a paucity of flashes. The reason for this is not entirely clear but seems to be linked the low LCL heights and thick WCDs present in this region. However, severe storms in Alabama are very large and electrically active consistent with the large and strong updrafts that must be present in those storms. These results presented here will be put in context of all regions of study after each region has been examined. A larger picture shows some interesting results that have implications for storms in all regions.

3.3. WASHINGTON, D.C. (DC)

3.3.1. OVERVIEW

During the period of study, over 14000 total cells were identified in the DC region. Nearly 1500 of these cells were classified as isolated and thus were included in this study. Roughly half of these cells produced at least one CG flash during the period of observation and 65% produced at least one flash of any kind. Therefore 16% of all cells produced IC flashes exclusively. The DC region produced the lowest +CG rates of any region as only 8% of all CGs were positive polarity. Due to the lack of inverted storms and +CG flash production in this region, which will be documented in the following sections, no attempt was made to classify storms in this region by dominant CG polarity. Rather, all storms in this region were treated together, regardless of dominant CG polarity.

3.3.2. LIGHTNING CHARACTERISTICS

Fig. 3.6 shows that nearly 90% of all cells included in this study produce total flash rates less than $10 \text{ flashes min}^{-1}$. This is typical of coastal and maritime regions where storms are common but are not electrically active (Williams et al. 1999; Orville and Spencer 1979). This region is characterized by the lowest overall flash rates of any region. Note that storms can produce superlative flash rates on rare occasions. A very small number of cells are able to produce greater than $50 \text{ flashes min}^{-1}$; some produce greater than $150 \text{ flashes min}^{-1}$. Similar to the Alabama region, storms with superlative flash rates in this region are associated with severe weather.

Production of +CG flashes is nearly non-existent in this region. Fig. 3.7 shows the CDF of CG flash rates of both polarities. The largest +CG flash rate of any storm in the DC region is less than 1 flash min^{-1} . These low +CG flash rates provide some evidence for the lack of inverted storms in this region as inverted storms typically produce anomalously high +CG flash rates due to the presence of mid-level positive charge. Negative CG flash rates behave differently however, as an appreciable number of cells are capable of producing large frequencies of CGs. The fraction of storms that produce greater than $10 \text{ CG flashes min}^{-1}$ (similar to Alabama), nearly 5% of all cells.

3.3.3. STORM PARAMETERS

Next we will describe relationships between storm parameters and total flash rates in the DC region. Fig. 3.8 shows multiple panels and multiple variables on the horizontal axis with total flash rate on each vertical axis. A power-law relationship is observed between total flash rates and the echo top heights of the 30 and 40 dBZ isopleths. This is shown more explicitly in the synthesis section. Similar to the Alabama region, this may have implications for estimating flash rates in models or remote regions where lightning data is not readily available. Note that the largest values of echo top heights are associated with the largest spread in flash rates, as to be expected. The

correlation coefficient values for these panels are moderately high, but since we do not observe a linear relationship between these variables, the R^2 value is essentially meaningless. The Spearman rank coefficient is nearly 1 for both relationships, indicating monotonic relationships between flash rates and echo top heights. Figs. 3.8c and 3.8d show the relationship between echo volumes above the freezing level and storm total flash rates. As expected, these quantities are correlated. Larger reflectivities, particularly ≥ 30 dBZ, signify the presence of rimed ice particles and an approximate non-inductive charging factory for charge separation to take place. More charge separation leads to more lightning. Note that the correlation coefficient for the 30 dBZ volume is modest but visual inspection reveals that it is skewed lower because of the anomalously high flash rate for the largest 30 dBZ volume. This is reflected in the much higher value of rho for these relationships. The spread for that largest value is also the largest of any on the panel. The 40 dBZ correlation coefficient is much higher. The maximum flash altitude displays a similar behavior to the echo top heights. A similar power-law behavior is observed as flash rates rapidly increase for flash heights above 12 km, a very similar behavior to the Alabama region. The highest flash altitudes are also associated with the largest spread as a relatively small portion of storms produce flashes above 12 km. Figs. 3.8f and 3.8g show similar phenomena, but from different perspectives. Fig. 3.8f shows the relationship between the total CG rate from the NLDN data and the total flash rate produced by the flash clustering algorithm. The behavior is nearly linear with a high correlation coefficient, suggesting that the IC:CG ratio in most storms is approximately constant, especially those with smaller flash rates. The slope of the best-fit line (not shown) is close to 4, meaning that total flash rates are 4 times larger than CG flash rates. Noting that IC flash rate is simply the difference between total and CG flash rates, the IC:CG ratio is approximately 3:1 for all storms in the DC region. This number is nearly identical to the value from the Boccippio et al. (2001)

study. Fig. 3.8g shows the total flash rate as a function of IC percentage, analogous to IC:CG ratio for storms that produce flashes. The result is a rapid rise in flash rates for higher IC percentages, similar to the Alabama region. Note that an appreciable number of storms have IC percentages less than 50%, indicating that the storm produces more CG flashes than IC flashes, a result similar to Alabama but differing from Oklahoma and Colorado, detailed in the following sections. The last panel illustrates the flash rate as a function of approximate location (and temperature) of the strongest positive charge. Low, and thus, warm positive charge regions are not conducive to flash rates. Flash rates begin to increase as the positive charge regions are located at or near -40°C . This is indicative of normal polarity storms with strong updrafts lofting positively charged ice crystals to great heights (cold temperatures). The largest flash rates are observed for mode temperatures colder than -50°C . These are likely the product of superlative updrafts usually found in severe storms. However, this is only speculation due to the lack of velocity data. The highest population of LMA mode temperatures is near -40°C , near the top of the mixed phase region and typical of ordinary strength normal polarity storms. This panel also provides strong evidence for the lack of inverted storms in this region. Inverted storms are typically strong and produce appreciable total flash rates with strong positive charge at temperatures near -20°C . This panel shows no increase in flash rates for storms possessing warmer positive charge.

The general behavior of IC vs. CG flash production is consistent with the Alabama region in that storms that produce larger flash rates tend to favor production of IC flashes over CG flashes. This is shown in Fig. 3.9. The correlation between CG fraction and total flash rate in this region is better than in Alabama. Like Alabama, the largest flash rates are not associated with the lowest CG fraction. The approximate IC:CG ratio for these high flash rate storms is 25:1, a number more typical of a continental region.

3.3.4. STORM ENVIRONMENT

The environment in this region is characteristic of maritime regimes with occasional continental influences. We will now examine the details of this environment and the reasons that strong storms do not exist in our sample. Fig. 3.10 shows multiple plot panels, each with different variables plotted on the horizontal axis. Fig. 3.10a shows the environmental CAPE and total flash rate. Higher CAPE does lead generally lead to higher flash rates but the correlation is modest. Anomalous CAPE values are indeed associated with anomalously high flash rates, like those in severe storms. Thicker WCD values in Fig. 3.10b are associated with larger flash rates in this region, in direct contrast with the Alabama region, where shallower WCDs produced higher flash rates. The reasons for this are not currently known. These values are fairly well correlated as well, although the large spreads in the majority of the WCD values cast some doubt on the quality of the correlation. Note that only a small fraction of cells have WCD values less than 2 km, similar to the Alabama region and tropical regimes (Williams 1989; Williams et al. 2005). The total flash rate relationship with AOD values is non-existent with this dataset. The correlation coefficient is essentially zero, that is, no trends are observed. We are again skeptical of the validity of the AERONET AOD dataset and look to augment it with other types of data not subject to the same limitations. Inspecting instability from a different perspective shows a well-behaved relationship between total flash rate and equivalent potential temperature (θ_e). The largest values of θ_e are associated with the highest flash rates, albeit with considerable spread. The correlation coefficient is also sufficiently high for both linear and monotonic relationships. No significant trend is observed in the 3 km shear data, especially considering the large flash rate spread in the majority of values. Mixed phase shear, as defined earlier, does show a trend with good correlation, with the highest flash rates being associated with the lowest shear values. Large spreads exist in storms with

small shear values indicating most of the higher flash rate storms have small mixed-phase shear. Large values of shear in this region of the cloud would likely destroy the updrafts likely present in the analyzed median storms. A modest correlation is found between LCL heights and total flash rates. Higher LCLs are associated with larger flash rates. Caution should be taken though, as the flash rate variations are fairly large. Perhaps not unrelated, total flash rates are correlated with surface dry bulb temperatures. Higher surface temperatures will result in higher LCLs if surface dew points are relatively low. If they are high, then larger values of instability will be produced. Either of these scenarios will tend to increase electrical activity in storms. This raises an interesting question: which is more important to produce high flash rates, LCL or instability? The following sections will shed some light on this question.

3.3.5. SEVERE WEATHER

Even though severe weather is relatively uncommon in the DC region, a discussion of lightning activity in relation to cases of severe weather is now described. Table 3.3 shows the comparisons of various storm parameter medians and environmental parameters between severe and non-severe storms in the DC region accompanied by the p-value from the Wilcoxon rank-sum significance test. Severe storm observations accounted for 2% of the total in DC during 2011, this number is presumably higher than other years given the unusually high severe weather activity of 2011. Although severe weather in DC is usually associated with synoptic events and strong forcing, many of the severe storms were classified as organized by the classification scheme and were not included in this study. Even with the small sample size of severe storms, the p-values in table 3.3 show that a large majority of parameters are significantly different between severe and non-severe storms. Similar to the Alabama region, LCL heights and WCD values are not significantly different. Surprisingly, some common environmental values associated with severe weather such

as CAPE and 6 km shear are not significantly different in this region. Even though the statistics suggest that severe storms are not feeding from environments conducive to severe weather, they are clearly much stronger electrically as determined by total flash rate, CG flash rate and maximum flash altitude. They are also stronger storms from a radar structure perspective as all radar areas, heights and volumes are all much larger in severe storms than non-severe storms. Note the similar qualitative results with Rudlosky and Fuelberg (2013).

3.3.6. SUMMARY

During the period of study, the environment in the DC region was very similar to that of the Alabama region. This is to be expected because of the geographic characteristics of these regions. These regions are maritime in nature, an environment that produces a large number of storms but rarely produces electrically active storms. Large CAPE and WCD values are relatively common here, while high LCL heights are not. Storms that occur here must have significant warm rain processes, which are related to the lack of lightning activity relative to other regions in this study by virtue of the small supercooled liquid water contents that are likely present in the mixed-phase regions of storms in this region.

3.4. OKLAHOMA

3.4.1. OVERVIEW

During the period of study, a total of nearly 9000 cells were identified by the cell tracking software in the Oklahoma region. Of those cells, 700 were classified as isolated and were included in the study. The number of cells included in this study is significantly lower than the previous regions by roughly a factor of two. The cells in this region are much more electrically active than the DC and Alabama storms. A large fraction, 85%, of all cells produced lightning in this

region, which is much higher than the previously examined regions. Fifty-eight percent of all cells produced at least one CG flash, so 31% of all cells produced exclusively IC flashes during the observation period. Production rate of +CG flashes is also much higher than the previous regions as 31% of all CG flashes in storms in the present study were positive polarity, in line with previous studies (Curran and Rust 1992; Smith et al. 2000). The Oklahoma region has a unique and transient weather regime. Because of its location relative to the Gulf of Mexico, very moist conditions are common, particularly in the eastern part of the region. Since Oklahoma is sufficiently far from the Gulf of Mexico, observed temperatures are often very high with triple digits being common. The western portions of the region are in reasonable proximity to the High Plains and the high elevations of the Intermountain West. These regions are characterized by hot and dry conditions. It is the proximity of distinct airmasses that gives rise to the drylines that are often observed in this region. Drylines serve as initiation points for storms, many of which become severe. For these reasons, we will investigate some of the storms in this region in more depth later in this section.

3.4.2. LIGHTNING CHARACTERISTICS

Fig. 3.11 shows the PDF of storm total flash rates in Oklahoma. Immediately apparent is the smaller portion of storms producing flash rates < 10 flashes min^{-1} . These storms constitute about 65% of all storms in the region, much lower than the 90% observed in Alabama and DC. The drop-off in frequency is not as rapid as previous regions. Note the scale of the horizontal axis: storms are capable of producing total flash rates approaching 500 flashes min^{-1} which is on par with the most electrified storms on Earth (Zipser et al. 2006). An appreciable amount of storms also produce more than 100 flashes min^{-1} which was exceptionally rare in the previously analyzed regions.

Similar to the increased total flash rate production, higher CG production rates are observed in this region. A large difference is observed in the +CG flash rates compared to the previous regions, a result similar to Zajac and Rutledge (2001). The highest +CG flash rates are more than 3 min^{-1} and nearly 40% of all cells produce +CG flashes. Carey and Buffalo (2007) and Wiens et al. (2005) postulate that this increased +CG production is caused by strong storms that can supply large liquid water contents to the mixed phase region, thereby reversing the polarity of charge gained by graupel and producing an inverted charge structure. These claims will be investigated in the following figures. Negative CG rates in this region are also high. While a similar number of storms produce CG flashes (50%), storms producing superlative CG flash rates are more common in this region. Nearly 10% of all cells produce CG flash rates greater than 10 min^{-1} .

3.4.3. STORM PARAMETERS

A more thorough examination of the storm parameters and their relationships with flash rates may identify the characteristics that are tied to flash production. Fig. 3.13 shows the storm variables and their relations to total flash rates similar to previous sections. Nearly identical relationships exist between echo top heights and flash rates in this region compared to the other regions. Figs. 3.13a and 3.13b show power-law increases in flash rates with increasing echo top heights. The key difference between Oklahoma and the previous regions is flash rates are much higher for a given echo top height in Oklahoma. Like other regions, the lack of linearity in these relationships demands that we discard the linear correlation coefficient but the monotonic coefficient is nearly 1. The reflectivity volumes above the freezing level correlate well with the observed flash rates in Oklahoma. Larger charging zones should produce greater charge separation and larger electric fields leading to more lightning. Note that volumes in this region are significantly larger in comparison to Alabama and DC storms. An appreciable amount of storms have 30 dBZ volumes larger

than 1000 km^3 whereas that is the exception in the previous regions. The relationships observed in other regions between a storm's maximum flash altitude and total flash rate hold here as well. Again the difference in this region is the much larger flash rates for a given maximum flash height, likely the manifestation of higher CAPE values and stronger updrafts. These grand flash heights must be caused by lofted particles making it to extreme heights and the associated charge separation taking place in these storms. Fig. 3.13f, showing the NLDN total CG rate and total LMA flash rate has remarkable correlation, suggesting an approximately constant IC:CG ratio for most storms in this region. With a slope of approximately 10, total flash rates are 10 times larger than CG rates for a majority of storms. This yields an IC:CG ratio of 9, which is higher than values from Boccippio et al. (2001). That study found a longitudinal gradient with a ratio near 3 for the eastern edge of the region, increasing to around 5 for the western edge of the region. This gradient is likely due in part to the varying moisture determined by the geographic location of the region discussed previously. The discrepancy in IC:CG ratio should receive further investigation but may be attributable to an increase of spatially small flashes as total flash rates increase (Bruning and MacGorman 2013). The small flashes produced by electrically active storms may be missed by the optical sensors described in Boccippio et al. (2001) producing artificially low flash rates and IC:CG ratios. Similar behaviors in IC percentage are observed in 3.13g where rapid increases in flash rates accompany increases in IC percentages. This lends credence to the previous claim that higher flash rate storms produce more IC flashes. Note that the lowest IC percentages observed in Oklahoma storms are 50%, while an appreciable amount of storms in the previously examined regions produced significantly fewer IC flashes. The LMA mode temperature relationship to flash rates exhibits similar characteristics to previous regions with warmer positive charge producing low total flash rates and cold positive charge (near $-40 \text{ }^\circ\text{C}$) producing higher flash rates. Some

peculiar behaviors appear though. First, the coldest positive charge is $-50\text{ }^{\circ}\text{C}$, which is not nearly as cold as the stronger storms in Alabama and DC. The coldest positive charge regions observed in those regions are near $-60\text{ }^{\circ}\text{C}$, and those storms produce the highest flash rates in their respective regions. For some unidentified reason, total flash rate decreases for storms with positive charge regions colder than $-40\text{ }^{\circ}\text{C}$. Another important distinction in the Oklahoma region is the slight increase in flash rates for positive charges near $-15\text{ }^{\circ}\text{C}$. This is consistent with an inverted charge structure with positive charge at mid-levels which is usually near 8 km MSL or $-15\text{ }^{\circ}\text{C}$. The inverted flash rate signature in Oklahoma is not as strong as in the Colorado region, which will be shown in the next section.

The behavior of CG fraction with total flash rate in Oklahoma storms is generally similar to the previous regions, as shown in Fig. 3.14. Storms with larger flash rates also have a tendency to produce larger fractions of IC flashes, which manifests as a lower CG fraction. The best fit line shows a nearly inverse relationship between CG fraction and total flash rate as the slope of the best fit line is -0.98 . It is important to note that the highest flash rate storms stray away from the best-fit line, similar to other regions. These superlative flash rate storms are not associated with the lowest CG fractions throughout the region. The maximum flash rate storms are those with CG fractions between 10^{-2} and 10^{-1} , a result observed in the previous regions as well. Note the modest correlation coefficient value. The whole story of electrical activity may not be explained with simple CG flash rates.

3.4.4. STORM ENVIRONMENT

In investigating the environment of the Oklahoma region, the transient nature of the region manifests as convoluted relationships with many of the environmental variables. This is also due in part to the framework of this study. Drylines are present here more than any other region of the

country. As storms form near the dryline, sharp gradients in moisture and other variables dependent on moisture are present. Storms near these sharp gradients are assigned inflow soundings and the associated various environmental parameters described in section 2. Storms moving across these sharp gradients may result in misleading environmental parameters. This framework is setup to treat each cell observation as its own cell which in theory, takes care of this problem. As a storm evolves and moves into different environments, it will be treated as a completely different cell. This may not be sufficient however, as storm characteristics may not respond on such a short observation time scale, which is 5 minutes in this study. The ability of the environmental data to represent the real environment is also crucial for this methodology to accurately prescribe environmental data as an inflow sounding. Also, since the environmental data are produced hourly, temporal interpolations to each 5 minute observation had to be carried out. The fine-scale temporal variations such as dryline movement may not be captured in this analysis. All of these potential inaccuracies may lead to a simple case study approach.

Nonetheless, Fig. 3.15 shows the environmental parameters and their relationships to total flash rates in the Oklahoma region. Immediately apparent is the lack of any relationship for many variables with total flash rates. CAPE and WCD show no systematic relationship with minute correlation coefficient values. This result is somewhat unexpected but may be attributable to the limitations of this framework discussed previously. Similar to other regions, the AERONET AOD data show no systematic relationship with flash rate. This is due in part to the highly variable AOD values around drylines and a lack of representative AOD values by virtue of a single sensor for each region. A well-behaved relationship is observed between total flash rate and surface θ_e , in contrast to the lack of relationship with CAPE. This result does generally agree with Smith et al. (2000) which states that storms east of a sharp θ_e gradient are more intense and produce higher

flash rates. Note the large spread in flash rates with the larger values of θ_e indicating that high flash rate storms are more likely to occur in higher θ_e values than lower values. Decreased values of 3 km shear are associated with higher flash rates. At first, this is counterintuitive because high values of shear are thought to be linked with severe weather and associated superlative flash rates (e.g. Klemp and Wilhelmson 1978; Weisman and Klemp 1982). Recall however, that this type of analysis tends to be resistant to outliers and strong storms. The Spearman rank coefficient for the 3 km shear relationship is striking and demonstrates the monotonic nature of the relationship. Mixed phase shear has little effect on total flash rates, differing from the DC region. LCL heights are modestly correlated with flash rates. The highest LCLs in the region are associated with the highest median flash rates and the largest flash rate spreads. The large variation in LCL heights is likely caused by storms near the dryline where storms that form west of the dryline with very high LCLs while storms just east of the dryline have much lower LCLs in a very small spatial proximity. These high LCLs are thought to be associated with broad updrafts more resistant to entrainment and loss of total liquid water and supply of liquid water to the mixed phase region for enhanced electrification. It is worthy noting that the vast majority of LCL heights in this region are below 1 km, more similar to the Alabama region than the Colorado region. The modest correlation between flash rate and surface temperature is consistent with other regions and the relationship is very monotonic.

3.4.5. ANOMALOUS STORMS

Given the slight increase in flash rates for LMA mode temperatures near $-15\text{ }^{\circ}\text{C}$ and the high +CG flash rates possible in Oklahoma, this suggests the existence of inverted storms in this region. We attempt to identify the important parameters associated with these inverted storms by investigating the relationships between storm parameters and positive charge temperature. Fig. 3.16

shows the same storm parameters as previous figures but the vertical axis is now LMA mode temperature decreasing upwards such that height is increasing. Given the relationships in Fig. 3.13 we would expect storms with greater magnitudes of storm variables, such as reflectivity heights and volumes, to have greater flash rates in general. Keep in mind that since the vertical axis is inverted the Spearman rank coefficient values will be of opposite sign. The echo top heights in panels 3.16a and 3.16b show colder positive charge for the highest echo top heights. These are connected by strong updrafts argued previously. Recall from Fig. 3.13 that colder LMA mode temperatures produced storms with generally higher flash rates. The relationship between echo volumes above the freezing level can hardly be considered linear. Figs. 3.16c and 3.16d show colder positive charges as the volumes increase from very small values to a modest value of approximately 400 km³ (100 km³) for 30 dBZ (40 dBZ) with an approximately constant LMA mode temperature for any larger storms. This indicates the region's largest storms tend to possess positive charge at similar temperatures to those of more modest size. Tropopause heights in this region are typically near -60 °C, which would suggest that positive charge could be lofted to these temperatures similar to Alabama and DC, but this is not the case. Further investigation is needed to shed light on this mystery. The relationship between maximum flash altitude and LMA mode temperature is very well-behaved. The relationship is not linear but is very monotonic. Increasing flash altitudes are associated with colder positive charge temperatures until reaching an asymptote value of -35 °C around 10 km MSL. A modest dependence of LMA mode temperature is observed on NLDN CG rate. This is not a surprising result because CG flashes are more of a by-product of the cloud charging, and the larger flash rate storms tend to favor IC flashes. However, the relationship is fairly monotonic. This effect can be observed in Fig. 3.16g which shows increasing flash rates for

increased IC percentages. No significant dependence is observed between LMA mode temperature and IC percentage.

Evidence exists that inverted storms with strong mid-level positive charge exist in this region. In this study, storms in Oklahoma are capable of producing large +CG rates and a modest increase in flash rates was observed for storms with positive charge regions at temperatures near $-15\text{ }^{\circ}\text{C}$. Combining this evidence with other studies (e.g. Bruning et al. 2010), it is clear that these storms exist in this region. However, Fig. 3.16 doesn't show evidence of them. Since the purpose of these figures and this analysis is to obtain bulk information and trends, rare storms will have little, if any, effect in this framework. It is clear then, that these strong inverted storms are rare in this region and we must employ a different strategy to find them.

In an attempt to objectively find these storms, a definition of an inverted storm was created within this framework. Rather than define these storms by a +CG production criterion, we defined them by their electrical activity. That means criteria involving location of positive charge and overall strength of the storm. The criteria prescribed in this study for a storm to be classified as inverted are any storms that have an LMA mode temperature between $-10\text{ }^{\circ}\text{C}$ and $-25\text{ }^{\circ}\text{C}$ and a total flash rate area density in the top 10% of all storms in the region. The reason for classifying by flash rate density rather than total flash rate is to avoid any large storms that may have been incorrectly classified. The strongest isolated cells should have high electrical activity regardless of size. Fig. 3.17 shows a scatter plot of total flash rate density and LMA mode temperature. The vertical black line represents the 90th percentile of flash density and the horizontal lines represent the temperature limits for the criteria, making it easy to inspect the number of storms classified as inverted in the Oklahoma region. The percentage of storms that satisfied the prescribed criteria in Oklahoma was 39 of the 703 total or about 5.5%, indicating that they are relatively rare by

these metrics and perhaps small enough not to produce a strong signal in the previous figures and analyses. While total flash rates in the inverted storms were significantly higher than their normal polarity counterparts, only WCD associated with inverted storms was significantly different than the normal counterparts. This methodology does not appear to produce significant results with the present number of samples and may also be limited to the same limitations described earlier, particularly in this region. Perhaps more samples will make this a useful classification system. For this study we must resort to case studies illustrating the unique nature of inverted storms in the Oklahoma region.

The case study presented here was chosen because of its location on Fig. 3.17. This storm had large flash rate densities throughout its lifecycle and was very strong in all measures. The synoptic situation is summarized on Fig. 3.18. The CAPE and dew point contours indicate that a dryline was present during this time. The storm of interest is denoted with its unique ID number of 40288 located around 100 km southeast of Norman. This storm initiated just east of the dryline around 0000Z on 21 May 2011 and quickly became strong. The storm was supported by a very unstable environment as CAPE values near 5000 J kg^{-1} were immediately south of the storm. This unstable environment was caused by very warm and moist air near the surface as temperatures were in the low 80's and dew point temperatures were above 70°F .

Taking an in-depth look at the storm, Fig. 3.19 shows a vertical cross section of the storm at 0135Z, the same time as the previous figure. The left panel displays the radar reflectivity and 2D LMA source density integrated through all latitudes of the storm. The upper right panel shows a plan view of the storm in composite reflectivity with height integrated 2D LMA source density. The X's indicate the locations of the +CG flashes that occurred within the 5 minute observation period and the open triangles denote locations of CG flashes. Investigation of the radar structure

indicates that the storm is highly vertically developed and intense with 50 dBZ echo top heights near 14 km MSL, putting it in the tail of the storm strength distribution. The approximate size of the storm is indicated underneath the radar cross section. Context is provided by the plan view of the radar reflectivity. Note that the storm appears to have some supercellular characteristics but this is very difficult to conclude without Doppler velocity data. A veering shear profile, conducive to supercells, is present during the observation period, although the magnitude of the shear is not particularly strong. The positive charge in this storm (inferred by high source rates) is located around 8 km MSL (-25 °C) and is near the maximum reflectivity core of the storm. This can also be observed in the rightmost panel, which shows a 1D vertical LMA source histogram. The small secondary maximum near -15 °C is the likely location of the negative charge caused by recoil leaders (Saba et al. 2008). Note the location of the +CG flashes, as they are all near the core of the storm and the location of the positive charge inferred from the LMA source data. The CG flashes tend to be located downshear from the core of the storm and may have bolt from the blue characteristics. The annotations near the top of the right panel give the number of NLDN CG flashes by polarity, total number of identified flashes and total number of LMA sources for the observation period. At this particular time, 9 +CG flashes, 7 CG flashes and 640 total flashes occurred during the 5 minute period of observation, which translates to a +CG flash rate of 1.8 flashes min⁻¹ and a total flash rate of 128 flashes min⁻¹. There is no doubt that this storm was highly electrically active. Given the present radar and lightning evidence, this appears to be an inverted storm. However, the temperature of the positive charge is colder than the typical mid-level definition of -10 °C to -30 °C. This could be caused by very strong updrafts continuing to carry positively charged graupel from warmer temperatures at this time. Also note the lack of LMA sources near the freezing level of the storm around the reflectivity core. This may be contributing

to the high IC:CG ratio observed at this time. While these storms do exist in the Oklahoma region, they are rare and do not show up in the bulk analysis of this study.

The problem of +CG production has been the subject of many previous studies. Some of these studies such as Lang and Rutledge (2011) and Carey and Buffalo (2007) have classified and compared storms that have produced anomalous amounts of +CGs, terming them predominantly positive CG (PPCGs) storms or positive dominated storms (PDSs) to those that produce a majority of CG flashes. The goal of these studies is to determine the environmental conditions that produce anomalous electrification and therefore produce large amounts of +CGs. These previous studies only investigate one region, though, and their results may not be applicable in all regions. For example, results in this study have shown that none of these PPCG storms exist in the Alabama or DC regions regardless of environment or storm strength. These previous studies have generally found that storms producing large amounts of +CGs exist in more unstable environments with larger shear, in other words environments more conducive to severe weather. These environments are typically associated with superlative electrification and high electrical activity. A similar study has been conducted here using the present dataset to compare storms that produce $\geq 50\%$ +CGs during an observation period, termed positive storms, to those that produce $> 50\%$ -CGs during an observation period, termed negative storms. Fig. 3.20 shows a comparison of storm variables, with the cumulative distribution of positive storms in red and negative storms in blue. Fig. 3.20a shows that although the median flash rates in negative storms are higher, the difference is not significant. Note that all storms with very high flash rates are exclusively negative in this region. The maximum flash altitudes are significantly higher in negative storms than positive storms but a difference of 0.5 km is on the order of the LMA resolution at distances near the radius criteria in this study and therefore should not be trusted. Figs. 3.20c and 3.20d show that both negative and

positive storms in this region are very similar from a radar perspective, as both the 30 dBZ echo top height and 30 dBZ total volume are not significantly different. It appears as if storms of both dominant CG polarities are capable of spanning a broad spectrum of strengths. This result is more similar to Lang and Rutledge (2011), who showed that small differences existed between storms of both polarities whereas Carey and Buffalo (2007) found larger differences and determined that positive storms were the stronger polarity storm.

An environmental investigation of dominant storm CG polarity shows a somewhat different story than the storm characteristics. Fig. 3.21 shows four relevant environmental quantities for both storm polarities. Fig. 3.21a shows CAPE to be significantly larger for positive dominated storms than for negative dominated storms, consistent with Carey and Buffalo (2007) and Lang and Rutledge (2011). WCD values are also statistically significantly smaller for positive dominated storms than for negative storms, but this very small difference in magnitude is likely within the model's ability to diagnose variables included in WCD calculation. While median LCL heights and AOD values were higher for positive dominated storms, the difference was not statistically significant. These environmental results are in agreement with previous studies that state positive dominated storms form and feed on environments more conducive to severe weather. The positive dominated storms in this study, however are not significantly stronger from an electrical (total flash rate or maximum flash height) or radar perspective. It should be noted that the previous studies mentioned only characterized lightning activity by CG flashes, and did not have total flash rates or flash statistics that are afforded by the flash clustering algorithm. One can only speculate if or how the results would differ if the previous studies had those data.

One possible factor contributing to the behavior of +CG producing storms in Oklahoma are drylines. Drylines are a common feature in the Oklahoma region, and it is of interest to investigate

any effects they may have on the formation of charge structures and dominant CG lightning polarity. Since the large-scale CLEAR approach has trouble with this region, especially when sharp environmental gradients are present, we decided to take a simple approach to study any effects of drylines on dominant CG polarity. Objective identification of drylines was carried out with a simple dewpoint gradient detection on the hourly RUC files. Drylines were detected if gradient magnitudes surpassed a prescribed threshold of 10 C per 100 km (Schultz et al. 2007; Markowski and Richardson 2010) and the dryline was found to be sufficiently linear by a polynomial fit. Any identified cells during dryline hours were accounted for and a comparison was made between these cells and all other cells. Drylines were identified on 24 of 91 days (27%) during the period of study. On those days, 130 positive and 145 negative storms were identified. Those storms make up 89% of the total identified positive storms during the period of study and 55% of the total identified negative storms in the region. Moreover, during the dryline days, 47% of all storms producing CG flashes were positive, compared to 35% of all CG producing storms during the entire period of study. The relative preference of positive storms to occur during the presence of a dryline is currently unanswered. Certainly CAPE values are high on dryline days, generally increasing farther east of the dryline. This was previously shown to have an impact on the polarity of dominant CG activity in Oklahoma. Another possible factor is dry air intrusion at mid-levels. This could modify the drop size distribution in the warm rain zone and enable the survival of smaller drops into the mixed phase region where anomalous electrification may occur (Williams et al. 2002). Differences in aerosol concentrations on either side of the dryline may also play a role in microphysical modification and lead to anomalous electrification. This simple approach cannot answer these questions but may serve as a basis for detailed future work.

3.4.6. SEVERE WEATHER

Using techniques previously described in other regions, comparisons of storms that produced severe weather are compared to those that did not. Table 3.4 shows the comparisons of various median storm parameters and environmental parameters between severe and non-severe storms in the Oklahoma region accompanied by the p-value from the Wilcoxon rank-sum significance test. Given the severe nature of the 2011 season and the propensity for severe weather in Oklahoma, it is not surprising that the highest rate of occurrence was in the Oklahoma region with 4% of all cells producing severe weather. This rate is double the Alabama and DC regions and is also higher than Colorado (to be discussed later). Severe weather in Oklahoma can be produced by synoptic events, but can also be forced by a dryline on the mesoscale, amongst other mechanisms. Storms that initiate on the dryline typically begin isolated because of the strong shear, but may merge or grow upscale to mesoscale complexes. A possible future study would be to include all storms regardless of isolation to get a more comprehensive study of severe weather behavior. Even with the small sample size, the p-values in table 3.4 show all environmental parameters are significantly different with the exception of WCD, 6 km shear and mixed-phase shear. In contrast with the previous regions, severe storm LCL heights are higher than non-severe storms. This is due in part to a storm's proximity to the dryline and the propensity of severe storms from the dryline. Severe storms are clearly much stronger electrically as determined by total flash rate, CG flash rate and maximum flash altitude. They are also stronger storms from a radar structure perspective as all radar areas, heights and volumes are all much larger in severe storms than non-severe storms.

3.4.7. SUMMARY

Oklahoma is a very distinct region in the United States. A plethora of conditions exist such as hot tropical air, hot and dry conditions associated with drylines and synoptic influences just to

name a few. Storms in this region are generally more electrically active than the Alabama and DC regions. The storm lightning and radar parameters exhibited similar relationships to previous regions such as flash rate scaling with reflectivity volumes. Due to the transient nature of this environment however, the framework had a difficult time with the storms in this region. This led to somewhat unclear results between electrical characteristics and environmental parameters. This is a limitation of the CLEAR framework and is deserving of future improvement attempts. From the previous analyses and case study, it is clear that inverted storms can exist in the Oklahoma region. However, they exist in the tails of the distribution and are a rare occurrence. It is not yet clear what environmental conditions cause storms to possess inverted charge structures and superlative flash rates. This is further investigated in the coming sections where we will examine the Colorado region in a manner similar to the Oklahoma region. We will also combine all storm observations in an attempt to put each region into perspective of the larger picture to determine the environmental controls on lightning behavior.

3.5. COLORADO

3.5.1. OVERVIEW

During the three months of study in 2012, roughly 45000 cells were observed in this region, only approximately 30% of the total cells in Alabama. Also due to availability of reliable LMA data in this region, only the months of May and June 2012 are included in this study. Due to the isolated nature of the storms in this region, 726 cells were still included in the study which was more than Oklahoma. The highest percentage of electrified cells is located in this region as 90% of all cells produced at least one flash during an observation period. While that number is highest of any region, only 53% of all cells produced a CG flash during an observation period. Therefore, nearly 40% of all cells produced exclusively IC flashes, the highest of any region. A remarkable

44% of all CG flashes were positive polarity in this region which is the highest percentage of any region by a large margin. The weather regime of this region is unique to the other regions in the study. The high surface elevation and large distance from any significant bodies of water severely limit the moisture supply to this region, making it the driest region overall. Moisture tends to be the limiting factor on most days in this region as the Rocky Mountains and ridges provide constant triggers for storms. Consistent with the claims of Williams et al. (2005), this region produced the largest flash rates of any region. The reasons for this are discussed below. Note that the easternmost regions of the Rocky Mountains are within the 125 km domain of the Colorado LMA so filtering of those storms was carried out. Storms over the High Plains are the focus of this study due to their unique characteristics.

3.5.2. LIGHTNING CHARACTERISTICS

As mentioned previously, the overall flash rates in this region were the highest of any region in the study. Roughly half of all cell observations produced fewer than 10 flashes min^{-1} as shown in Fig. 3.22, compared to nearly 70% in Oklahoma and around 90% in both Alabama and DC. A large fraction of storms also produce greater than 50 flashes min^{-1} , something unique to this particular region. An appreciable number of storms produced flash rates in excess of 100 min^{-1} and 200 min^{-1} , and not all of them were associated with severe weather.

While total flash production is greatest in Colorado, total CG rates are not. Fig. 3.23 shows the CDF of +CG and CG flashes for all storms in Colorado. Negative CG rates in this region are the lowest of any in the study, however +CG rates are 2nd highest only to Oklahoma. Interestingly, more than half of the storms in this region did not produce any CG flashes in an observing period even though the fraction of electrically active storms in this region is the highest of any region. Only about 1% of all storms in this region produce CG flash rates greater than 10 min^{-1} , the

smallest of any region. Previous studies have postulated that inverted storms are more frequent in this region because of the unique environment, but inverted storms are usually associated with anomalously high production of +CG flashes. High production of +CG flashes is not as prevalent as the Oklahoma region. We attempt to shed light on this in the coming sections.

3.5.3. STORM PARAMETERS

Relationships between total flash rates and storm parameters are mostly consistent with other regions in that they are monotonic for most parameters, as shown in Fig. 3.24. A monotonic behavior between total flash rates and 30 and 40 dBZ echo top heights is observed, similar to all other regions. The main difference here is that storms in this region produce larger flash rates for a given echo top height. Strong flash rate correlations are observed for both reflectivity volumes above the freezing level, a behavior in line with all other regions. Note that the largest volumes have considerable spread, meaning that some very large flash rates are observed in those storms. Interestingly, the volumes of a large portion of storms in this region are very similar to those in Oklahoma, yet storms in this region produce larger overall flash rates. Also, a flash rate decrease is observed for storms with moderate reflectivity volumes in both Figs. 3.24c and 3.24d. No physical explanation is offered for this behavior. A quasi-exponential relationship between maximum flash height and storm total flash rate is observed, in general agreement with the other regions. The magnitudes of these behaviors are remarkably similar between Colorado and Oklahoma. Flash rates on the order of $150 \text{ flashes min}^{-1}$ are common in storms with maximum flash heights near 14 km. The first evidence for the distinction between this region and Oklahoma is shown Fig. 3.24f. A near-linear and monotonic relationship exists between total flash rates and NLDN CG rates, suggesting an approximate representative IC:CG ratio for storms in this region. Examination of the slope of the best fit line is roughly 50, which means that storms produce 50 total flashes

per CG flash. This implies that the approximate IC:CG ratio in this region is approximately 50. This number is approximately 5 times larger than the Oklahoma region and an order of magnitude larger than either Alabama or DC. With the behaviors in total flash rates and CG rates previously discussed between Oklahoma and Colorado, the IC:CG ratio must be significantly higher to explain those behaviors. Comparison with Boccippio et al. (2001) reveals a qualitative agreement that a maximum in IC:CG ratio is centered near the Colorado region in this study. Quantitatively, a large disagreement exists between these studies. Boccippio et al. (2001) quotes an IC:CG ratio near 10, a factor of 5 lower than observed in this study. We offer a similar explanation for the disagreement that satellite measurements have difficulty measuring the smaller flashes that are more common in high flash rate storms. The Colorado LMA network is also the newest network with the best detection efficiencies. This is due to the enhanced technologies, number of stations and lowest RF noise floors of any network, making it possible to detect weaker VHF signals and more signals during electrically active times and at long distances (P. Krehbiel, personal communication). Also note that the IC:CG ratio becomes much higher with superlative flash rate storms. This is a similar behavior to other regions and will be discussed further on the next figure. The next panel shows a very similar behavior, where flash rates rapidly increase in storms as the IC fraction approaches 100%. Note the large spread in the highest IC percentage point, indicating that nearly all storms with high flash rates are those with IC percentages above 95%. Another key distinction of this region is illustrated in Fig. 3.24h which shows flash rate as a function of positive charge layer temperature. The general trend is for flash rates to increase as the positive charge shifts to colder and greater heights. However, a large spike in flash rates is observed near -20°C . This is the inverted storm signature as strong storms with positive charge in the mid-levels (near -10°C to -20°C) are capable of producing appreciable flash rates. This is presumably caused by a charge

reversal of graupel particles due to strong updrafts producing copious amounts of supercooled liquid water. The population of storms with positive charge between -10 °C and -20 °C is high with a maximum at -15 °C. These storms are clearly stronger and more common in Colorado than they are in Oklahoma, and all other regions for that matter. This raises the question as to the cause of this distinct behavior. We will investigate this further in the coming sections.

Given the results from the previous section showing that IC flashes are much more favored over CG flashes in this region, Fig. 3.25 comes as no surprise. Colorado has the best (negative) correlation between CG fraction and total flash rate. This is due to the largest flash rate storms producing much lower CG fractions than the highest flash rate storms in other respective regions. The highest flash rate storms produce CG fractions around 10^{-2} , lower than any other region. Colorado also has the lowest CG fractions of any region in the study. CG fractions lower than 10^{-2} or IC:CG ratios greater than 100 are observed in this region.

3.5.4. STORM ENVIRONMENT

In an effort to determine what causes Colorado storms to be electrically distinct by total flash rate measures and positive charge locations, we turn to analysis of the environment. Previously we discussed in general terms what makes this environment different from the others, now we will investigate the details of this distinct region. Fig. 3.26 shows the lightning behaviors as a function of various environmental parameters similar to the previous regions. The flash rate relationship with CAPE is very weak in this region, although the largest flash rates are associated with relatively high instability. Note the lack of large CAPE values in this region. As mentioned before, storms in Colorado do not need large values of CAPE to produce strong storms. The reasons for this are not immediately clear. It is important to note that CAPE values can be misleading in this region due to elevation effects. The surface in this region is located near 850 mb while tropopause heights

are broadly similar to other regions. This results in a smaller depth to accumulate CAPE and may partially explain the lack of large CAPE values in this region. The effects of the environment on parcel theory are also different in this region compared to other regions. This is discussed in coming sections. The correlation coefficient value between flash rate and WCD is nearly zero, but that does not mean WCD does not affect total flash rates. Fig. 3.26b shows a tendency for high flash rate storms to be associated with shallow WCD values, less than 1 km in particular. There exists a class of storms with WCD values around 3 km with exceptionally high flash rates, although these storms are relatively rare. Also note the horizontal axis of Fig. 3.26b and compare with the other regions. The most common values of WCDs in other regions are greater than 3 km. That value is the upper limit of WCD values in Colorado. The largest population of WCD values is between 1.0 and 1.5 km, less than half of other regions. This provides evidence that parcels in Colorado storms spend less time in the warm region of a storm. This would decrease the loss of liquid water from a parcel and thereby increase the supply of liquid water to the mixed phase region, where it can assist in updraft intensification and superlative electrification. The AERONET AOD data in this region is again tenuous at best, although the highest AODs are associated with large flash rates. No significant trend is observed between surface θ_e and total flash rate. θ_e may also be misleading in this region due to the high elevations since θ_e is measured relative to 1000 mb. Modest positive correlation exists between flash rate and 3 km shear, a result contrary to other regions. Similar to other regions, flash rate is negatively correlated with the mixed phase shear. This is likely due to shearing of updrafts, especially shear in the upper levels of the storm. Higher LCL heights tend to produce more flashes, in support of the hypothesis put forth by Williams and Stanfill (2002), although the correlation coefficient is fairly weak. They suggest that higher cloud bases lead to broader and stronger updrafts, less prone to entrainment. They suggest that higher

cloud bases over land are the leading cause in the land/ocean contrast in lightning throughout the globe. Also note that an appreciable number of storms have LCL heights more than 2 km above ground level, this is much higher than other regions. Storms in Oklahoma have an overwhelming majority of storms with LCL heights less than 1.5 km while DC does not have a storm LCL higher than 2 km and Alabama only has 1% of all storms with an LCL height greater than 2 km. While the correlation is not very strong between LCL heights and flash rates in Colorado, this region has the highest overall LCL heights and has the greatest flash rates. All of the regions will be combined in the following sections to put all of the regions into perspective. With the exception of one set of storms, dry bulb surface temperatures are also well correlated with total flash rates, in agreement with Williams et al. (2005). Since this region is moisture limited, warmer dry bulb temperatures assist in raising the LCL heights.

3.5.5. ANOMALOUS STORMS

In an effort to understand the characteristics of the inverted storms discussed previously, we inspect Fig. 3.27 which is the same plot as Fig. 3.16 for the Colorado region. This figure gives us a little more information because the inverted storm signature is stronger in Colorado. The 30 and 40 dBZ echo top heights show similar behavior with respect to both LMA mode temperature and flash rate. Very low echo top heights are common in weak storms with low flash rates and warm positive charge regions. These should not be confused with inverted storms as they are not the same. These storms are usually decaying convection near the end of a storm's lifecycle. Flash rates and positive charge heights increase as echo top heights increase, mostly due to stronger updrafts. These are accompanied by modest increases in flash rates. A peculiar behavior in this region is the modal temperatures become warmer again for storms with echo top heights between 12-14 km. This is where the majority of the inverted storms lie. A similar behavior is observed in the 30 dBZ echo

volume above the freezing level. A general increase in positive charge height is observed at the 30 dBZ volume increases, but once a certain volume is reached, the characteristic mode temperature drops down to around -15°C . This means that a portion of inverted storms are very large volume storms, further evidence for the strength of these storms, similar to Lang and Rutledge (2011). A similar signal is not evident in the 40 dBZ echo volumes. Further investigation is needed to understand this relationship. A familiar relationship with maximum flash altitude is evident in Fig. 3.27e. Increasing maximum flash altitudes are associated with greater total flash rates, similar to Oklahoma storms, but a distinct warmer positive charge is evident for 14 km flash altitudes. These storms are also associated with large flash rates. There is no significant relationship between total CG rate and LMA mode temperature, in contrast to the Oklahoma region where larger CG rates were associated with colder and higher positive charge. The lack of relationship is due in part to the lack of CG production is nearly all storms in Colorado. Another distinct behavior in this region is illustrated in Fig. 3.27g where the highest flash rates (for storms that are electrically active) and IC fractions are associated with the lowest positive charge heights. Given the relatively large bars, this may be a dubious claim. Regardless, this is a different behavior from the Oklahoma storms where the highest IC percentages were associated with the coldest positive charge. Aside from the higher flash rates, Fig. 3.27h has shown other evidence for strong storms with warmer positive charge around -15°C . The task now is to investigate the environmental factors that contribute to strong storms with large flash rates and warm positive charge regions.

Fig. 3.28 is a 6-panel plot that shows various environmental parameters similar to those shown in previous figures. The difference is this plot shows the relationship between an environmental parameter and positive charge temperature (or height). Given that inverted storms exist in this region and tend to be strong, Fig. 3.28a shows some surprising results. LMA mode temperature

is strongly correlated with CAPE. This means that more unstable environments tend to produce stronger storms with colder positive charge centers that are more indicative of normal charge structures. This is evidence that normal polarity storms in Colorado can be very strong. It is important to remember that strong, normal polarity storms are still common in this region, although inverted storms are more common in this region than any other region in the study. The relationship between the WCD and LMA mode temperature is murky at best. There are a large number of points with LMA modes around $-15\text{ }^{\circ}\text{C}$ and these points are associated with WCD values around 1.5 km, which are nowhere near the shallowest values in the region although the flash rate spreads are large for the majority of the points so this statement is very tenuous. The AOD data shows some interesting tendencies. Lower AODs are typically associated with lower and warmer positive charge typically associated with inverted storms, with considerable spread. The highest AOD values are associated with colder positive charge centers indicative of normal polarity storms. These storms produce relatively large flash rates as well. We have been skeptical of the AERONET AOD data during this entire thesis so we are not inclined to put much stock into this result. If the signal were real, it would support the aerosol invigoration of convection hypothesis (Andreae et al. 2004) with larger flash rates and colder positive charge centers of assumed normal polarity storms. However, increased aerosols are thought to increase the amount of liquid water in the mixed phase region by suppressing collision-coalescence processes thereby increasing the likelihood of charge reversal on graupel particles and creating an inverted charge structure (Williams et al. 2002). Little stock is put into this result, given the uncertainties associated with AOD measurements. Similar to the CAPE relationship, warmer θ_e values lead to increased positive charge altitude. Also note that an increase in θ_e does not result in colder positive charge temperatures until a certain values is reached, similar to the CAPE behavior. The higher positive charge temperatures are representative of normal

polarity storms. The relationship in Fig. 3.28e does not show a systematic relationship between mixed phase shear and positive charge height. Perhaps this is to be expected because mixed phase shear would just displace the vertical charge layers rather than have an effect on their vertical position. An increase in LMA mode height is observed for small values of mixed phase shear, then much warmer positive charge is observed for moderate values of mixed phase shear. While the correlation is weak and the spreads are fairly large in Fig. 3.28f, a general trend of colder LMA mode temperatures for higher LCL heights is evident. This is consistent with previous results that show colder positive charge is generally associated with stronger storms with higher flash rates and higher flash rates are associated with higher LCL heights.

In our search for the important environmental variables that determine the location of positive charge within a storm, it appears that the approach in this framework does not highlight any one factor as the most important to forming inverted charge structures. Based on the instability and thermodynamic variables presented here, a majority of inverted storms form in moderately unstable environments with modest LCL heights (in this region) and relatively thick WCD values. This does not support the idea of strong storms with superlative updrafts and flash rates. However, this analysis is designed to avoid the outliers on both ends of the spectrum. This is likely where the strong inverted storms are located. Nevertheless, this analysis has shown that storms with inverted structures exist in the Colorado region and can be strong. Even though the focus on this region has been shifted towards inverted storms, keep in mind that the majority of very strong storms in this region are normal polarity. These normal polarity storms that have been presented in recent figures generally have the highest echo top heights, largest volumes and form in environments conducive to strong and severe weather.

Fig 3.29 is a scatter plot of total flash rate area density and positive charge temperature. The goal of this technique is to isolate the storms that are very electrically active and possess mid-level positive charge defined by earlier criteria. The total flash rate density must be in the top 10% of all storms in the region and the positive charge must be located between -10°C and -25°C . The fraction of storms that satisfy these criteria is almost 9% of all storms, nearly double the amount in Oklahoma. However, after investigation of the environmental variables associated with the inverted storms, only the WCD was significantly different. Surprisingly the WCD values for inverted storms were actually higher than those of other storms. This is in direct contrast with the Oklahoma region. This indicates that other means must be used to find strong inverted storms. The next section investigates a case study of an inverted storm.

Similar to the Oklahoma region, the previous analysis does not produce conclusive results about inverted storms but does provide a means of identifying appropriate case studies of inverted storms. Fig 3.30 shows the environmental setup on 6 June 2012. Warm and dry conditions were present throughout the region as temperatures were near 90°F with dew point temperatures near 50°F . Noteworthy was the presence of a Denver Cyclone (Crook et al. 1990), common on summer days with southeasterly winds near the surface. This is not particularly present in the wind barbs but surface analysis near this time shows winds turning towards the east near Greeley and Longmont, both of which are north of Denver.

A detailed look at cell number 7316 on Fig. 3.31 shows some anomalous behavior in the radar and lightning structure of the storm. Since this snapshot was taken early in the lifetime of the storm, the radar structure is relatively simple with one updraft core. The storm is not very expansive at this current time as indicated by the size scale under the left panel. The right panel shows the height of the maximum LMA sources is located around -15°C , indicating the likely position of

the positive charge at this time. The 2D source density plot shows the region of highest source rates between the altitudes of 6-8 km MSL. Note that the highest source densities are mostly confined to the higher reflectivity core. This behavior is typical of developing convection. The wind barbs indicate veering directional shear present, although the magnitude is not particularly strong. Despite the small size of the storm, it produced nearly 20 flashes min^{-1} at this current time but only produced 2 CG flashes, one of each polarity. This means the IC:CG ratio at this time was 41.

While an automated search of inverted storms to produce bulk statistics between inverted storms versus normal polarity storms was fruitless with the present data, a comparison of storms producing anomalous +CG flash rates can be carried out similar to the Oklahoma region. Previous studies have investigated this comparison of storms in nearby regions, but this is the first study detailing the differences between dominant CG polarity storms in northeast Colorado. This region is closer to the maxima in both +CG percentage and IC:CG ratio Boccippio et al. (2001). The results shown in Fig. 3.32 for the Colorado region are very different from the Oklahoma region. Fig. 3.32a shows flash rates in positive storms are much higher than in negative storms in this region, and the difference is significant. These flash rates are also much higher than storms of either polarity in Oklahoma. Maximum flash altitudes are also significantly higher in positive storms than in negative storms in Colorado. These results clearly show that positive dominated storms in this region are more electrically active than negative storms, although negative storms can produce superlative flash rates and maximum flash altitudes. Along with the electrical characteristics, the radar characteristics of positive storms are also much stronger than negative storms as shown in Figs. 3.32a and 3.32b.

Positive storms in Colorado are overall stronger storms, both from an electrical and a radar perspective, than negative storms in the region. It follows that positive storms are associated with stronger instabilities which are represented by higher CAPE values shown on Fig. 3.33a. In agreement with Lang and Rutledge (2011), however, no significant difference is observed between the WCD values of positive and negative storms. The WCD values for both storm polarities are still much smaller than storms in all other regions. LCL heights in 3.33c also show a lack of significant difference between positive and negative storms. AERONET AOD values are significantly higher for positive storms than for negative storms but the median difference is small, which casts some doubt regarding the role of aerosols contributing to polarity differences. If significant, this would support the aerosol invigoration of convection. The overall magnitudes of AOD values are relatively low compared to the Alabama and DC regions however, which are characterized by the lowest overall flash rates in the study. In contrast with the Oklahoma region, the positive storms in Colorado are stronger, as indicated by electrical and radar characteristics. The environments that produced positive storms in both regions were similar as characterized by higher CAPE values and AOD values, although more aerosol data is needed to confirm this. This distinct behavior will require further investigation with more detailed data such as dual-Doppler velocity data and polarimetric radar data to investigate the microphysical and dynamical differences between storms in these regions.

3.5.6. SEVERE WEATHER

Using techniques previously described in other regions, comparisons of storms that produce severe weather are now compared to those that did not produce severe weather. Table 3.5 shows the comparisons of various storm parameters and environmental parameters between severe and

non-severe storms in the Colorado region accompanied by the p-value from the Wilcoxon rank-sum significance test. Recall the period of study in this region is May and June of 2012 since the Colorado LMA was not operational until spring 2012. This year was not particularly severe for the region, but noting that the climatological hail maximum is located near this region, an occurrence of 3% is not surprising. This number falls between Oklahoma and the Alabama and DC regions. In contrast to the other regions, severe weather is only weakly associated with synoptic forcing and may be more associated to dynamical forcing. A large fraction of severe weather occurs largely due to local mesoscale effects such as the Denver Cyclone which is theorized to be produced by the Palmer Divide ridge near Denver, Colorado and the Cheyenne Ridge near Cheyenne, Wyoming. A possible future study would be to include all storms regardless of isolation to get a more comprehensive study of severe weather behavior, even though a large fraction of severe weather is isolated in this region. Even with the small sample size, the p-values in Table 3.5 show all environmental parameters. Most environmental parameters are not significantly different such as 6 km shear, CAPE, and WCD. Regardless of the environmental differences, severe storms are clearly much stronger electrically as determined by total flash rate, CG flash rate and maximum flash altitude. They are also stronger storms from a radar structure perspective as all radar areas, heights and volumes are all much larger in severe storms than non-severe storms. The peculiar lack of environmental differences between severe and non-severe storms in this region is puzzling and deserves future investigation. Perhaps the local mesoscale effects contribute to this.

3.5.7. SUMMARY

The results in the Colorado region clearly show its distinct behavior from other regions of study. The Colorado region is characterized by a dry climate with warm temperatures common. This combination gives rise to moderate instability and shear values as well as high LCL heights

and shallow WCD values, when compared to other regions. While the trends between flash rates and positive charge temperatures with flash rates and other intensity measures are less defined in this region, comparisons between Colorado and other regions show some clear trends. The storms in this region have the highest LCL heights and the shallowest WCD values of any region. These storms also have the highest overall flash rates, largest fraction of electrified storms and highest percentage of +CGs. These quantities have been linked in previous studies and results here support those findings. Controls on these factors are further elucidated in the following section when all regions are treated together.

3.6. LIGHTNING BEHAVIOR AND ENVIRONMENT IN ALL REGIONS

Starting to build a bigger picture requires that we consider all storms simultaneously to identify the environmental differences and their relationships to lightning behavior. The previous sections have shown that lightning behavior across the regions is distinct to each environment. This section will attempt to attribute those distinct regional behaviors to large scale differences in environmental factors.

Initially, we detail the differences in storm total flash rates throughout the regions. This is illustrated in Fig. 3.34 which shows the CDF of storm total flash rates for each region. The Colorado region is the most electrically active region. This has been alluded to in previous results but is now shown explicitly in this figure. Colorado has the smallest fraction of storms with the lowest flash rates but also has the highest fraction of storms with flash rates greater than 120 flashes min^{-1} . While storms in the Oklahoma region are not quite as active as in Colorado, they are still more electrically active than the other regions of study. The highest flash rates of all storms in the study are in the Oklahoma region and associated with severe weather. The Alabama and DC

regions have the lowest overall flash rates as they have the highest fraction of low flash rate storms but also the lowest fraction of high flash rate storms.

Now that the flash rate differences have been explicitly shown, we must identify the factors that cause these differences throughout the regions. Our first step is to examine single variables thought to be important contributors to total flash rates and their relative frequencies in each region. Fig. 3.35 shows the log of total flash rate as a function of LCL height for all included storms in the study. This results in a total sample size of around 4000 cell observations. The colors of the points indicate relative population showing that most of the storms have LCL heights less than 1000 m. Recall the relative number of cell observations in each region, as the Alabama and DC regions contributed more valid cell observations than the Oklahoma and Colorado regions. The bars indicate the locations of the 25th and 75th percentiles of the flash rate distributions for each bin. It is important to note that these bars are different from the previous 6 and 8 panel plots. Total flash rate is very well correlated with LCL height with an R^2 value of 0.95, albeit with considerable spread for each bin. This relationship is monotonic as represented by the Spearman rank coefficient of 1. The quasi-symmetric error bars on the log scale mean that the data is non-symmetric. A large portion of the flash rates are clustered at lower values while a long tail exists at larger flash rates. This strong relationship between the medians means that LCL height is a connecting factor between regions in determining the flash rate differences between the regions. A comparison between Fig. 3.35 and Fig. 3.36 taken from Williams et al. (2005) shows a very similar trend in the tropics as measured from the TRMM LIS instrument. Flash rate magnitudes are also similar between the two figures. This result is striking. The fact that very similar flash rate magnitudes and trends are observed between the two studies even though these studies used completely different data sets and studied completely different regions may support the robustness of this relationship between LCL

height and total flash rate. It is impossible to state the reasoning for the slightly differing values but the differing lightning data may be a contributing factor. Flash rates for this study are likely higher and more accurate than satellite based measurements (Boccippio et al. 2000; Christian et al. 2003) because the VHF LMA data and flash clustering algorithm are able to detect small flashes much better. The distributions of LCL heights are shown in Fig. 3.37. Immediately apparent is the anomalous nature of the Colorado region, which is characterized by much higher LCL heights than the other regions (recall that Colorado storms also had the largest flash rates of all regions). The DC region has the lowest LCL heights characteristic of an oceanic regime. Storms in the DC region also had the lowest flash rates of any region in an overall sense. Surprisingly, the Oklahoma and Alabama regions have very similar LCL heights. Note however that Oklahoma has slightly higher flash rates than Alabama. This may point to a difference in network sensitivities which is very difficult to characterize in a large sense. Other environmental factors are also a possibility, which will be examined later.

Fig. 3.39, taken from Williams et al. (2005) compares the flash rates to surface dry bulb temperatures. Fig. 3.38 presented here shows a similar trend with a near-linear relationship between log flash rate and higher dry bulb temperatures. Note the high linear and Spearman rank correlation coefficient. The correlation between these variables follows the results observed in each individual region. The most common dry bulb temperatures were observed near 20 °C and the least common were very high and low temperatures. The magnitudes of flash rates in this figure are strikingly similar than those in the Williams et al. (2005) figure for similar temperatures. Note that lower temperatures occur in extratropical regions such as these and that demands the dry bulb temperature scale to be different in this study. The results presented here, while not exactly the same,

follow a very similar trend to that of the Williams et al. (2005) study even though that study investigated tropical regions and this study investigates continental regimes, although Alabama and DC have a lot of maritime characteristics, namely low LCL heights and thick WCDs, especially in the framework of this analysis where outliers are not considered. These outliers in Alabama and DC are likely to be strong storms that are synoptically forced during severe weather episodes early in the warm season.

Alluded to before was the fact that storms with higher LCL heights should have lower WCD values by virtue of their relation to the freezing height. Fig. 3.40 shows a plot of median flash rates as a function of WCD values. These quantities are negatively correlated with the highest observed flash rates occurring for storms with WCDs less than 1000 m. These storms also have the smallest inter-quartile range (IQR; difference between 25th and 75th percentile) of all the storms, indicating that they are consistently electrically active. Note that these storms make up a small fraction of the total storms, consistent with the relative LCL populations. Storms with deep WCDs (around 3000 m) have median flash rates that are an order of magnitude lower than storms with less than 1000 m WCDs. These shallow WCD values are almost exclusively in the Colorado region, as shown by Fig. 3.41. The largest WCD value for any storm in Colorado is around 2.5 km while that value is very near the median in all other regions. It is surprising that WCD values in Oklahoma are similar to the Alabama and DC regions, although very shallow WCDs are slightly more common in the Oklahoma region compared to either of those regions. Flash rate distributions are nearly identical all storms with WCD values greater than 2000 m, when observing the medians as well as the IQRs for each WCD bin. The negative correlation observed here corroborates the earlier claim that storms with smaller WCD values tend to have higher flash rates, likely because the parcel residence time inside the warm rain zone of the cloud has been shortened. WCD is

not exactly correlated with LCL height, as evidenced by the weaker flash rate correlation than with LCL height. This correlation is modulated by the freezing height. The weaker flash rate correlation also suggests that LCL heights may be a more important control on total flash rate than WCD. This may be because the vertical updraft speed increase may be a bigger controller of warm cloud residence time than the distance traveled to reach the freezing level.

CAPE has been offered to explain a large portion of the total flash rate variations between individual storms in addition to the global differences in lightning. We attempt to quantify its effect with Fig. 3.42 which shows the flash rate relationship with CAPE in all 4 regions. A clear correlation is observed as the highest flash rates are observed at the highest CAPE values, although there is considerable spread in flash rates with each bin. Note that the highest population of CAPE values lies in the first bin and a rapid population decrease is observed as CAPE values increase. This correlation with flash rate is the poorest of all the variables that we have investigated and raises questions about the relative controls of each thermodynamic variable on total flash rate. The distribution in storm CAPEs is also of interest when investigating the effects of CAPE on storm flash rate. This is shown in Fig. 3.43. While the median CAPE values (represented by 0.5 cumulative frequency) in Oklahoma and Alabama are very similar, the CDFs show that higher CAPE values are much more common in Oklahoma. The CAPE values in Oklahoma are the highest and may help explain the higher flash rates in Oklahoma than the Alabama and DC regions which have similar LCL heights and WCD values. Note that Colorado has some of the lowest CAPE values of any region.

While single variable analysis has illuminated some very important relationships between total lightning activity, it does not take environmental interactions into account. This is precisely what will now be investigated. Fig. 3.44 shows median flash rates for all storms within a 2D bin as

determined by the variables on both axes. Note that the number of storms in a particular bin must meet a specified criterion to be plotted on the figure. This is because we do not want one outlier storm to affect or dwarf the rest of the results. In an effort to quantify the significance of the data, the number of cell observations in each valid bin is indicated by the white text. It is immediately clear that higher flash rates tend to favor storms with higher values of both CAPE and LCL height. The highest flash rates are observed in storms with high LCL heights and moderate CAPE values rather than high CAPE values and low LCL heights, consistent with Williams and Stanfill (2002) and previous figures. It is no surprise that storms with small values of CAPE and low LCL heights have small total flash rates. Note the lack of observations in the upper-right corner of the figure, this is because environments with high LCL heights tend to have smaller values of CAPE and vice versa. The bins with the largest number of contributing storms are in the lower-left corner of the figure where CAPE and LCL heights are both low. This is also where the lowest median flash rates are located.

Fig. 3.45 shows the relationship between WCD and CAPE to total flash rates. The highest flash rates are observed in storms with moderate CAPE and WCD values, coincidentally both around 1500 in their respective units. High flash rates are also observed in storms with moderate CAPE values and very shallow WCD values < 1000 m. Storms with the highest CAPE values also tend to be the ones with large WCD values, and is because both values are tied to low-level environments, particularly moisture. Note the overall behavior of CAPE and WCD: large values of CAPE cannot be possible without the coexistence of large WCD values. High flash rates in shallow WCDs are consistent with the previous results and the fact that LCL heights and WCD values are intimately related and negatively correlated based on the height of the freezing level. Given these results, it

is surprising that storms with the largest flash rates are not those with the highest CAPE values but rather those with moderate CAPE values which have high LCL heights and shallow WCDs.

Previous figures have shown that storms with higher LCL heights and shallower WCD values tend to produce higher flash rates. We have also claimed that LCL heights and WCD values are inversely related by their relation to the freezing height altitude. Fig. 3.46 shows this explicitly. With WCD values on the horizontal axis and LCL heights on the vertical axis, it is clear that the highest flash rates occur within storms that have higher LCL heights and shallower WCDs. Also note the behavior of the two variables. There are no observations on the top-right portion of the figure which suggests an inverse relation between the variables. There are also no observations in the bottom-left portion of the figure as that region represents an environment with very low freezing heights. Those environments are not conducive for isolated convection.

Since LCL heights are determined by surface dry-bulb temperature and surface dew point temperature as per Bradbury (2000), it is useful to look at the effects of these two parameters on total flash rates. Fig. 3.47 shows a clear preference for high flash rate storms to occur in environments with high dry-bulb temperatures and modest dewpoint temperatures. This figure shows very similar trends to those in Fig. 3.48, taken from Williams et al. (2005). The highest flash rates are observed where dewpoint depressions are near 20 °C. This corresponds to LCL heights greater than 2 km AGL, which is where the highest flash rates are observed in Fig. 3.35. These results, along with Williams and Stanfill (2002) suggest this is the reason for the superlative flash rates in Oklahoma and particularly Colorado. It may be possible that this is simply a residence time argument. If the Morton et al. (1956) fixed-angle hypothesis holds true such that higher LCL heights produce broader updrafts which are less prone to dry air entrainment, then these storms will produce higher liquid water contents closer to the adiabatic value. Coalescence growth in parcels with

strong updraft speeds rising through their WCDs will be very limited. Since LCL heights are anti-correlated with WCD values via the relation to the freezing height, storms with high LCL heights will have broader and stronger updrafts via decreased entrainment. These same storms will also have reduced WCD values, leading to a decrease in distance in warm region of the cloud. These factors conspire together to decrease the residence time of an ascending parcel in the warm rain zone, resulting in decreased loss of liquid water below the freezing level, and more liquid water surviving into the mixed phase region. Takahashi (1978) and Saunders et al. (1991) state that more supercooled liquid water available for riming increases the amount of charge transfer per collision. These same storms that contain larger amounts of liquid water in the mixed phase region also have stronger updrafts via previous arguments. It is these stronger updrafts that will produce more collisions and greater charge separation, conducive to higher total flash rates. It is this same argument that many studies (e.g. Wiens et al. 2005) have made to explain the graupel charge reversal that results in the inverted charge structures observed in the High Plains. One then expects higher flash rates to be related to enhanced production of +CG flashes. This relationship is explored in the coming sections.

While simple flash rate quantities have been shown to be related (strongly in some cases) to environmental variables, that is not the sole purpose of this study. We also want to investigate the role of charge structures in determining lightning characteristics and the relationships between these factors. The slope of the contours in Fig. 3.49 represents the overall relationship between maximum flash altitude and positive charge temperature. These relationships were demonstrated in each region in previous sections. The median flash rates for each bin show some interesting behaviors. There exist two maxima in flash rates, both at the highest flash altitudes. One of these maxima is located at the coldest positive charge temperatures indicative of strong normal polarity

storms in all regions. Note these flash rates are near $100 \text{ flashes min}^{-1}$ for the coldest positive charge regions. The other maximum is located at high flash altitudes but warm positive charge near $-15 \text{ }^\circ\text{C}$, these are indicative of electrically active storms with inverted charge structures. This is evidence that there exist at least two types of charge structures that are capable of producing superlatively electrified storms. Finally, the maximum in storm occurrence is near 10 km maximum flash altitude and positive charge near $-40 \text{ }^\circ\text{C}$ where relatively low median flash rates are observed in these cases.

It is clear from the previous results that high altitude flashes and echo top heights are coincident with higher flash rates. This has also been documented in previous studies (e.g. Shackford 1960; Jacobson and Krider 1976; Williams 1985) where a fifth-power law was determined between cloud top height that Price and Rind (1992) used to build a simple global lightning parameterization. This parameterization is used in some global models to produce lightning-generated NO_x , for example. It is then important to have correct total lightning relationships. This is the purpose of Fig. 3.50. It shows the median flash rate for each height bin for 0-50 dBZ echo top heights. The near-linear relationships are evident in all regions and for all reflectivity values. The linear fit parameters for all relationships are listed on table 3.1. Given that 0 dBZ height is most comparable to the relationships used in Price and Rind (1992) it is surprising that the slopes are near 10 in all regions, indicating that flash rates are proportional to the 10th power of cloud top height. This may be due to the different flash detection efficiencies with the different datasets, as alluded to before. Higher flash rate storms will have more numerous smaller flashes that may be missed by satellite observations (Bruning and MacGorman 2013). The general trend is for the slope to decrease and the intercept to increase with higher reflectivity values. For example, the slopes are near 4-5 for the 40 dBZ echo top heights. Note that the majority of R^2 values are above 0.95 indicating that the

relationships are very close to linear. Inter-region comparisons reveal that different fit parameters exist in different regions, especially at higher reflectivities. Given some of the past results shown here, this is not surprising. Perhaps future simple flash rate parameterizations should employ these relationships and consider moving away from one parameterization for the entire globe.

Simple results shown previously in this study have linked the production of +CG flashes and higher flash rates together in a simple regional comparison. We will now investigate the production of +CG flashes in more detail to better understand if the same environmental variables that produce superlative flash rates produce higher +CG flash rates. Fig. 3.51 shows a scatter plot of total flash rates and percentage of total CG flash rates that are of positive polarity. A positive correlation is observed between these lightning behaviors with a modest correlation coefficient of 0.4. These quantities are expected to be correlated because inverted storms tend to be strong storms with high flash rates and ordinary convection is typically weak with very low production rates of +CG flashes. This was observed in the section comparing storms producing a majority of +CG flashes in both Colorado and Oklahoma. Storms producing anomalous amounts of +CG flashes in those regions existed in more unstable environments. These storms produced larger amounts of total flashes than storms producing a majority of CG flashes in the Colorado region. Conversely, these storms produced smaller amounts of total flashes than storms producing a majority of CG flashes in the Oklahoma region. These results will require further investigation with a more detailed dataset including microphysical and dynamic information.

Investigating all storms included in the study has elucidated some significant results and provided some evidence for the differences between lighting behavior in the various regions of study. Relationships between total flash rates and environmental variables shown in this section are somewhat striking in the similarities with other studies investigating completely different regions with

different data sets. Flash rates were found to be nearly exponential with varying LCL heights and dry bulb temperatures, very similar to Williams et al. (2005). WCD values were shown to be inversely correlated with log of flash rate, which follows from the relationship between LCL heights and WCD values. Examining median flash rate variations with two variables also showed similar behaviors as storms with high LCL heights and shallow WCD values produced the highest flash rates. Those variables seemed to exhibit more control over total flash rates than CAPE, which is typically associated with the thermodynamic perspective of thunderstorm intensity. It was also shown that at least two types of charge structures, as determined by LMA modal temperature, are capable of producing large flash rates. This is suggestive of the anomalous charging and presence of inverted charge structures in thunderstorms.

3.7. SENSITIVITY STUDIES

The sensitivity of these results is tested both for LMA flash counting performance and autocorrelation between storm parameters. The details of the flash counting are located in Appendix A while the simple autocorrelation tests are detailed below.

Since each cell observation at every 5 minutes is treated as a different cell, it is possible that consecutive observations of the same storm may be correlated with each other. This phenomenon is known as autocorrelation and violates assumptions made when performing rank-sum statistical significance tests in this study. Rudlosky and Fuelberg (2013) conducted an autocorrelation study of various storm parameters to investigate the amount of time needed for samples from the same storm to become independent. They concluded that the decorrelation time for most parameters was between 5-10 minutes which is on the order of samples in this study. To test for the effects of autocorrelation in the results of this study, a sensitivity study was performed in which every other radar file was included for statistical processing. This resulted in an observation time of 10 minutes

instead of 5 minutes. Most prominent storm radar, lightning and environmental characteristics were compared with the new subset of data versus the whole dataset of the study. Rank-sum tests were performed on all included storm radar, electrical and environmental quantities. All quantities in question were not significantly different to the 95% confidence level between the subset of data and the whole original dataset in all regions. This is shown in tables 3.6 to 3.9 that show some of the pertinent storm and environmental variables. This gives some confidence to independent nature of the samples taken at regular 5 minute intervals.

The decision to have a large requisite cell size resulted in more efficient processing of the data by virtue of fewer number of identified cells. Allowing smaller cells to be included in the study increased the number of identified cells and also decreased the average size of identified cells. While excluding smaller cells did result in a slight loss in number of electrified cells, the processing speed gain outweighed the drawbacks of missing a couple of cells. The number of cells is still significant and comprises a large sample of observations.

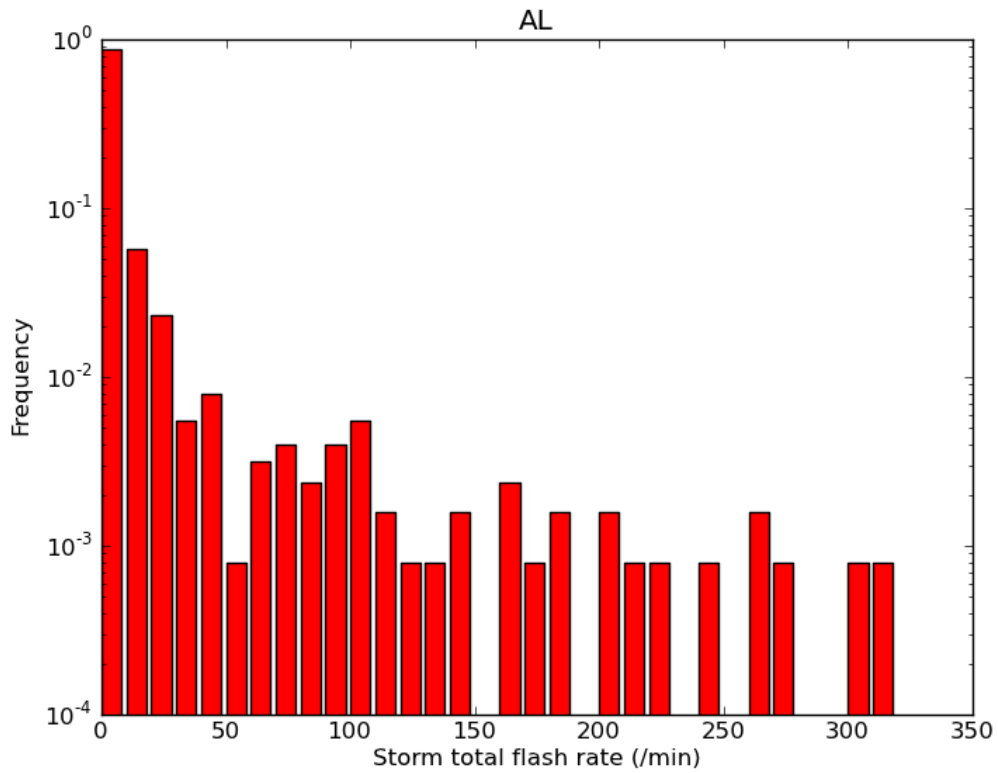


FIG. 3.1. Probability Distribution Function (PDF) of storm total flash rates in isolated Alabama convective cells. Colors here will remain consistent throughout the study. Note the log scale on the vertical axis.

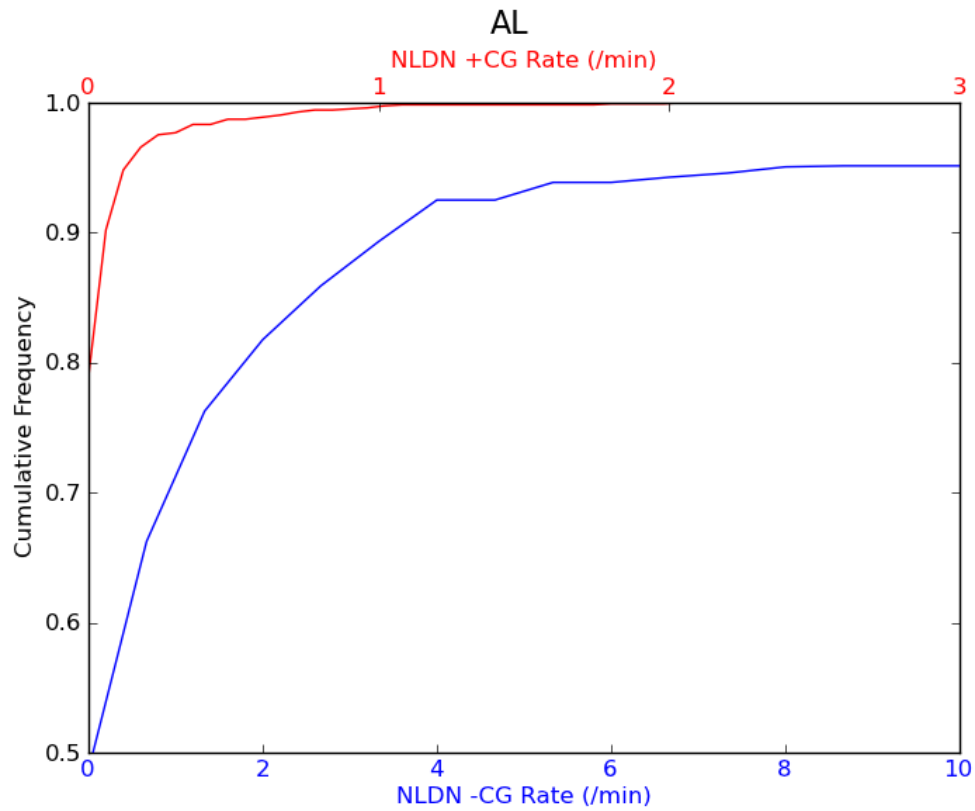


FIG. 3.2. Cumulative distribution function (CDF) of +CG rate (red) and CG rate (blue) for all storms in the Alabma region. Note that the vertical axis starts at 0.5 because many storms did not produce any CG lightning.

Storm variables AL

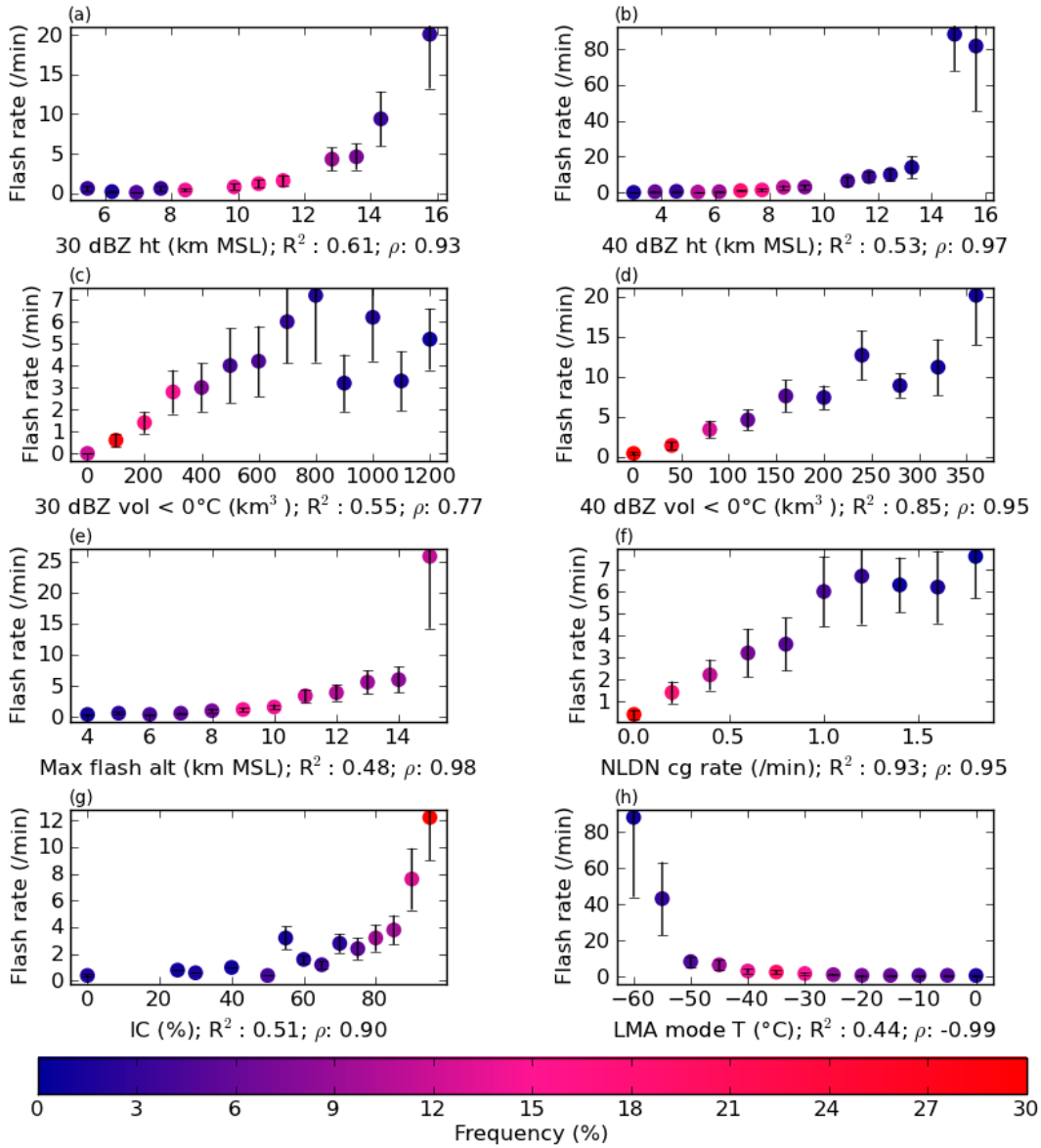


FIG. 3.3. 8 panel plot of storm variables and flash rates for the Alabama region. Each point represents the median flash rate for all storms within a particular bin. Error bars indicate the median absolute deviation of the flash rate distribution for each bin. Points are colored by the relative population of the horizontal variable following the bottom colorbar. R^2 value represents the goodness of fit to a linear function. ρ value represents the how well the relationship can be represented by a monotonic function.

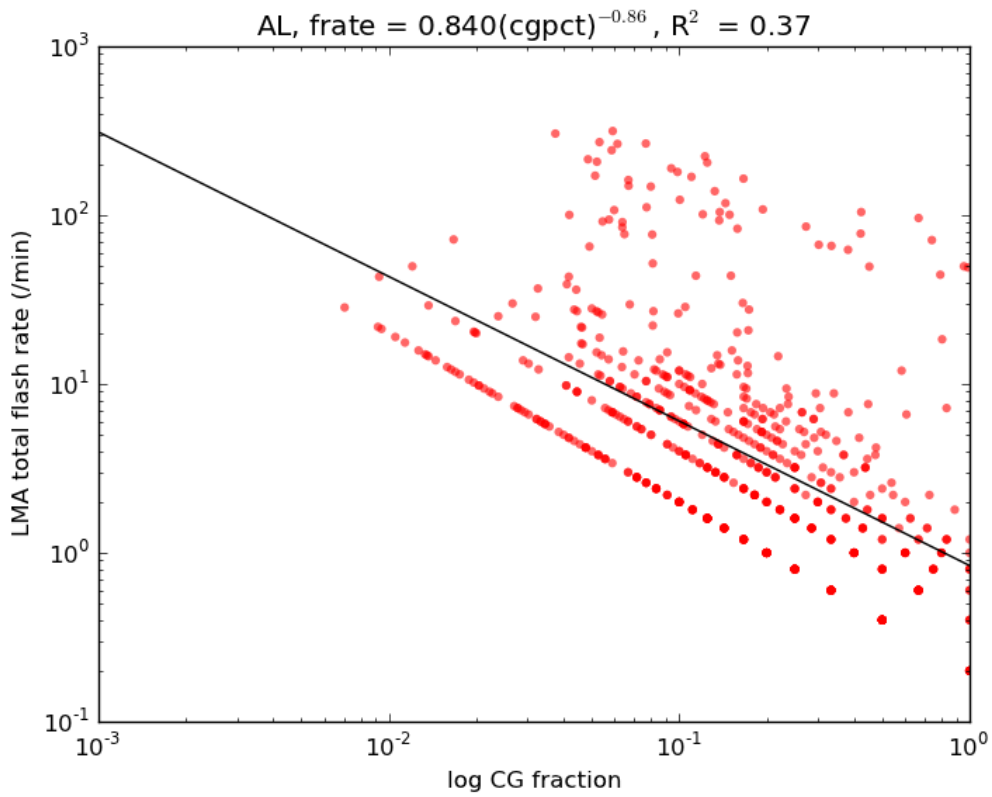


FIG. 3.4. Log of total flash rate versus log of CG fraction for Alabama storms. The best fit line parameters are displayed in the title along with the linear correlation coefficient

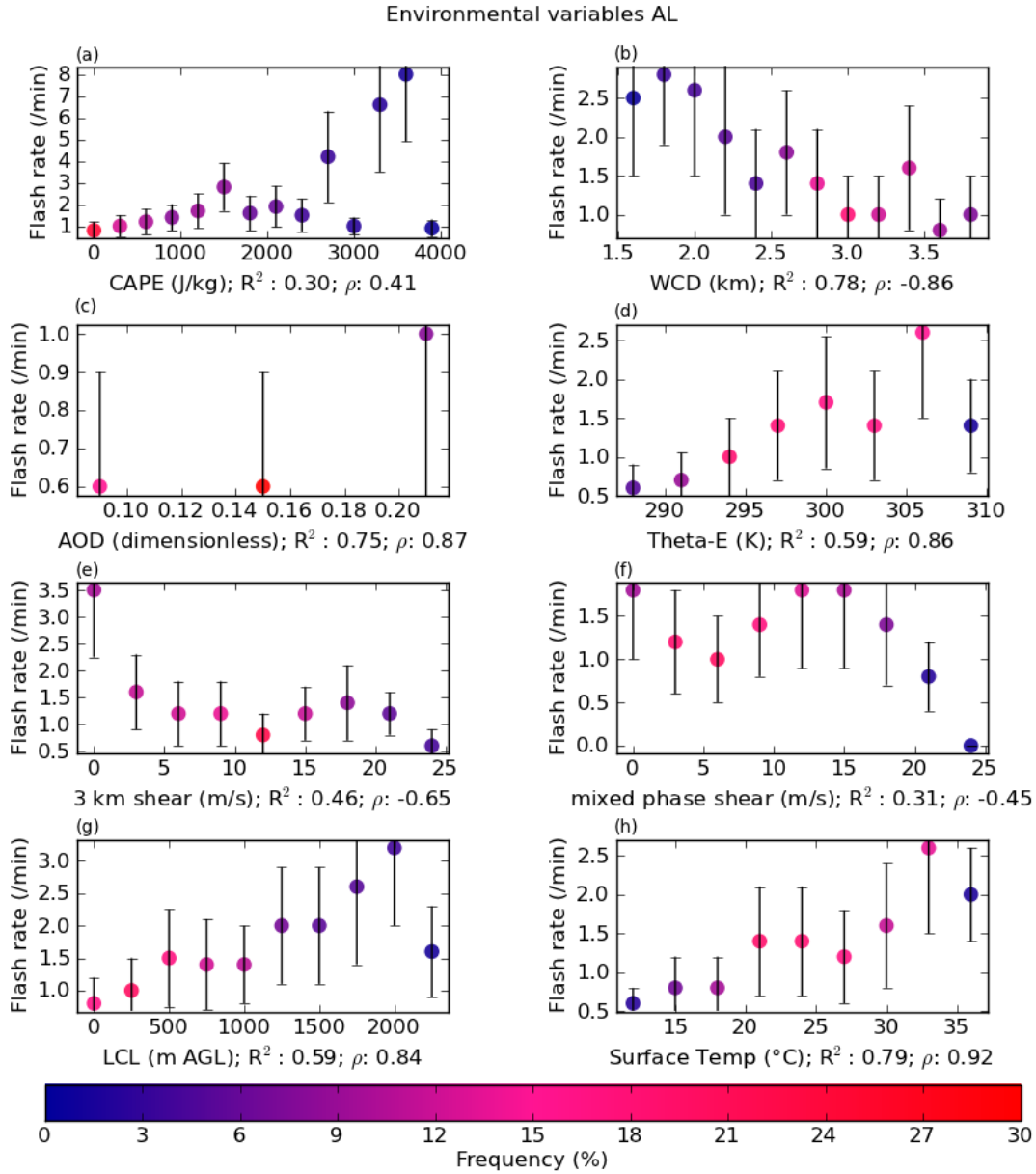


FIG. 3.5. 8 panel plot of environmental variables and flash rates for the Alabama region. Each point represents the median flash rate for all storms within a particular bin. Error bars indicate the median absolute deviation of the flash rate distribution for each bin. Points are colored by the relative population of the horizontal variable following the bottom colorbar. R^2 value represents the goodness of fit to a linear function. ρ value represents the how well the relationship can be represented by a monotonic function.

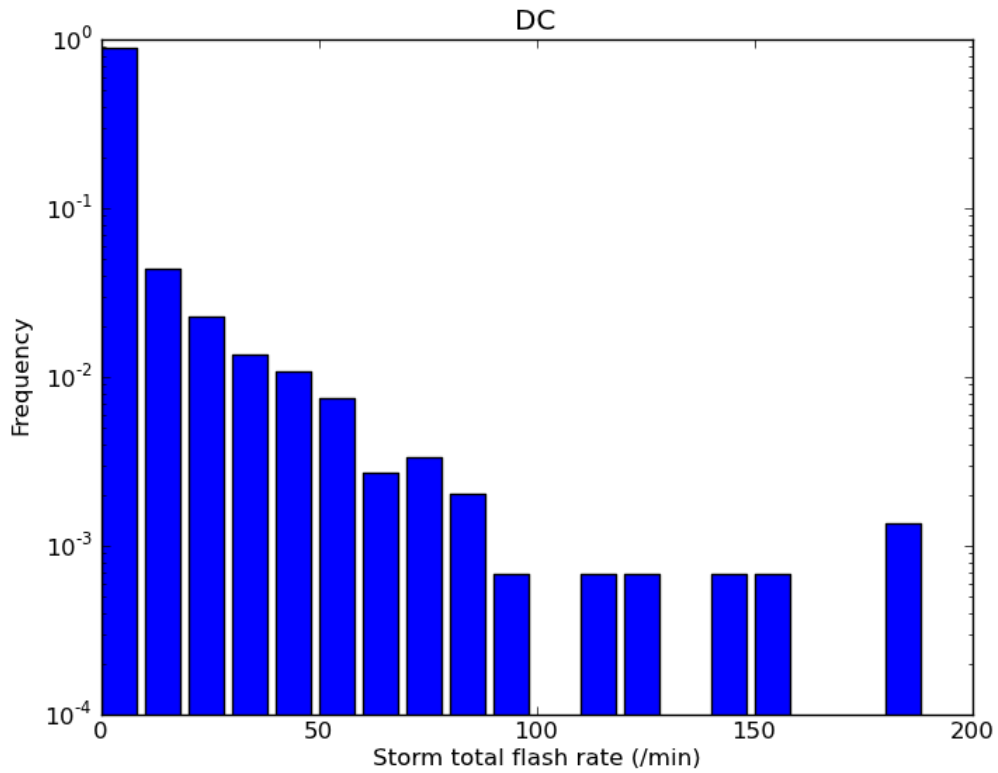


FIG. 3.6. Probability Distribution Function (PDF) of storm total flash rates in isolated DC convective cells. Colors here will remain consistent throughout the study. Note the log scale on the vertical axis.

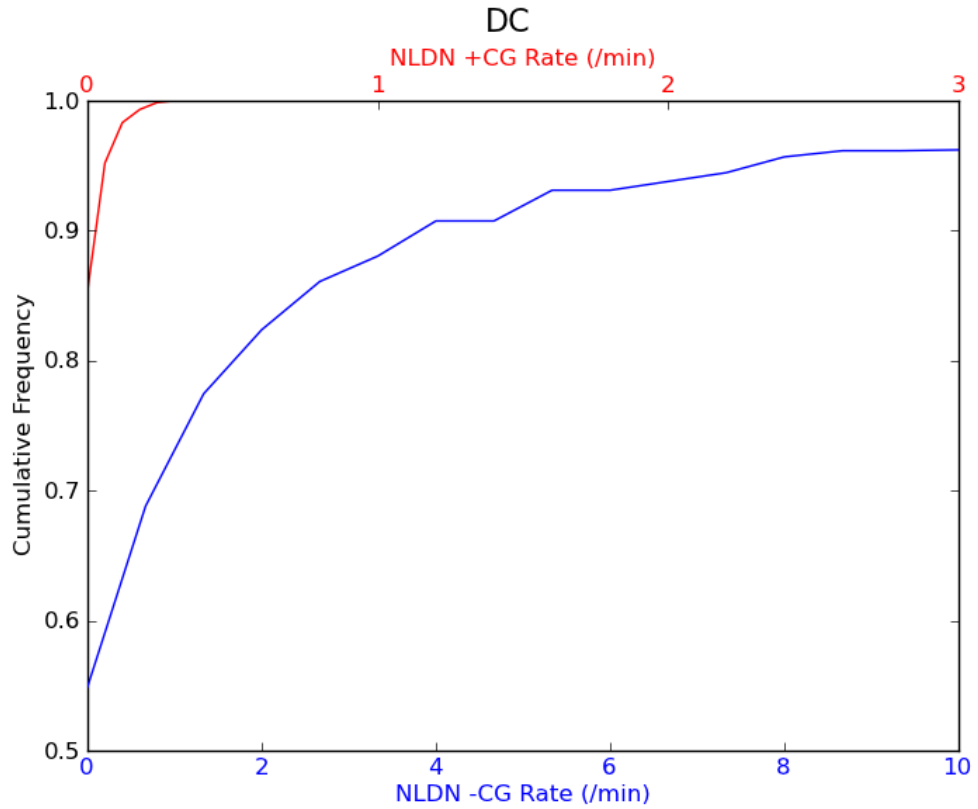


FIG. 3.7. Cumulative distribution function (CDF) of +CG rate (red) and CG rate (blue) for all storms in the DC region. Note that the vertical axis starts at 0.5 because many storms did not produce any CG lightning.

Storm variables DC

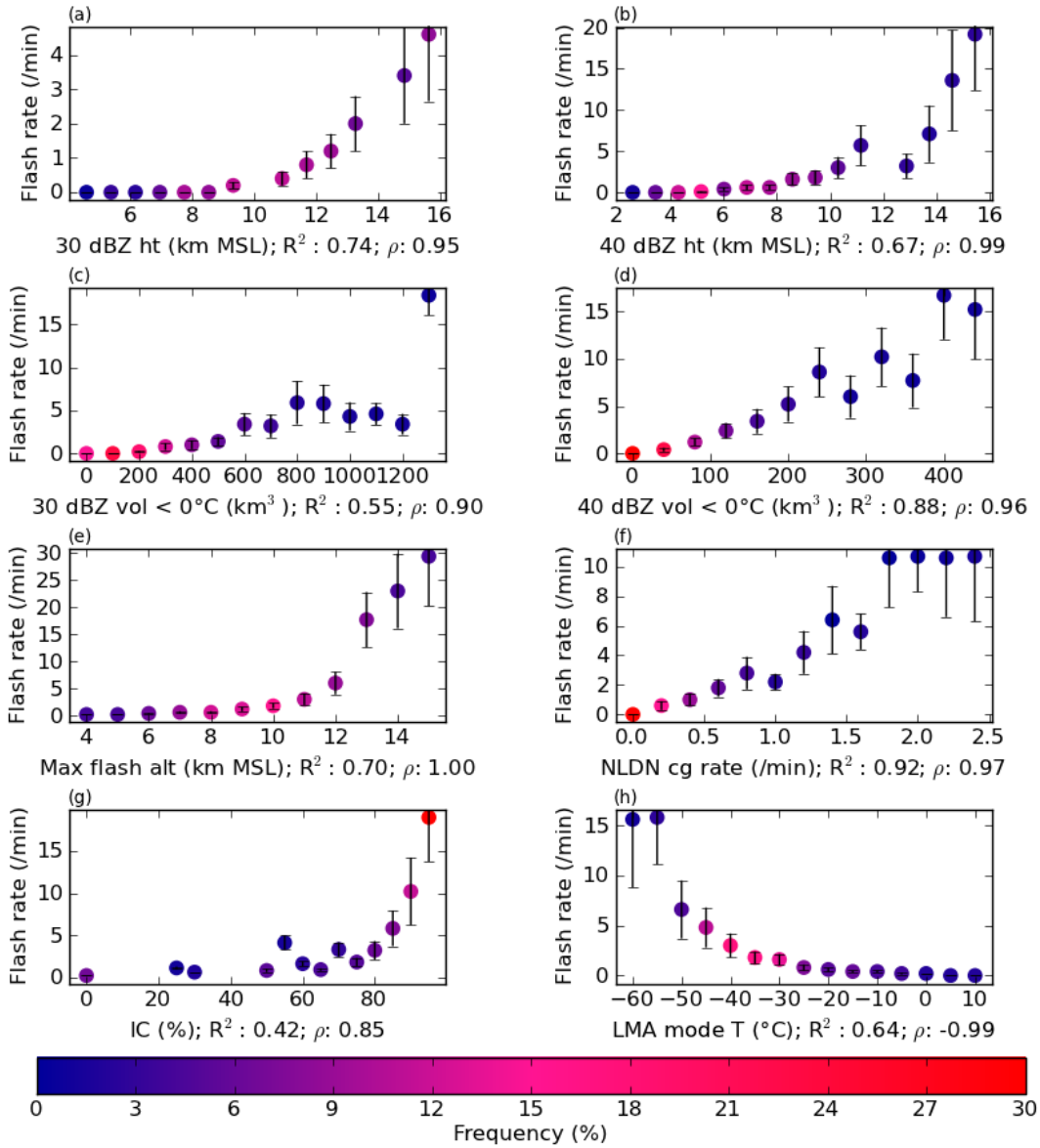


FIG. 3.8. 8 panel plot of storm variables and flash rates for the DC region. Each point represents the median flash rate for all storms within a particular bin. Error bars indicate the median absolute deviation of the flash rate distribution for each bin. Points are colored by the relative population of the horizontal variable following the bottom colorbar. R^2 value represents the goodness of fit to a linear function. ρ value represents the how well the relationship can be represented by a monotonic function.

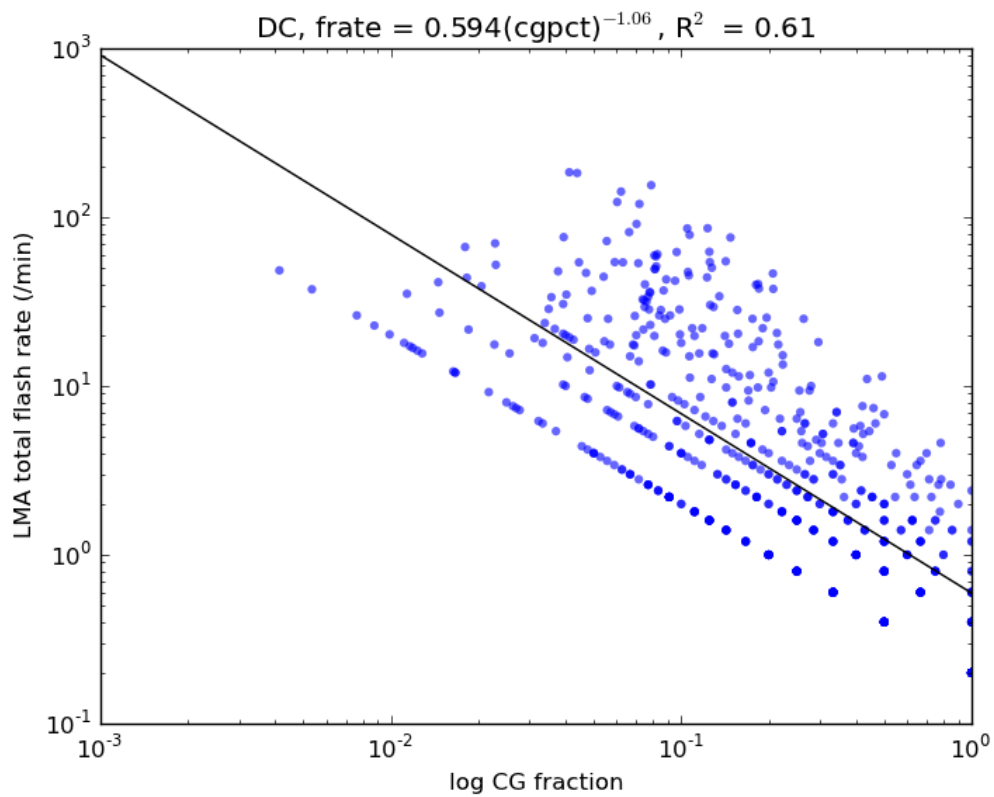


FIG. 3.9. Log of total flash rate versus log of CG fraction for storm in DC. The best fit line parameters are displayed in the title along with the linear correlation coefficient

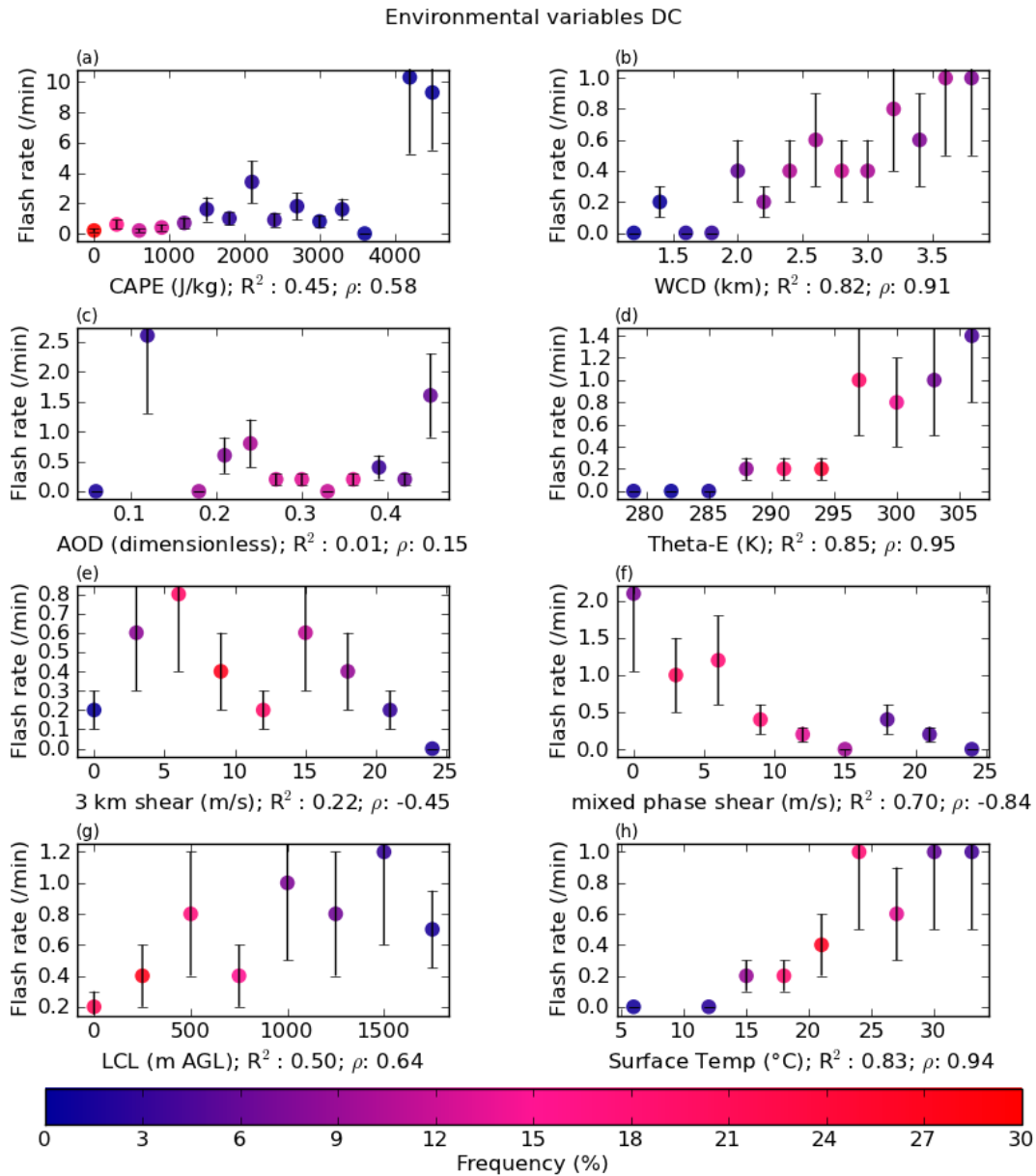


FIG. 3.10. 8 panel plot of environmental variables and flash rates for the Alabama region. Each point represents the median flash rate for all storms within a particular bin. Error bars indicate the median absolute deviation of the flash rate distribution for each bin. Points are colored by the relative population of the horizontal variable following the bottom colorbar. R^2 value represents the goodness of fit to a linear function. ρ value represents the how well the relationship can be represented by a monotonic function.

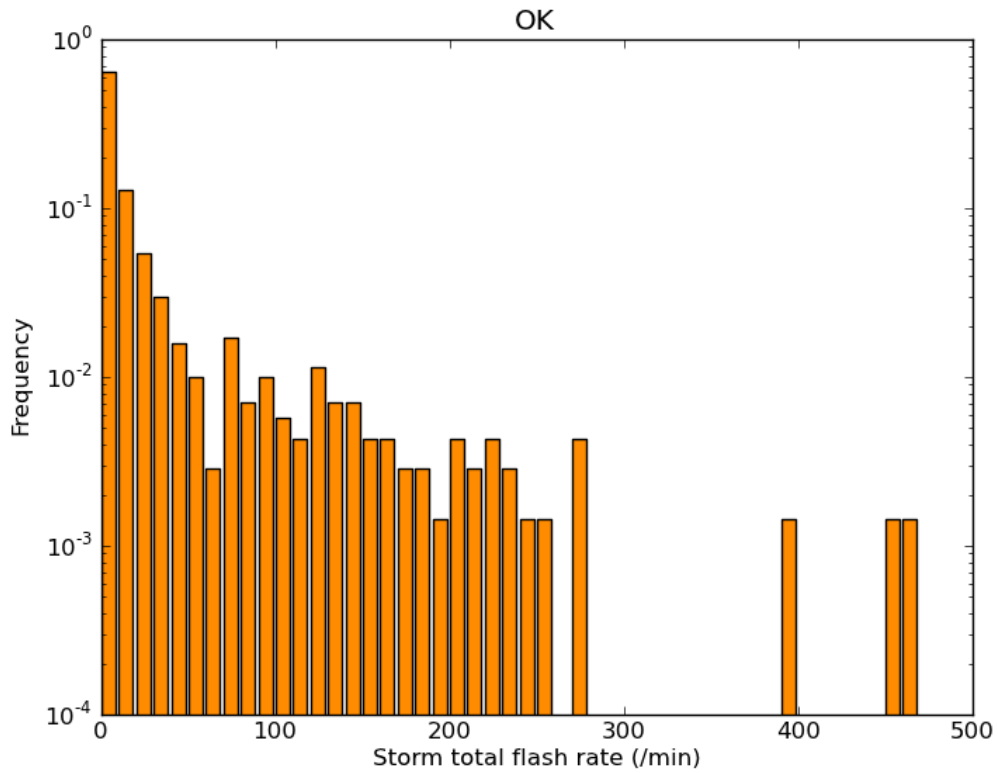


FIG. 3.11. Probability Distribution Function (PDF) of storm total flash rates in isolated Oklahoma convective cells. Colors here will remain consistent throughout the study. Note the log scale on the vertical axis.

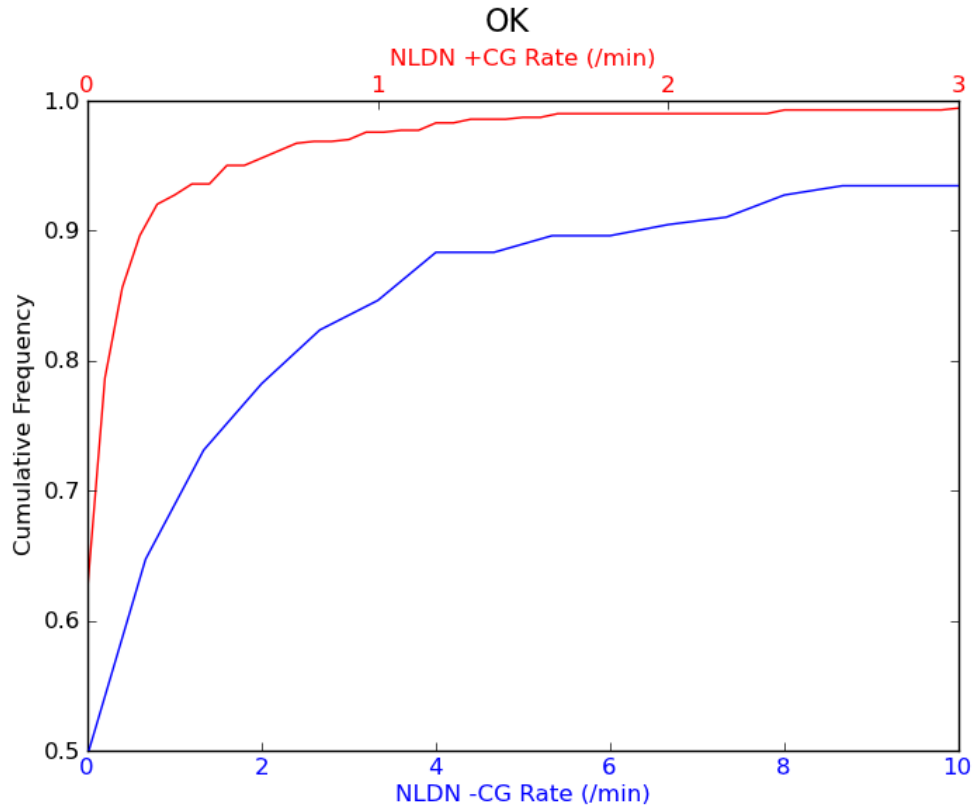


FIG. 3.12. Cumulative distribution function (CDF) of +CG rate (red) and CG rate (blue) for all storms in the Oklahoma region. Note that the vertical axis starts at 0.5 because many storms did not produce any CG lightning.

Storm variables OK

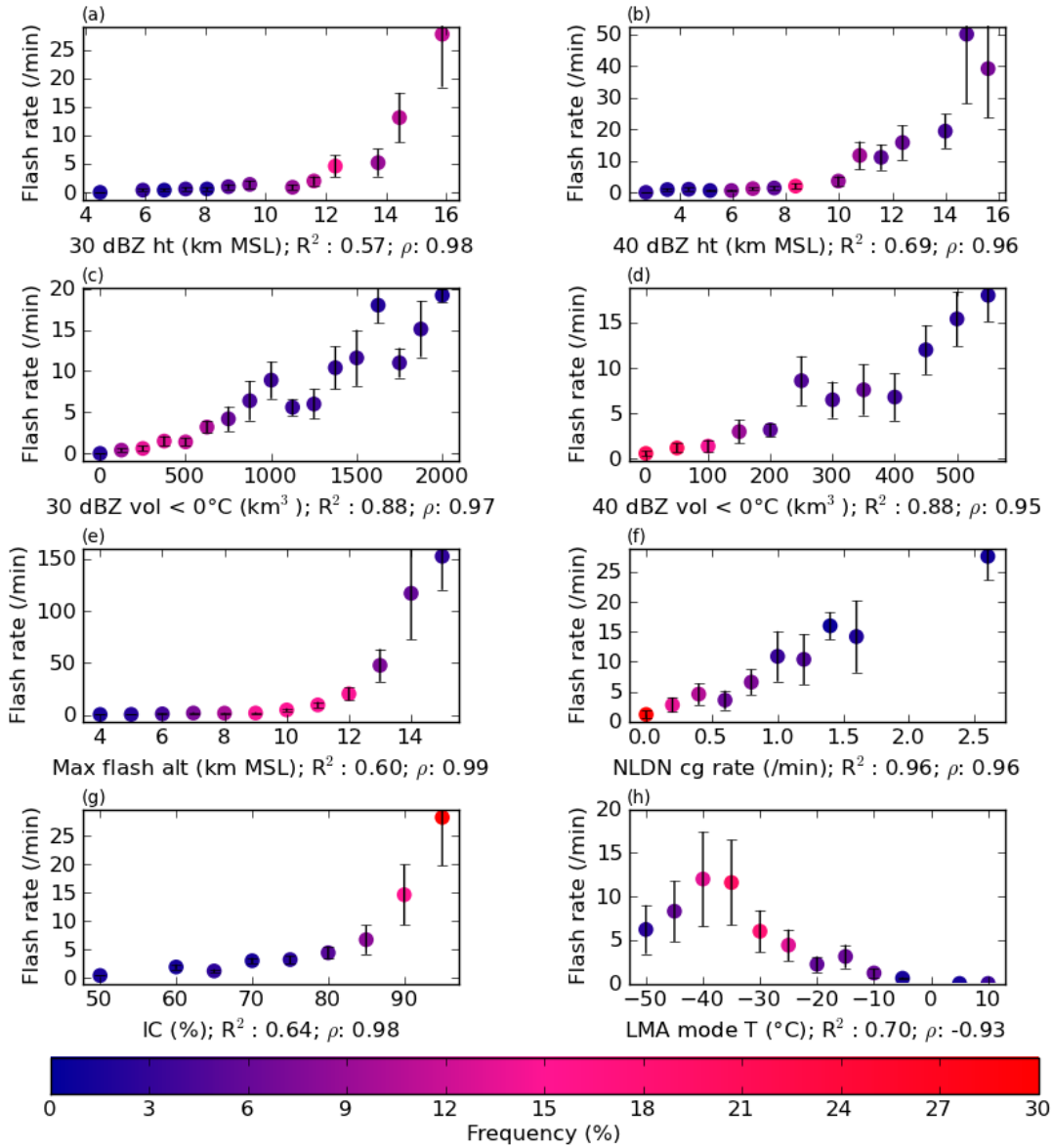


FIG. 3.13. 8 panel plot of storm variables and flash rates for the Oklahoma region. Each point represents the median flash rate for all storms within a particular bin. Error bars indicate the median absolute deviation of the flash rate distribution for each bin. Points are colored by the relative population of the horizontal variable following the bottom colorbar. R^2 value represents the goodness of fit to a linear function. ρ value represents the how well the relationship can be represented by a monotonic function.

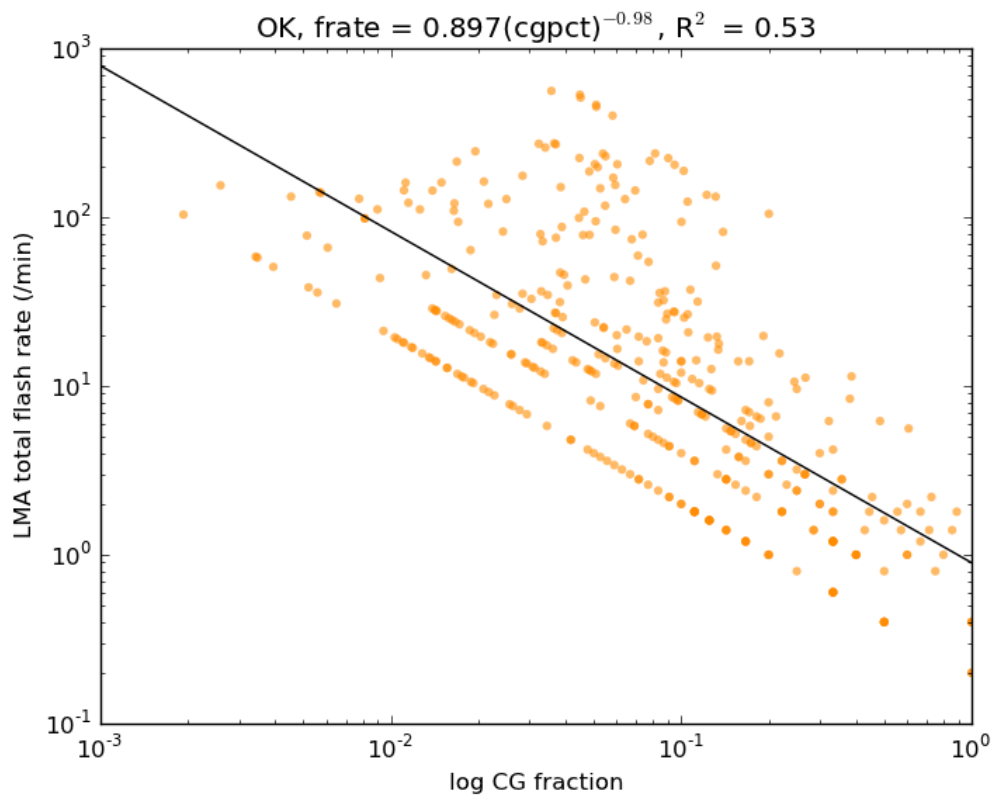


FIG. 3.14. Log of total flash rate versus log of CG fraction for storms in Oklahoma. The best fit line parameters are displayed in the title along with the linear correlation coefficient

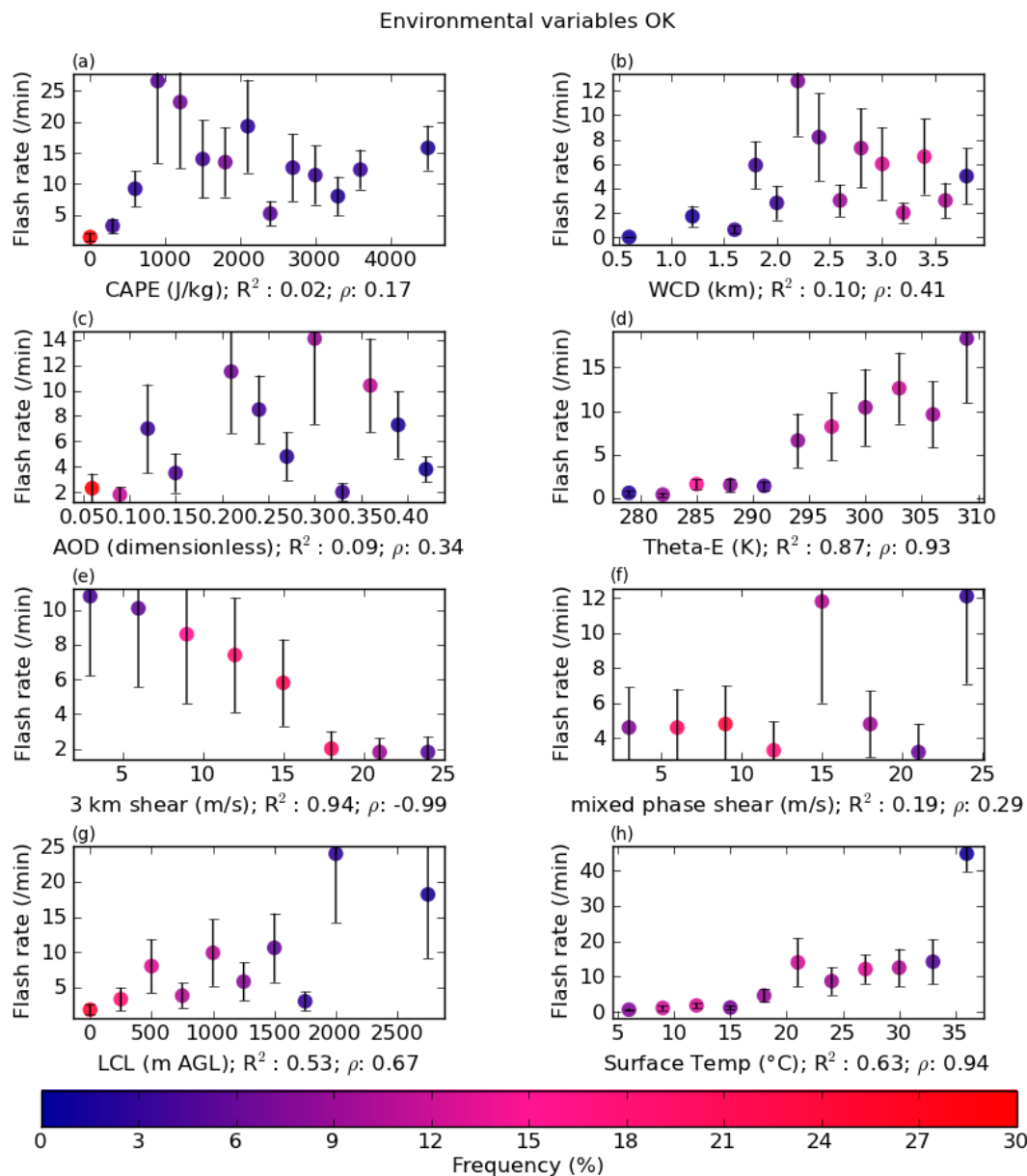


FIG. 3.15. 8 panel plot of environmental variables and flash rates for the Oklahoma region. Each point represents the median flash rate for all storms within a particular bin. Error bars indicate the median absolute deviation of the flash rate distribution for each bin. Points are colored by the relative population of the horizontal variable following the bottom colorbar. R^2 value represents the goodness of fit to a linear function. ρ value represents the how well the relationship can be represented by a monotonic function.

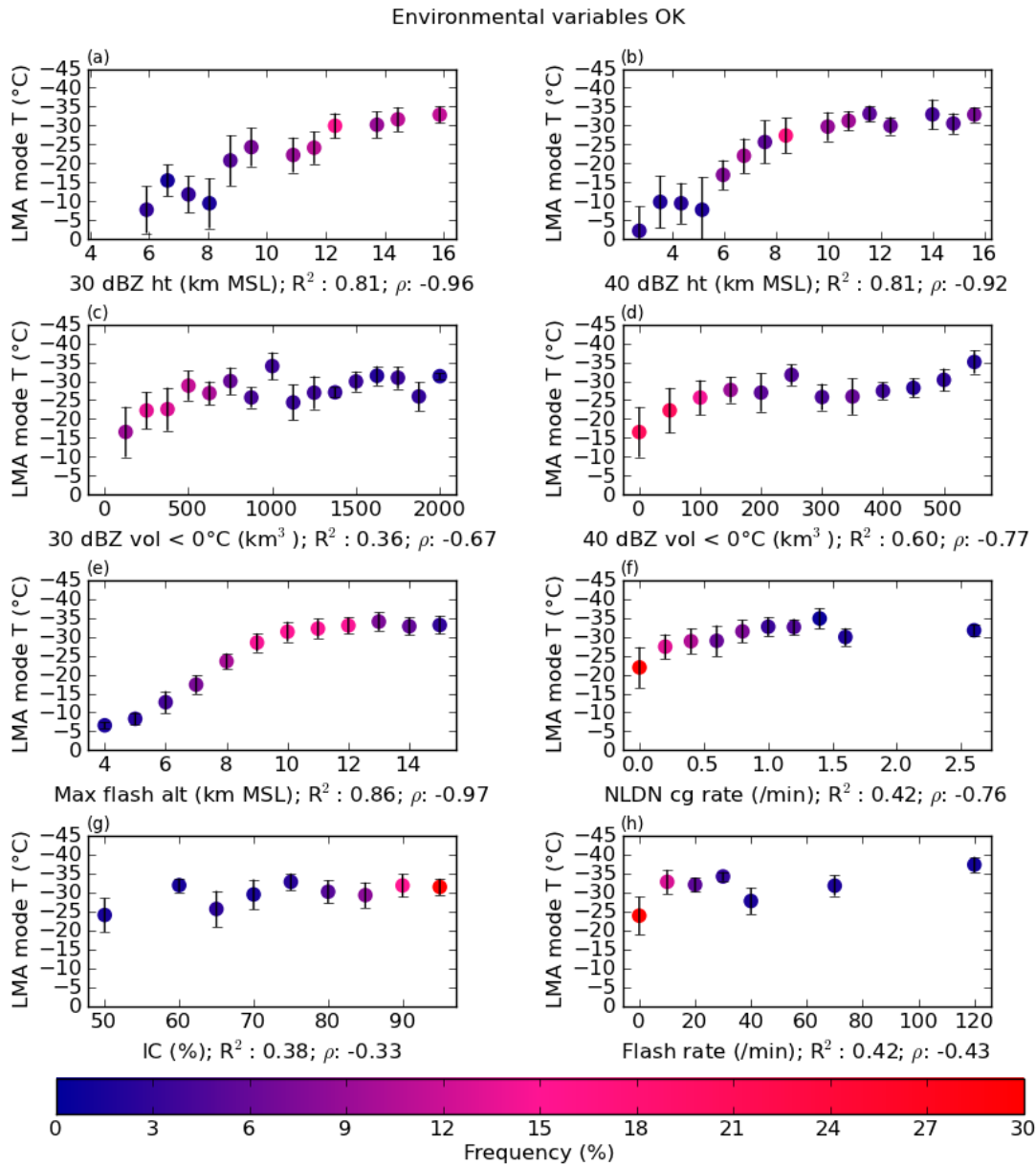


FIG. 3.16. 8 panel plot of environmental variables and LMA mode temperature for the Oklahoma region. Each point represents the median LMA mode temperature for all storms within a particular bin. Error bars indicate the median absolute deviation of the LMA mode temperature distribution for each bin. Points are colored by the relative population of the horizontal variable following the bottom colorbar. R^2 value represents the goodness of fit to a linear function. ρ value represents the how well the relationship can be represented by a monotonic function.

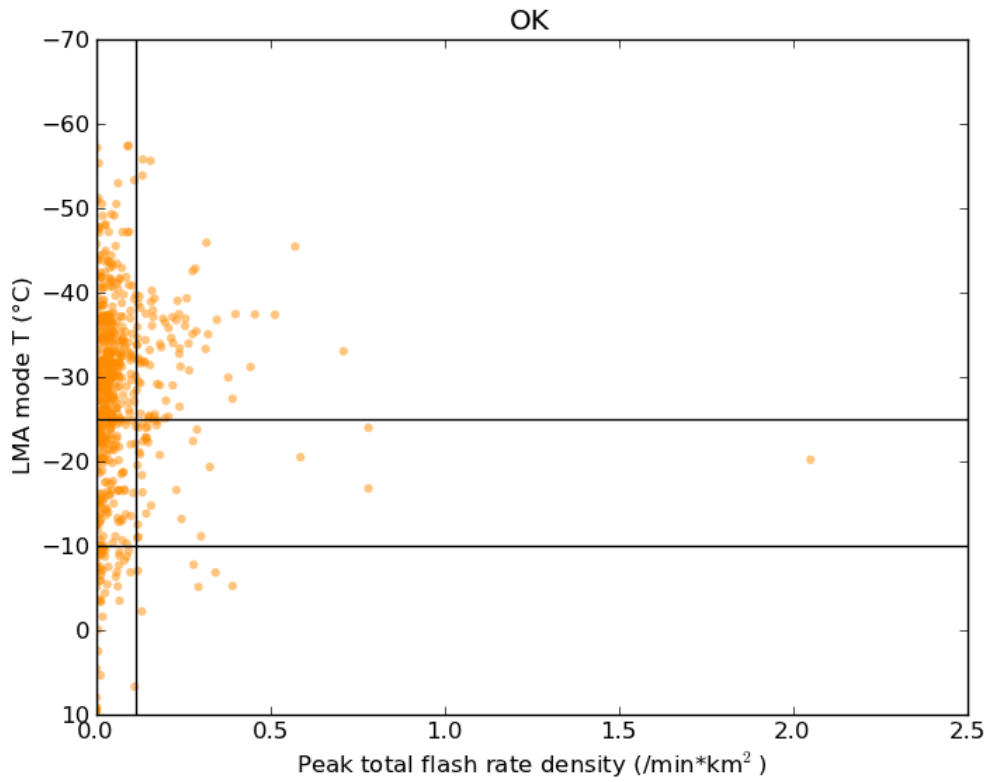


FIG. 3.17. Total flash rate density normalized by storm 30 dBZ composite area and LMA mode temperature for Oklahoma storms. The vertical line represents the 90th percentile of flash rate density for all storms in the region. The horizontal lines represent the LMA mode temperature criteria. Storms in that box are considered inverted by this method.

OK 05/22/2011 - 01:35Z Composite Reflectivity and Surface Temp (filled),
sfc winds (black barb), 500 mb winds (green barb), CAPE (color contour), Dew Point (dashed)

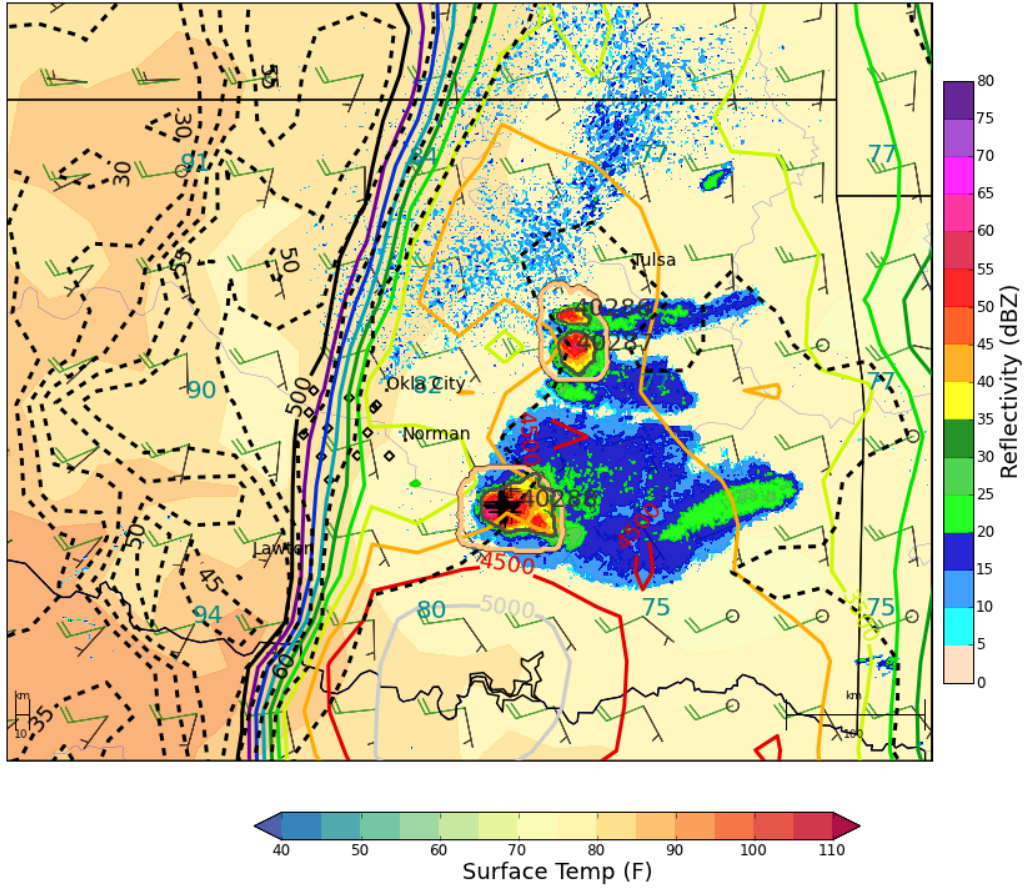


FIG. 3.18. Synoptic setup and composite radar reflectivity for Oklahoma inverted case study. Reflectivity follows colorbar on the right, surface temperature follows the bottom colorbar. Other contours indicated in title. Unique cell identification number is indicated near cell.

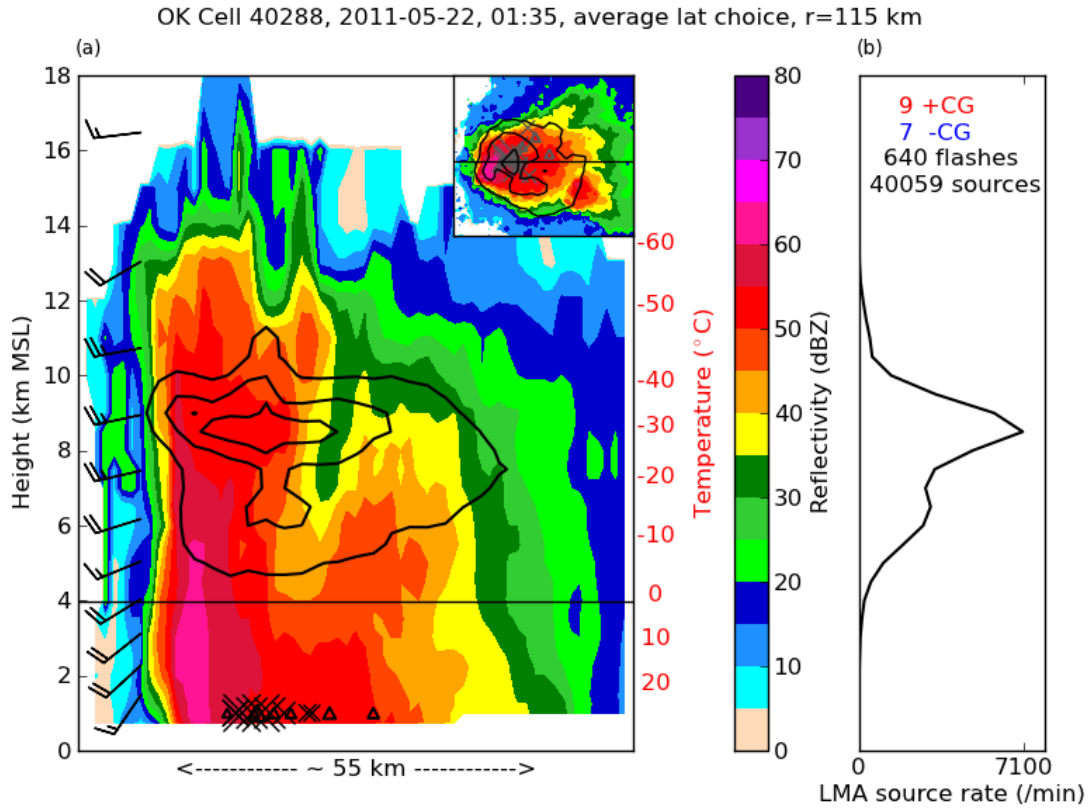


FIG. 3.19. Radar and LMA source density structure of Oklahoma case study. Black contours indicate 2D LMA source density. Barbs on left are wind profile from inflow sounding point. Upper-right panel is a plan view of composite reflectivity with a 2D height integrated source density and the black line indicates the latitude choice of cross section. Temperature is indicated in red text. Total number of flashes and sources are located on the top of the right panel.

Environmental variable CDFs in OK for positive (red) and negative (blue) storms

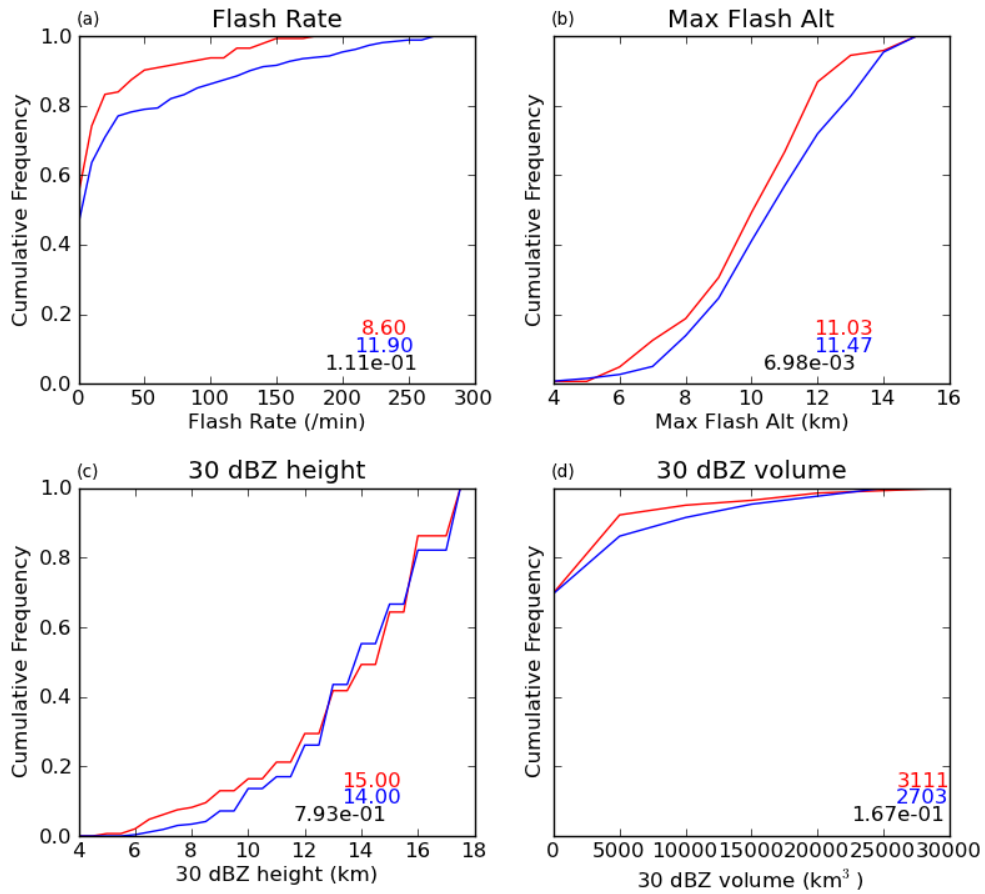


FIG. 3.20. 4 panel plot comparing storm variables between positive (red) and negative (blue) storms in the Oklahoma region. The red number represents the median quantity of the positive storms and the blue number is the median quantity of the negative storms. The black number is the 2-sided p-value of the Wilcoxon rank-sum test.

Environmental variable CDFs in OK for positive (red) and negative (blue) storms

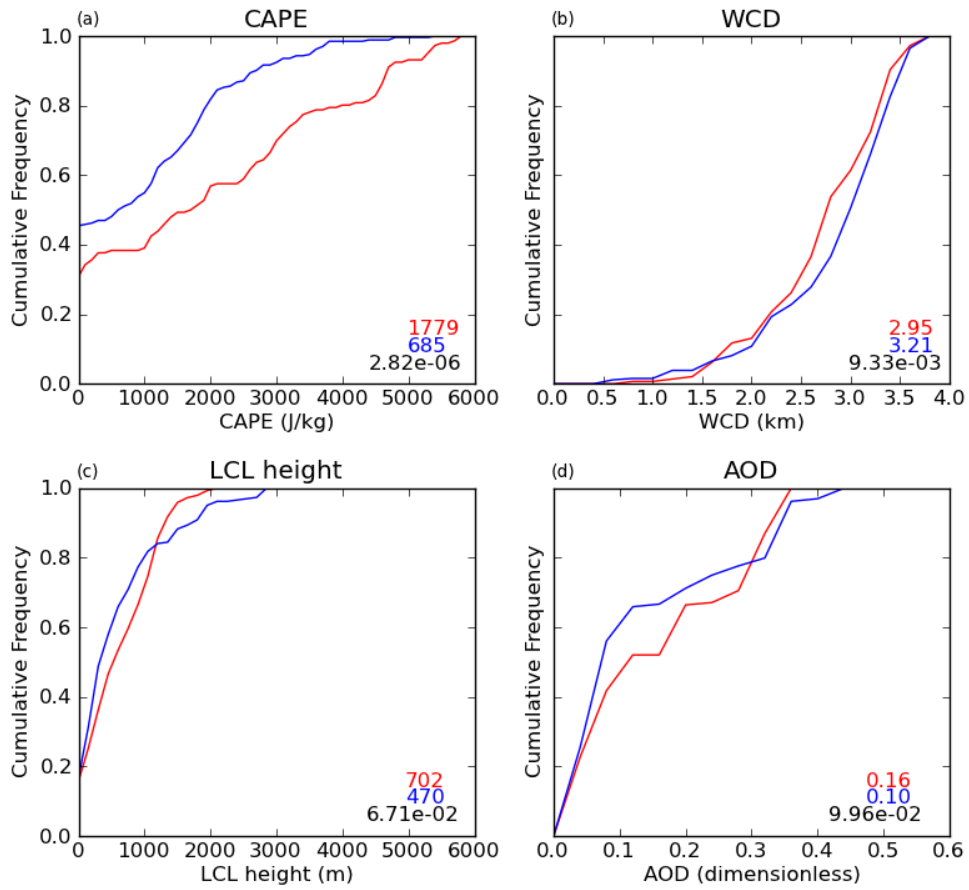


FIG. 3.21. 4 panel plot comparing environmental variables between positive (red) and negative (blue) storms in the Oklahoma region. The red number represents the median quantity of the positive storms and the blue number is the median quantity of the negative storms. The black number is the 2-sided p-value of the Wilcoxon rank-sum test.

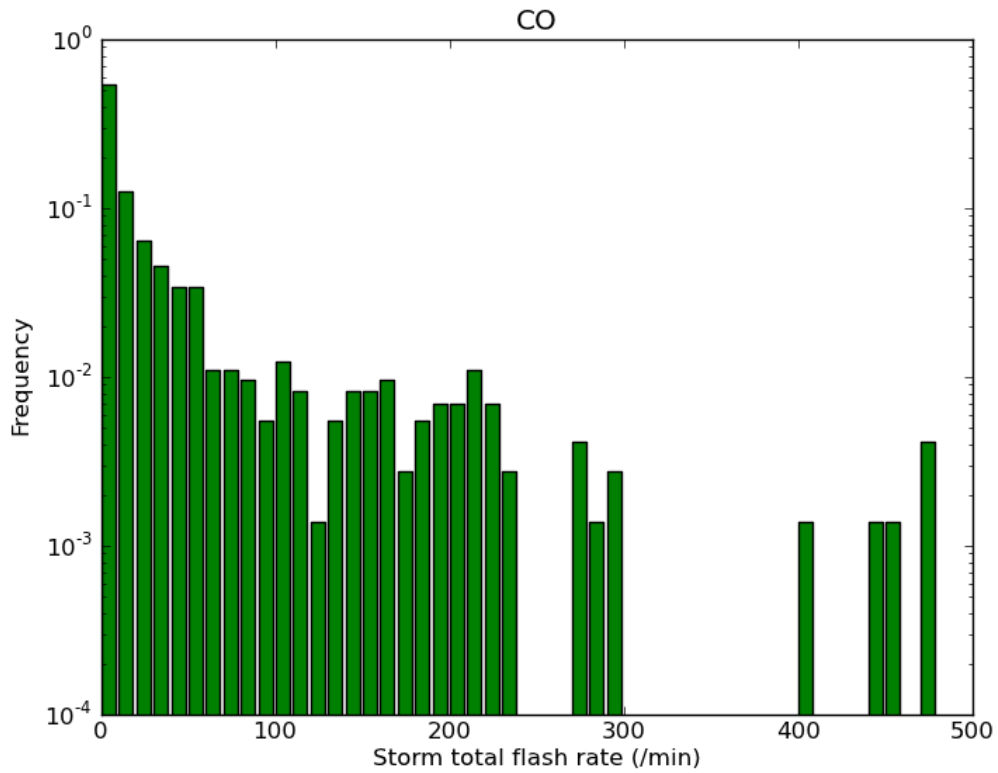


FIG. 3.22. Probability Distribution Function (PDF) of storm total flash rates in isolated Colorado convective cells. Colors here will remain consistent throughout the study. Note the log scale on the vertical axis.

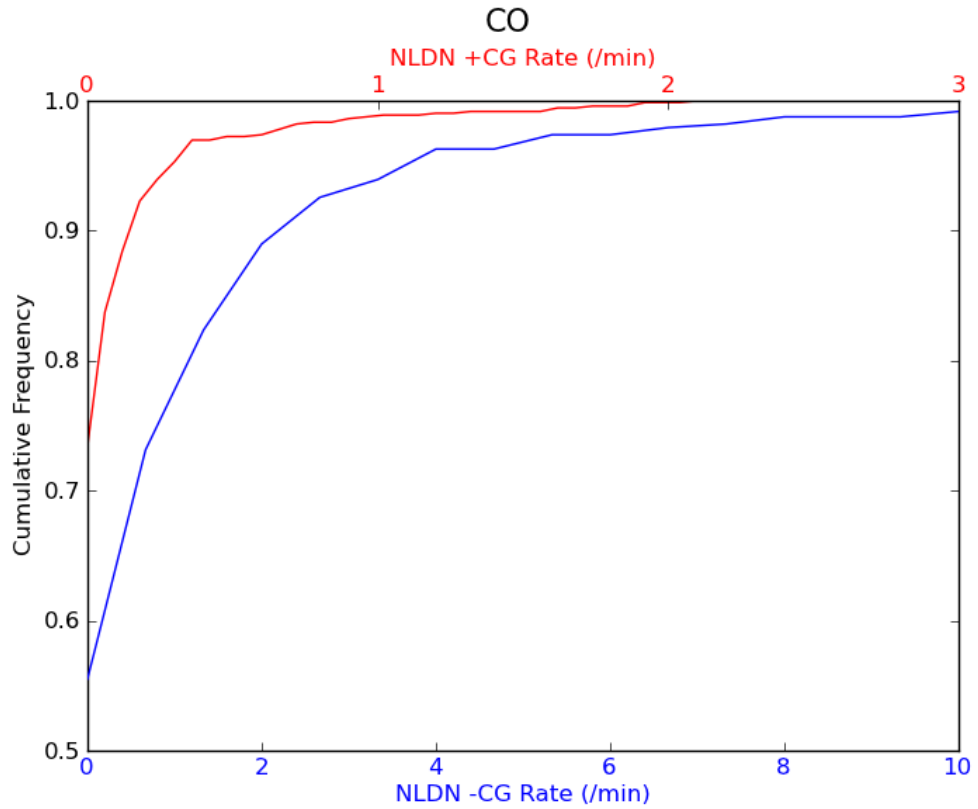


FIG. 3.23. Cumulative distribution function (CDF) of +CG rate (red) and CG rate (blue) for all storms in the Oklahoma region. Note that the vertical axis starts at 0.5 because many storms did not produce any CG lightning.

Storm variables CO

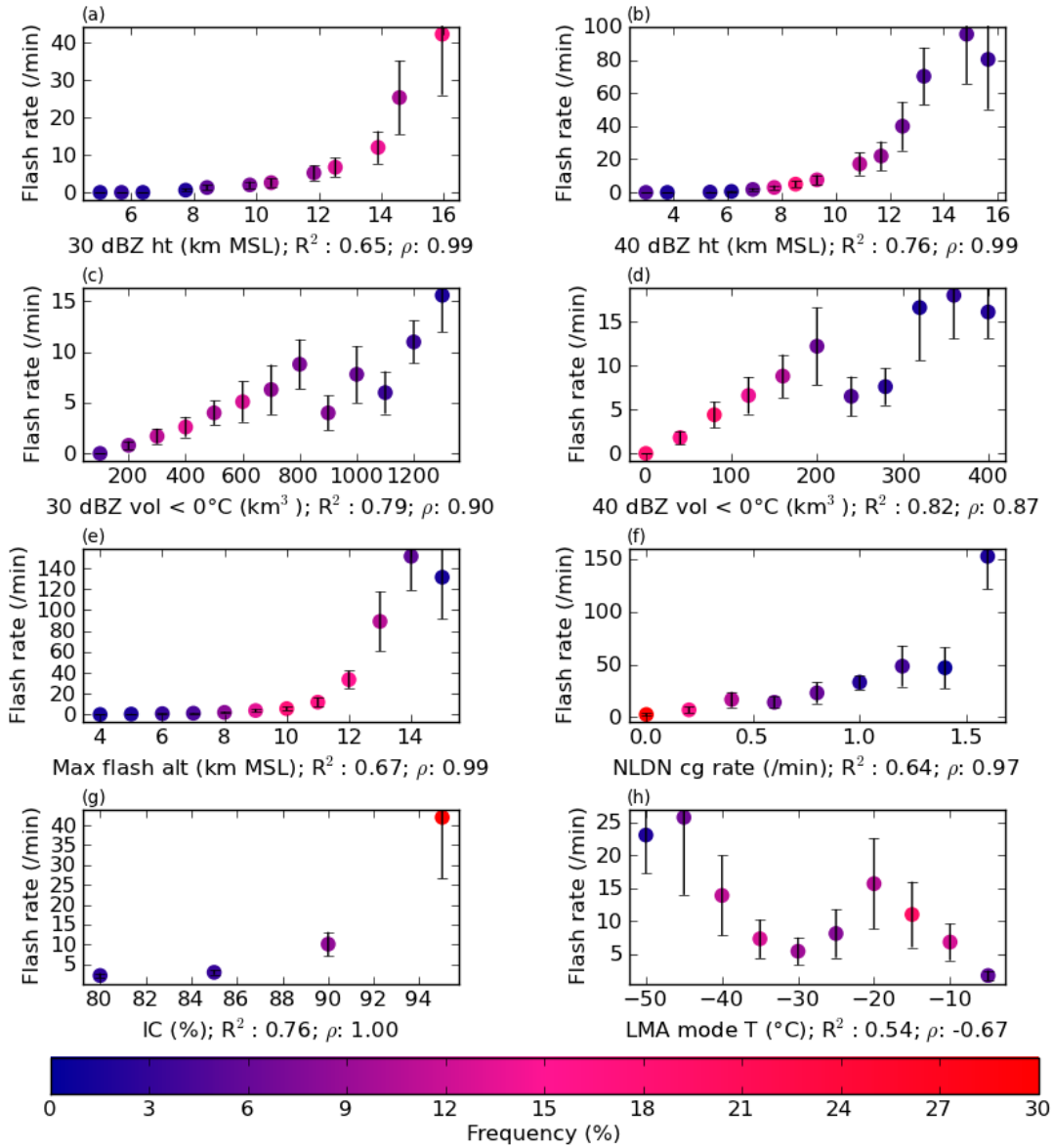


FIG. 3.24. 8 panel plot of storm variables and flash rates for the Oklahoma region. Each point represents the median flash rate for all storms within a particular bin. Error bars indicate the median absolute deviation of the flash rate distribution for each bin. Points are colored by the relative population of the horizontal variable following the bottom colorbar. R^2 value represents the goodness of fit to a linear function. ρ value represents the how well the relationship can be represented by a monotonic function.

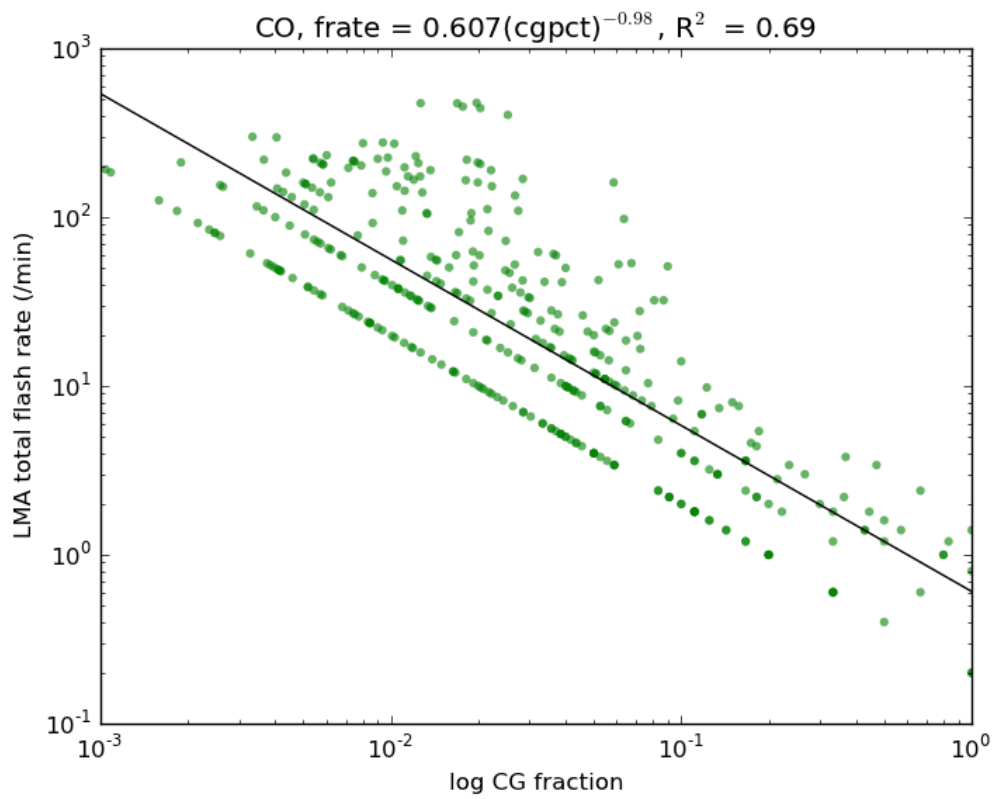


FIG. 3.25. Log of total flash rate versus log of CG fraction for storms in Oklahoma. The best fit line parameters are displayed in the title along with the linear correlation coefficient

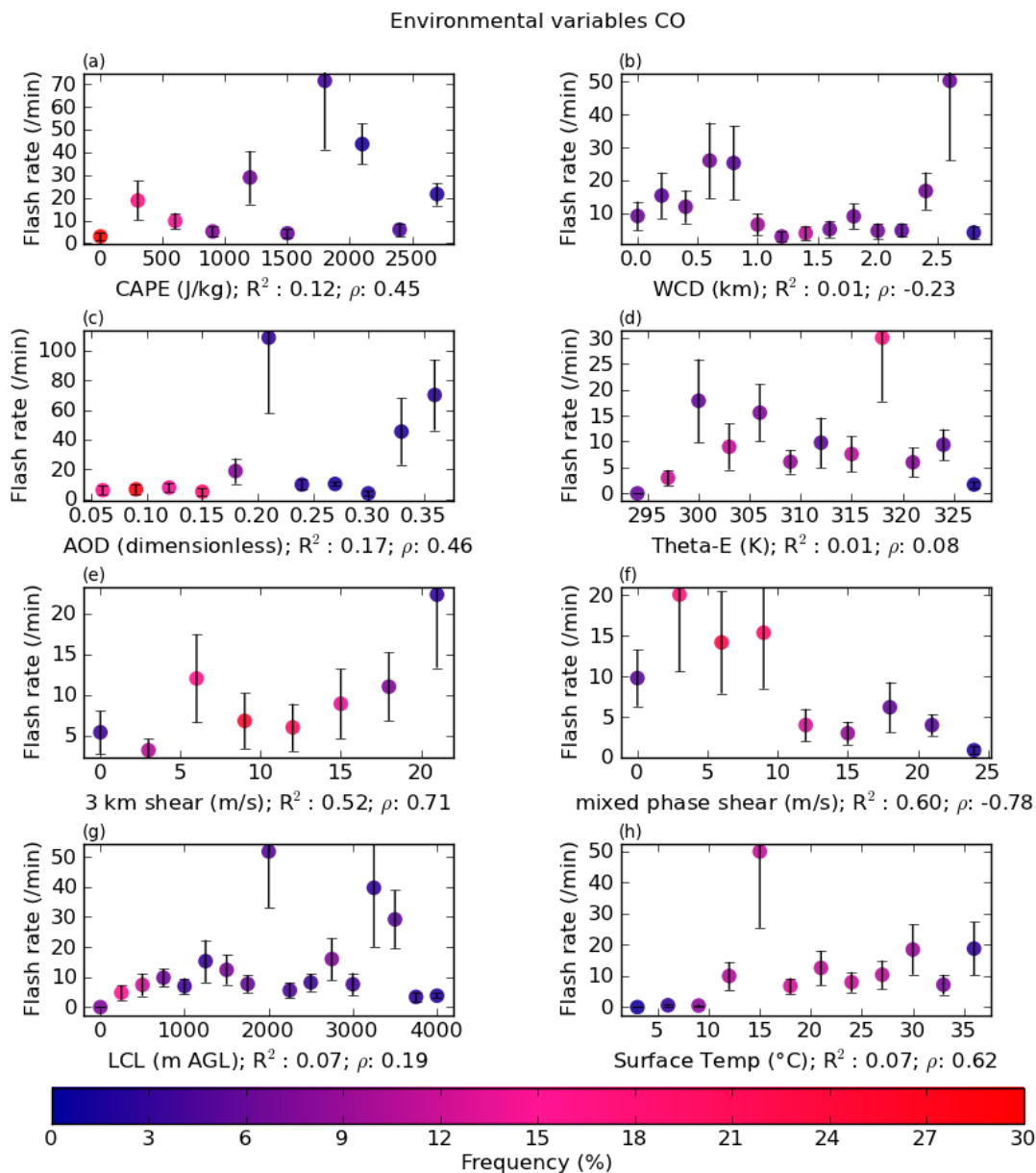


FIG. 3.26. 8 panel plot of environmental variables and flash rates for the Oklahoma region. Each point represents the median flash rate for all storms within a particular bin. Error bars indicate the median absolute deviation of the flash rate distribution for each bin. Points are colored by the relative population of the horizontal variable following the bottom colorbar. R^2 value represents the goodness of fit to a linear function. ρ value represents the how well the relationship can be represented by a monotonic function.

Environmental variables CO

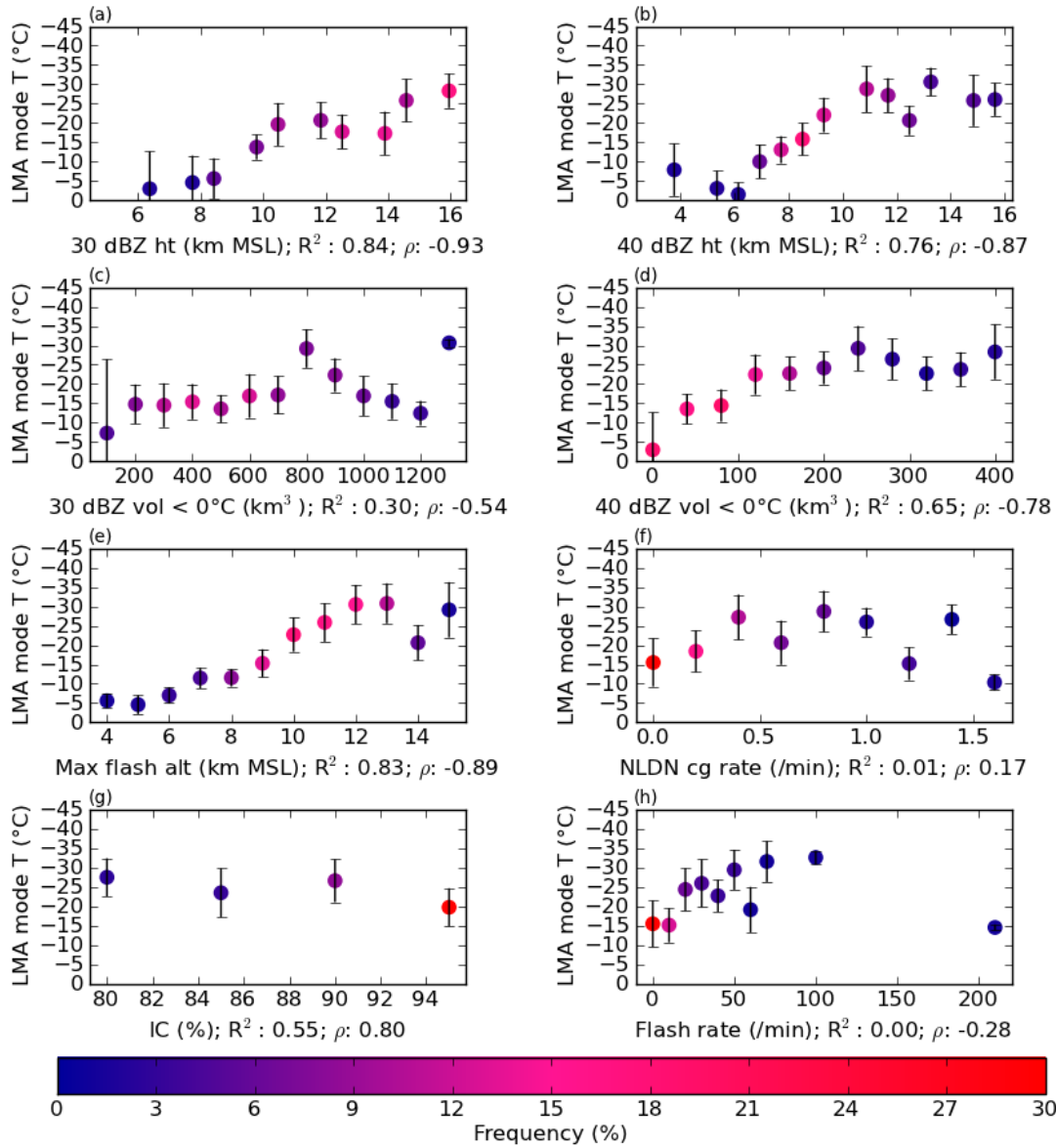


FIG. 3.27. 8 panel plot of environmental variables and LMA mode temperature for the Colorado region. Each point represents the median LMA mode temperature for all storms within a particular bin. Error bars indicate the median absolute deviation of the LMA mode temperature distribution for each bin. Points are colored by the relative population of the horizontal variable following the bottom colorbar. R^2 value represents the goodness of fit to a linear function. ρ value represents the how well the relationship can be represented by a monotonic function.

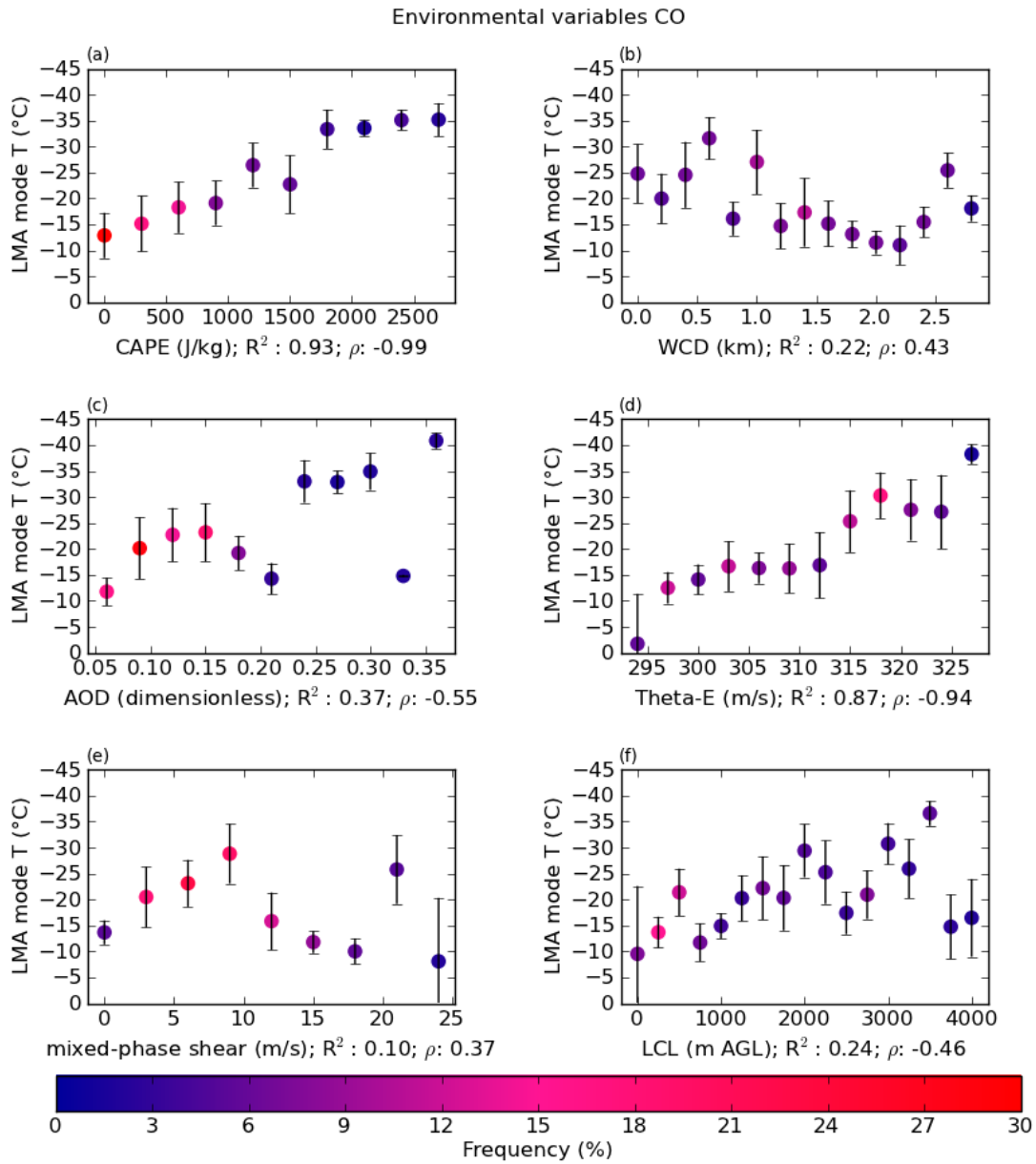


FIG. 3.28. 6 panel plot similar to previous plot but shows relationships between environmental parameters and LMA mode temperatures in Colorado. Points, colors and bars all follow previous figures.

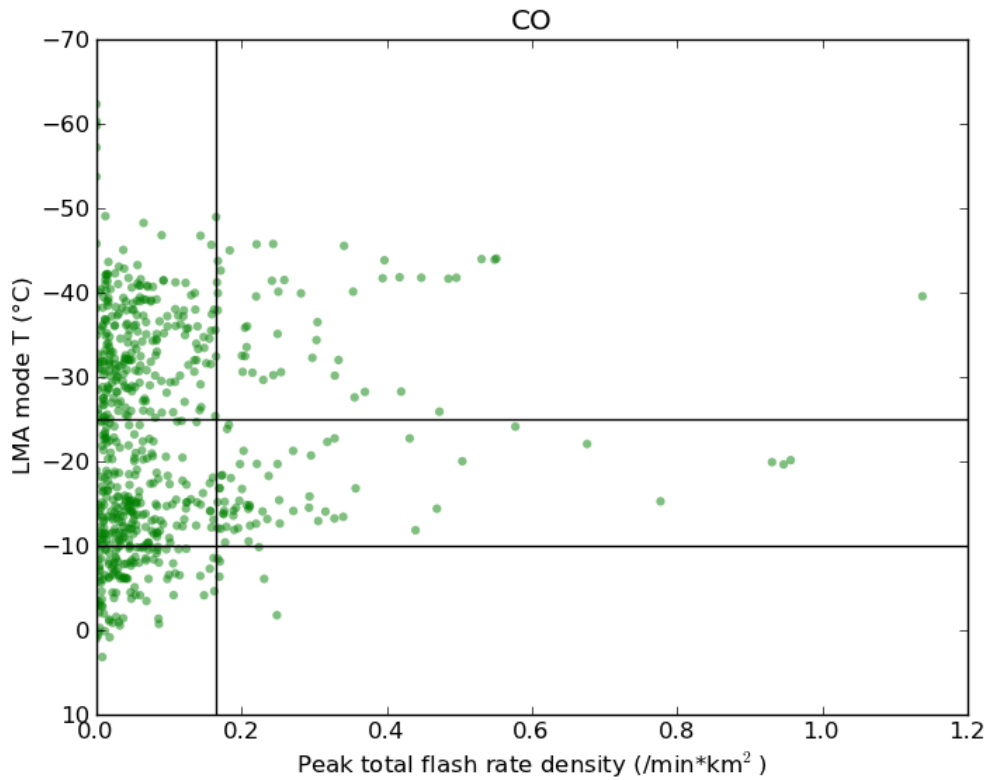


FIG. 3.29. Total flash rate density normalized by storm 30 dBZ composite area and LMA mode temperature for Oklahoma storms. The vertical line represents the 90th percentile of flash rate density for all storms in the region. The horizontal lines represent the LMA mode temperature criteria. Storms in that box are considered inverted by this method.

CO 06/06/2012 - 21:35Z Composite Reflectivity and Surface Temp (filled),
 sfc winds (black barb), 500 mb winds (green barb), CAPE (color contour), Dew Point (dashed)

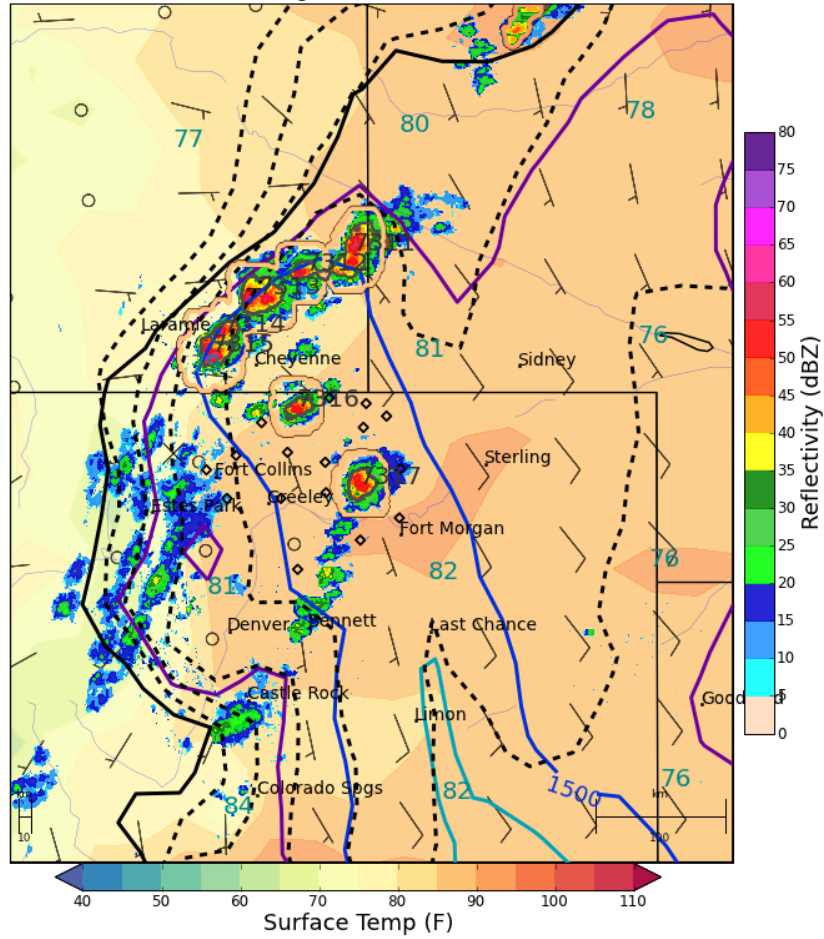


FIG. 3.30. Synoptic setup and composite radar reflectivity for Oklahoma inverted case study. Reflectivity follows colorbar on the right, surface temperature follows the bottom colorbar. Other contours indicated in title. Unique cell identification number is indicated near cell.

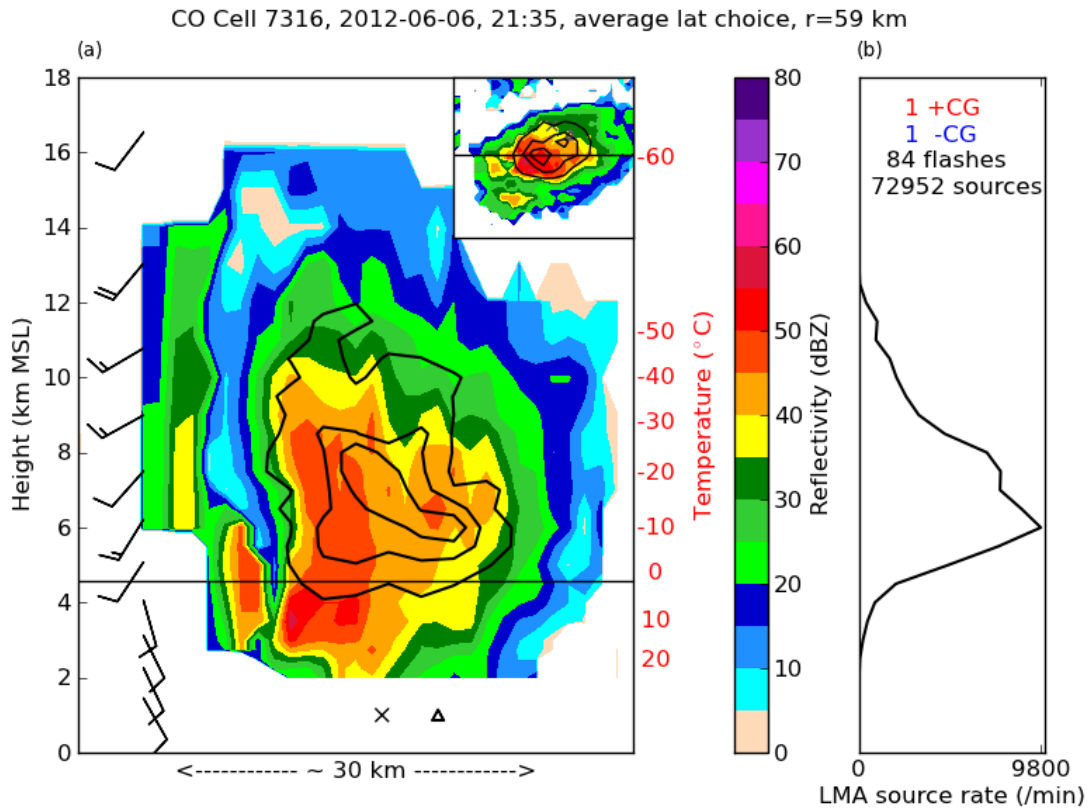


FIG. 3.31. Radar and LMA source density structure of Oklahoma case study. Black contours indicate 2D LMA source density. Barbs on left are wind profile from inflow sounding point. Upper-right panel is a plan view of composite reflectivity with a 2D height integrated source density and the black line indicates the latitude choice of cross section. Temperature is indicated in red text. Total number of flashes and sources are located on the top of the right panel.

Environmental variable CDFs in CO for positive (red) and negative (blue) storms

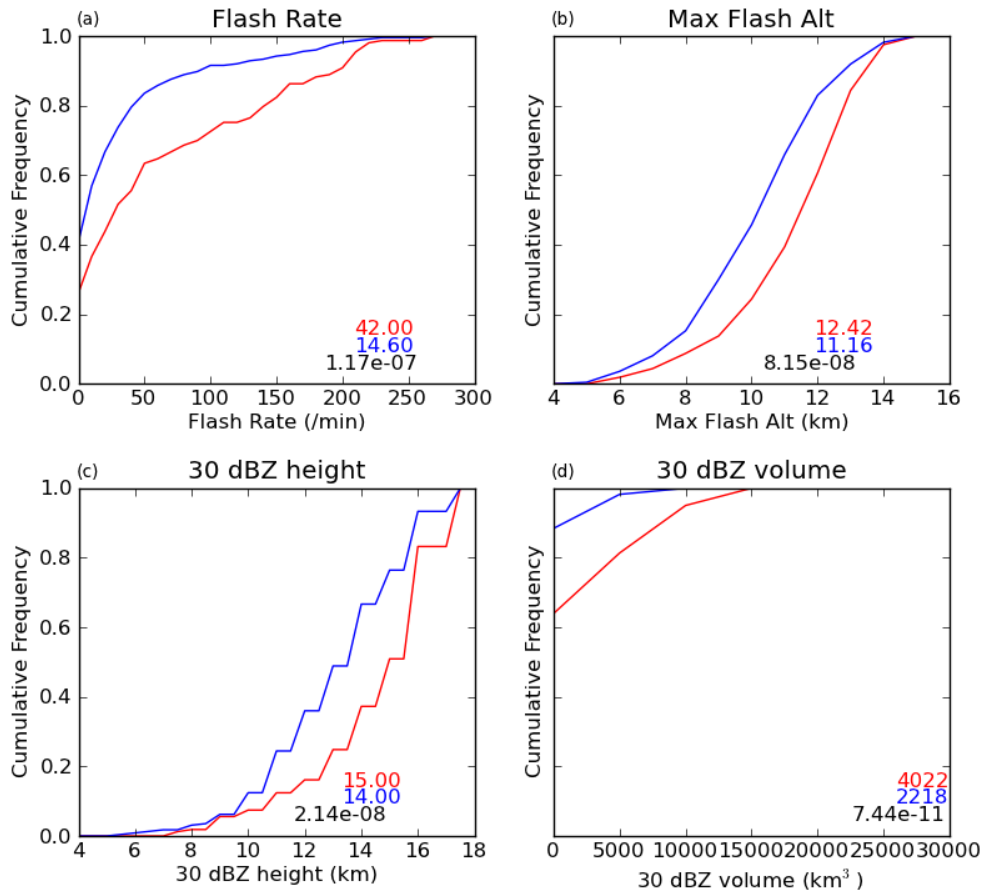


FIG. 3.32. 4 panel plot comparing storm variables between positive (red) and negative (blue) storms in the Oklahoma region. The red number represents the median quantity of the positive storms and the blue number is the median quantity of the negative storms. The black number is the 2-sided p-value of the Wilcoxon rank-sum test.

Environmental variable CDFs in CO for positive (red) and negative (blue) storms

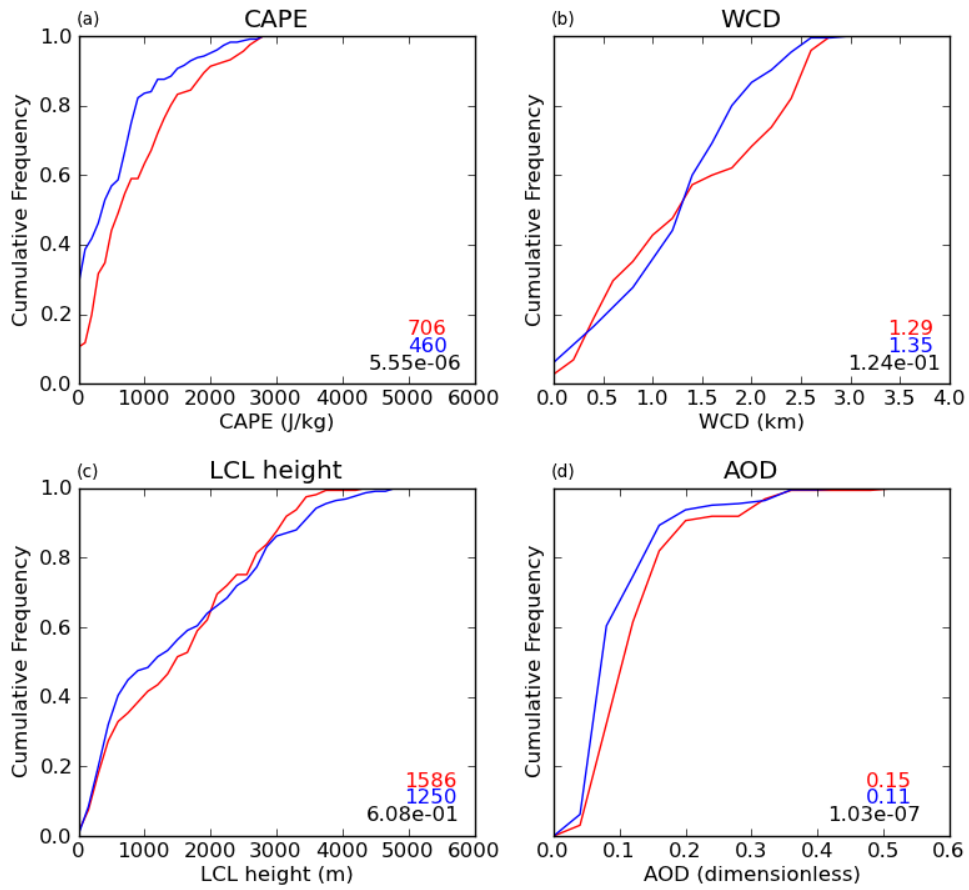


FIG. 3.33. 4 panel plot comparing environmental variables between positive (red) and negative (blue) storms in the Oklahoma region. The red number represents the median quantity of the positive storms and the blue number is the median quantity of the negative storms. The black number is the 2-sided p-value of the Wilcoxon rank-sum test.

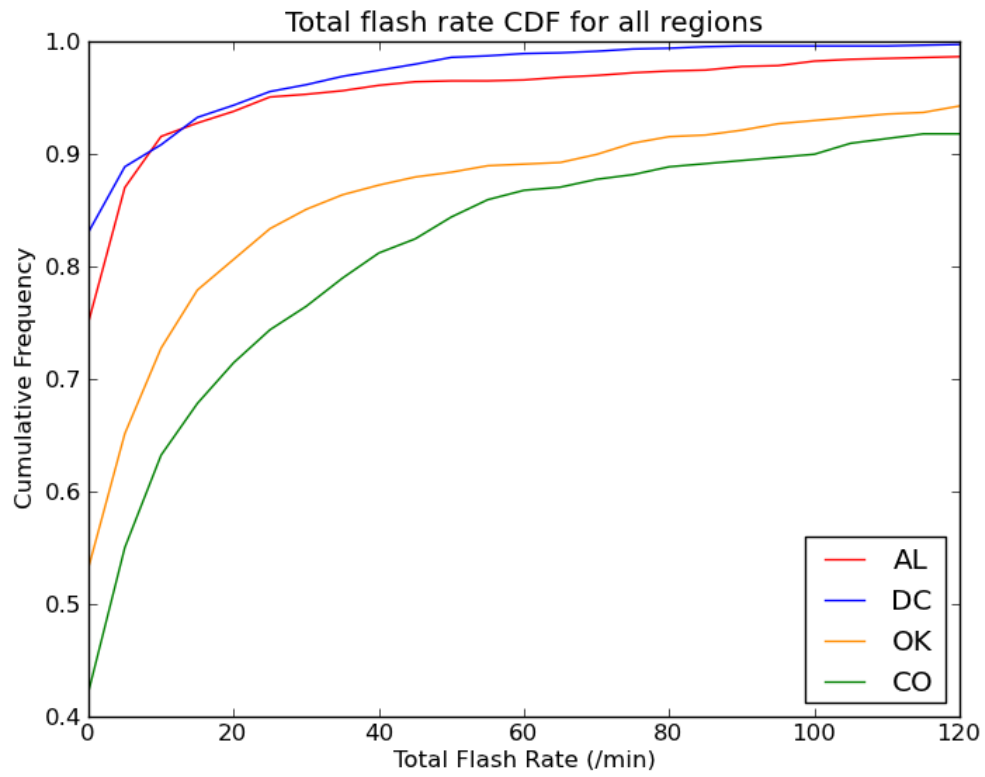


FIG. 3.34. CDF of storm total flash rates for each region. Colors are indicated in the legend.

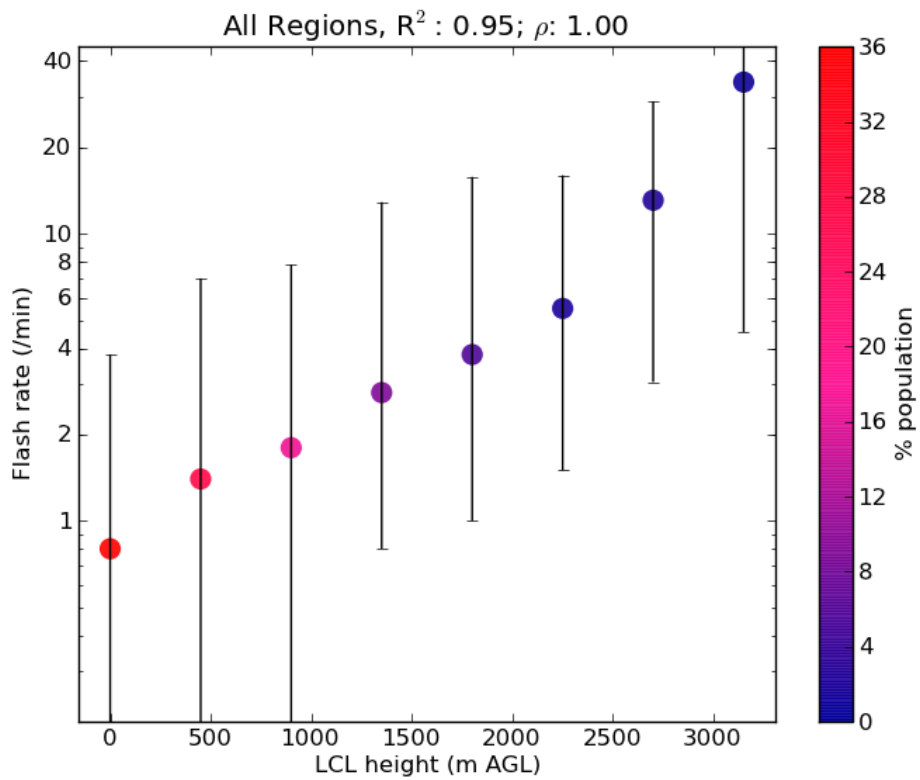


FIG. 3.35. Log flash rate and LCL heights for all storms in all regions of study. Points denote the median flash rates for each LCL bin. Bottom error bar denotes the 25th percentile of the flash rate distribution for each LCL bin. Top bar denotes the 75th percentile of flash rate distribution for each LCL bin. Color of point indicates relative population of LCL heights following the colorbar.

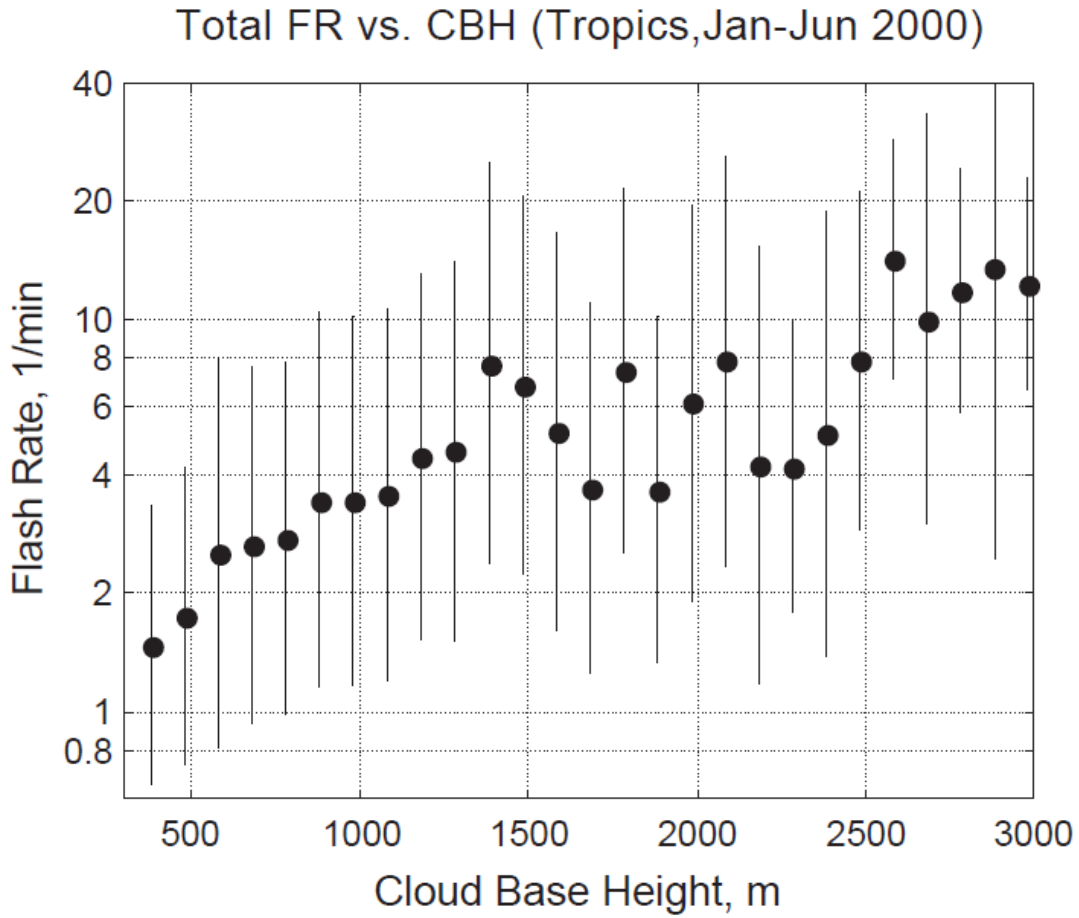


FIG. 3.36. Figure 1 from Williams et al. (2005), showing log of total flash rate measured by the TRMM LIS instrument and maximum dry bulb temperature approximately 1700 storms less than 35 degrees latitude. Figure included for comparison purposes.

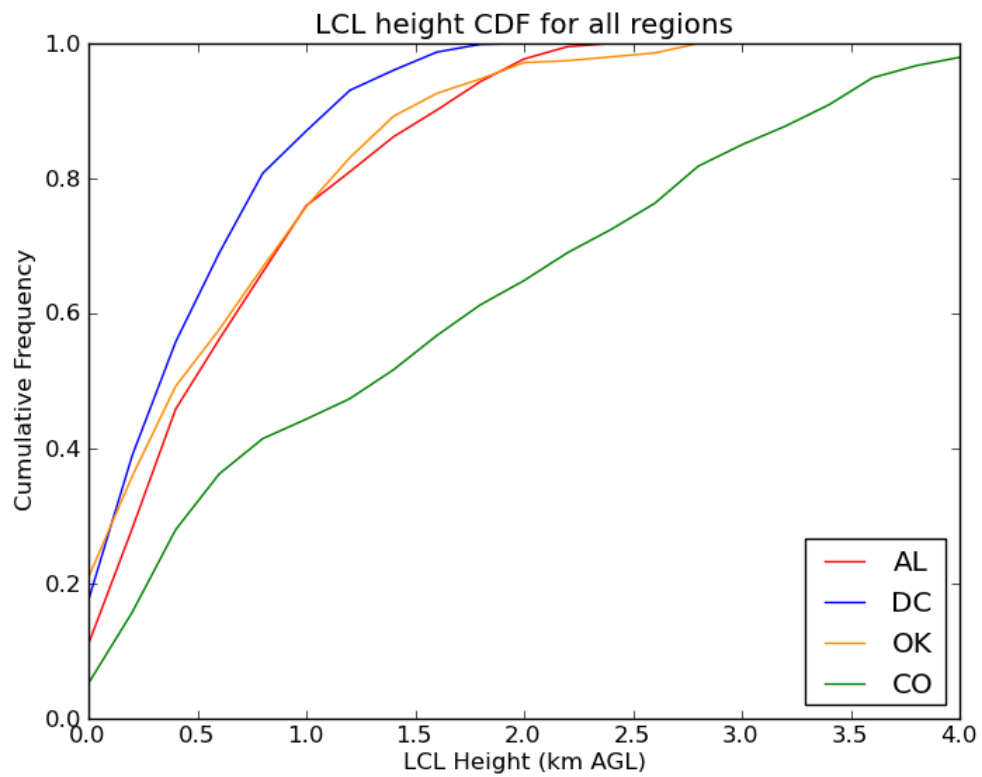


FIG. 3.37. CDFs of LCL heights for each region. Colors follow each region and are indicated in the legend.

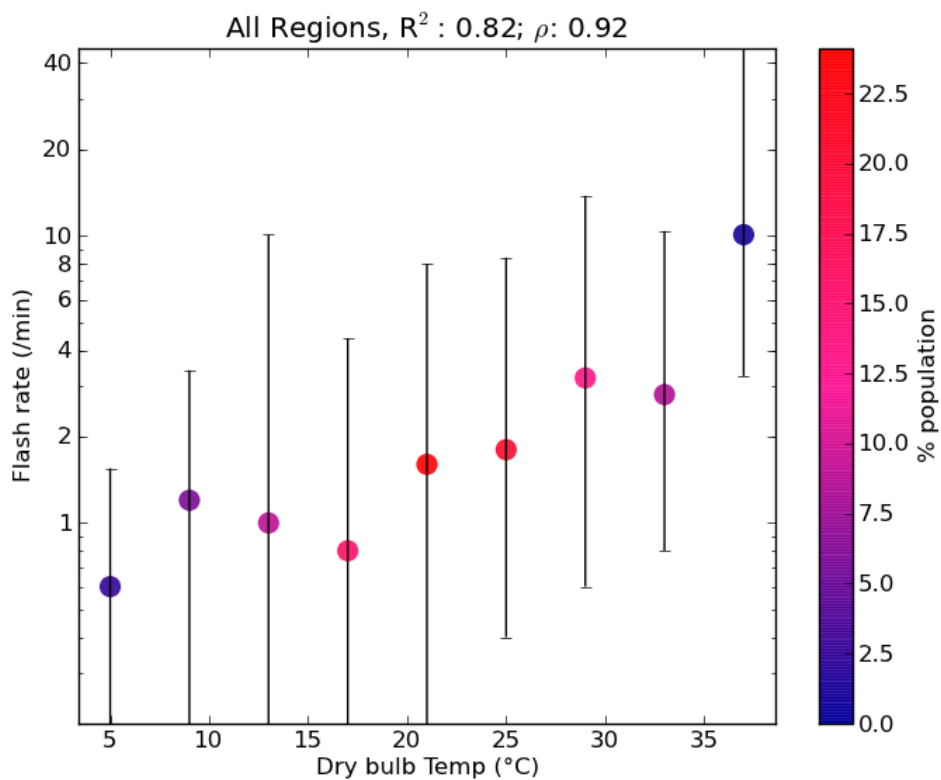


FIG. 3.38. Log flash rate and dry bulb temperatures for all storms in all regions of study. Points denote the median flash rates for each dry bulb temperature bin. Bottom error bar denotes the 25th percentile of the flash rate distribution for each dry bulb temperature bin. Top bar denotes the 75th percentile of flash rate distribution for each dry bulb temperature bin. Color of point indicates relative population of dry bulb temperatures following the colorbar.

Total FR vs. DBT (Tropics, Jan-Jun 2000)

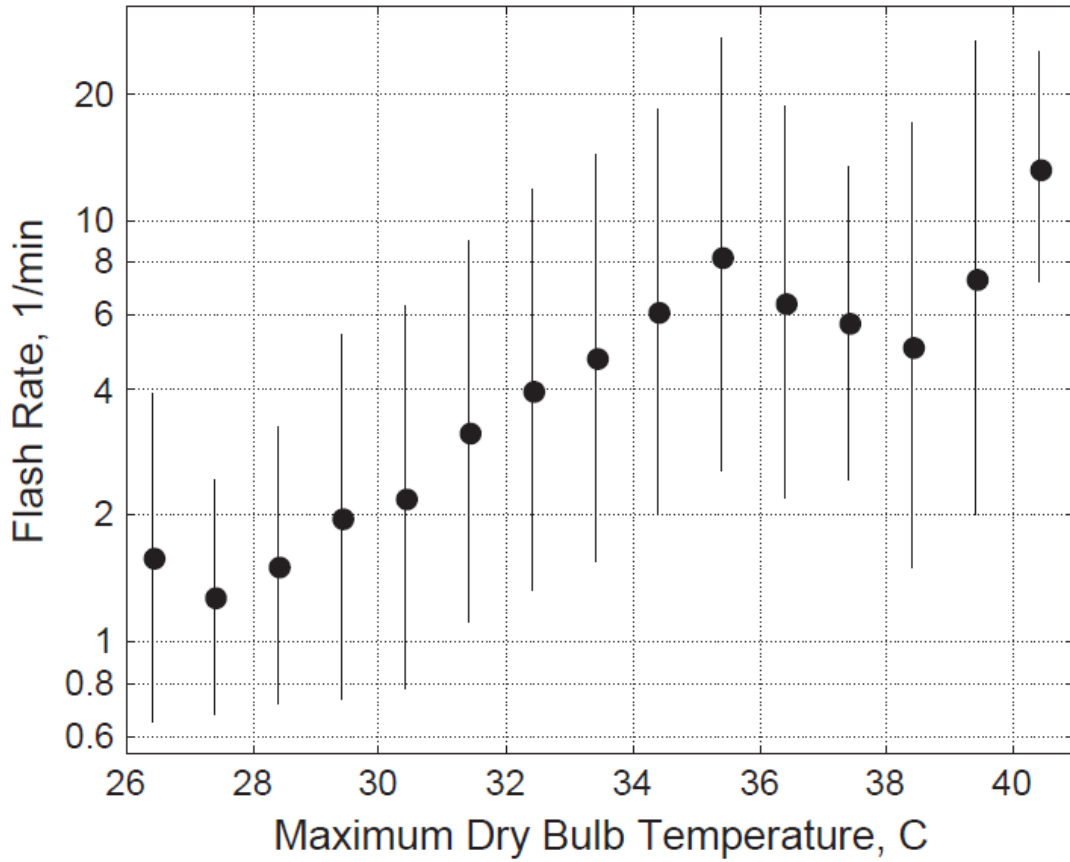


FIG. 3.39. Figure 2 from Williams et al. (2005), showing log of total flash rate measured by the TRMM LIS instrument and maximum dry bulb temperature approximately 1700 storms less than 35 degrees latitude. Figure included for comparison purposes.

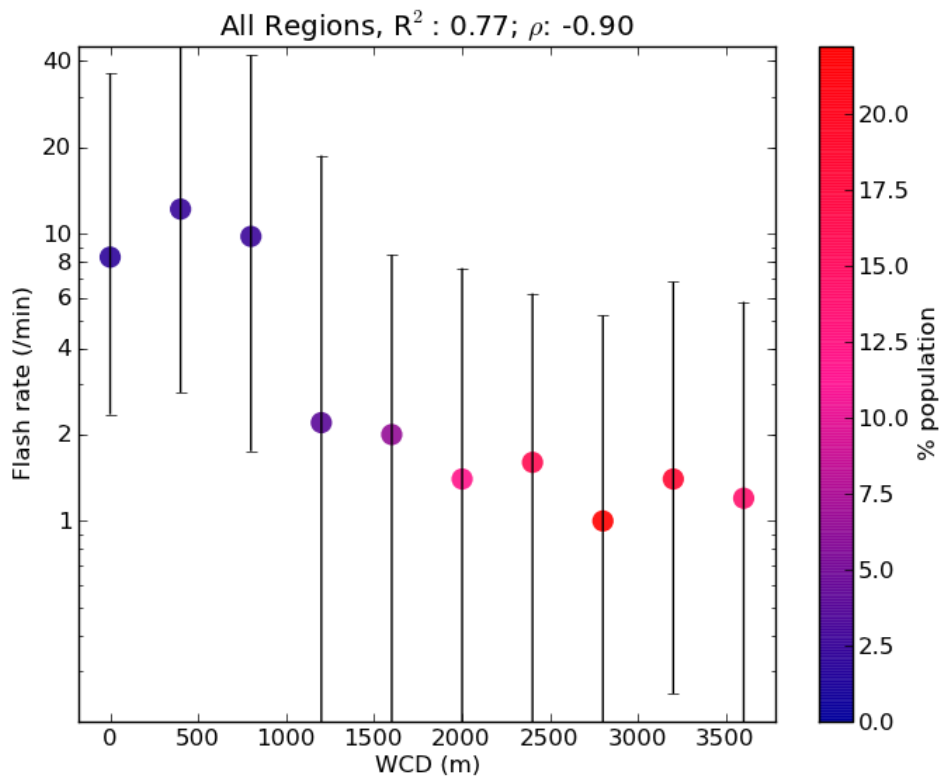


FIG. 3.40. Log flash rate and WCD values for all storms in all regions of study. Points denote the median flash rates for each WCD bin. Bottom error bar denotes the 25th percentile of the flash rate distribution for each WCD bin. Top bar denotes the 75th percentile of flash rate distribution for each LCL bin. Color of point indicates relative population of WCD values following the colorbar.

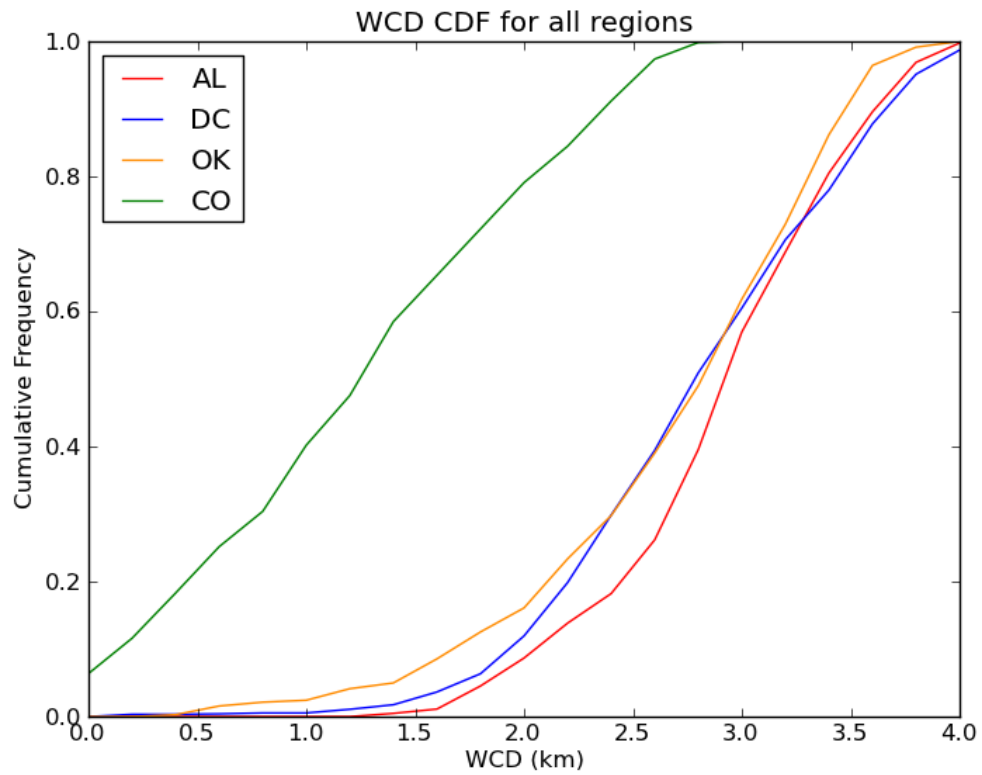


FIG. 3.41. CDFs of WCDs for each region. Colors follow each region and are indicated in the legend.

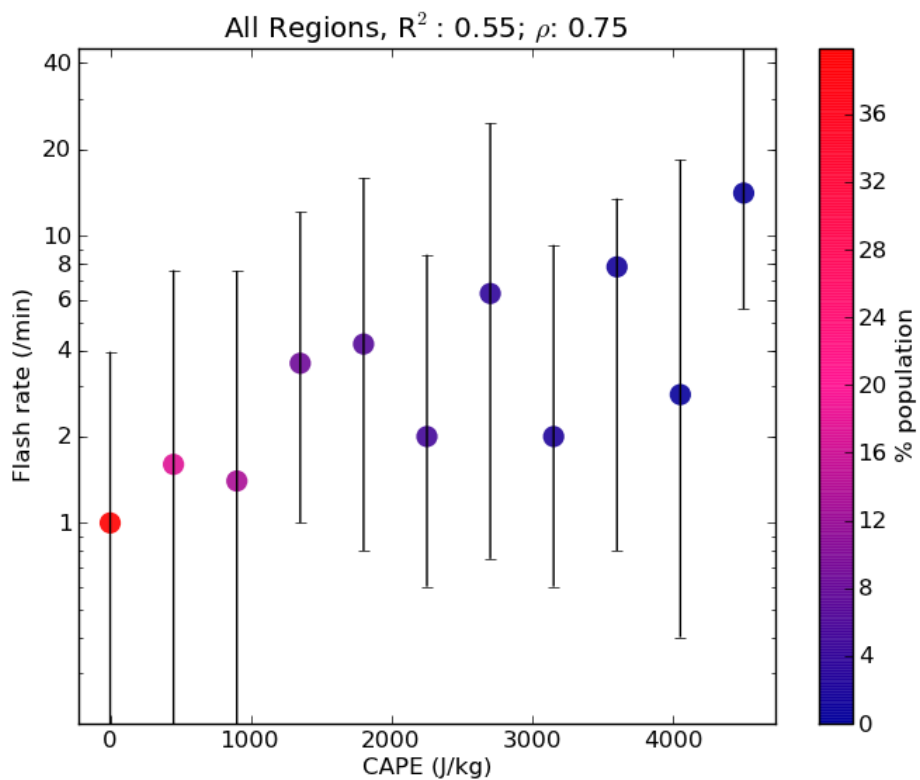


FIG. 3.42. Log flash rate and CAPE values for all storms in all regions of study. Points denote the median flash rates for each CAPE bin. Bottom error bar denotes the 25th percentile of the flash rate distribution for each CAPE bin. Top bar denotes the 75th percentile of flash rate distribution for each CAPE bin. Color of point indicates relative population of CAPE values following the colorbar.

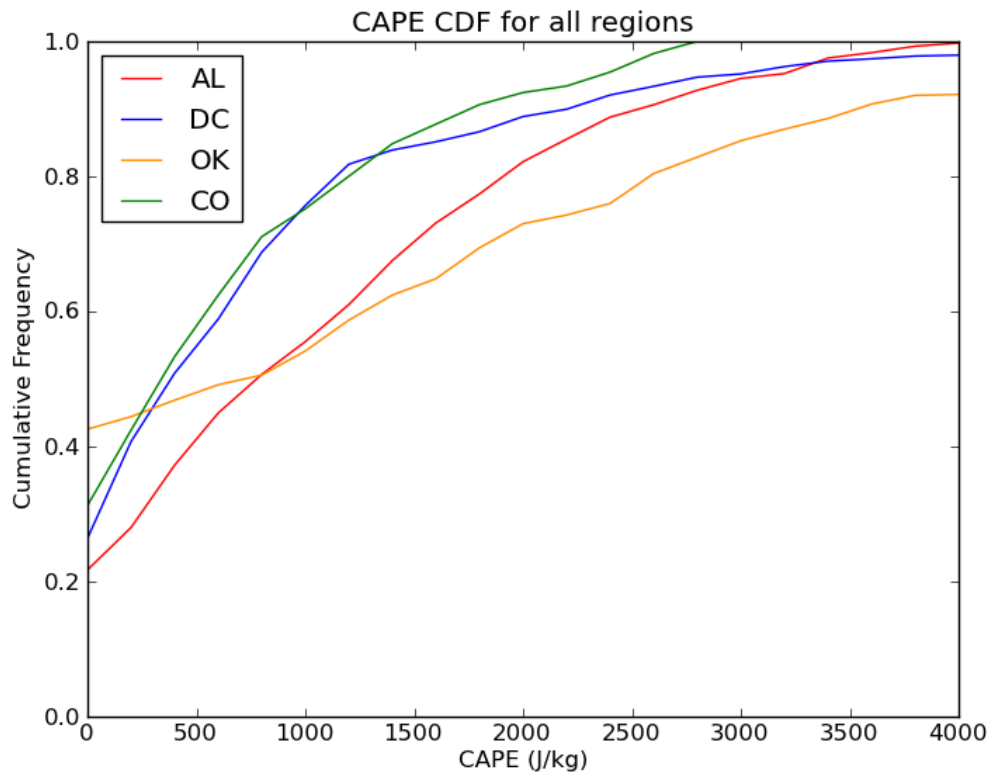


FIG. 3.43. CDFs of CAPE values for each region. Colors follow each region and are indicated in the legend.

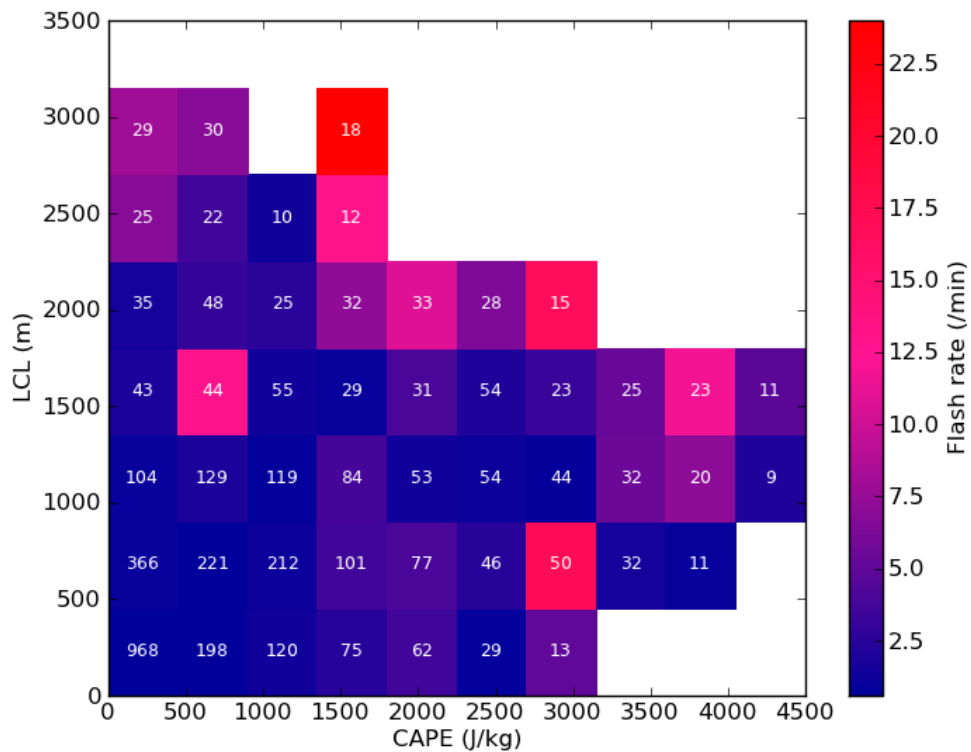


FIG. 3.44. Flash rates as a function of LCL height and CAPE for all storms of study. Median flash rate for each 2D bin is colored following the colorbar. The white numbers denote the number of storm observations in the bin.

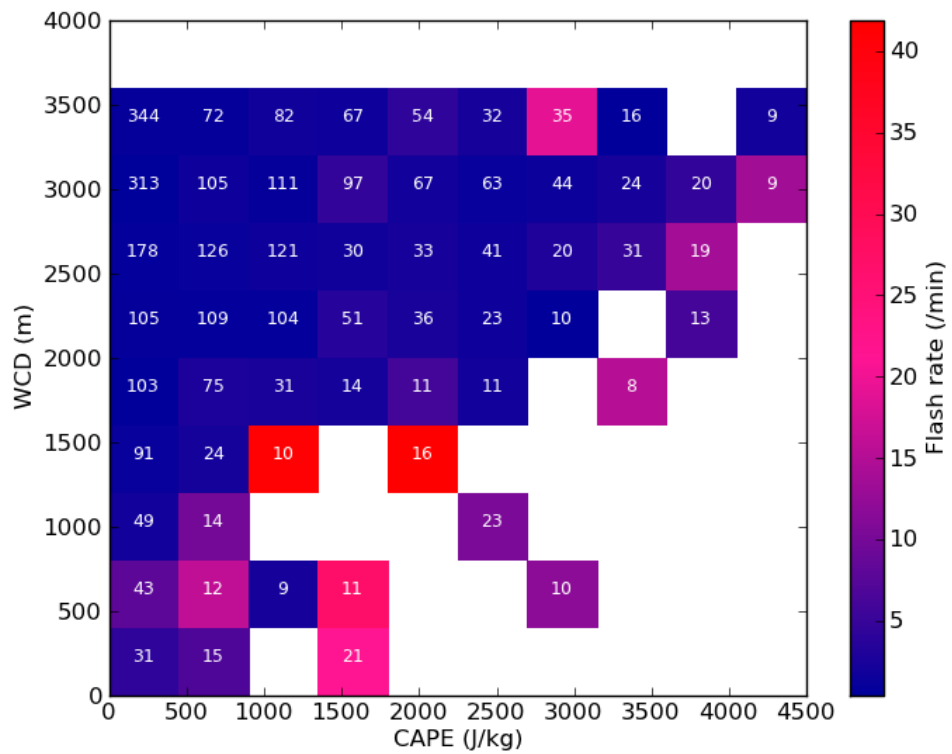


FIG. 3.45. Same as previous figure, but for CAPE and WCD.

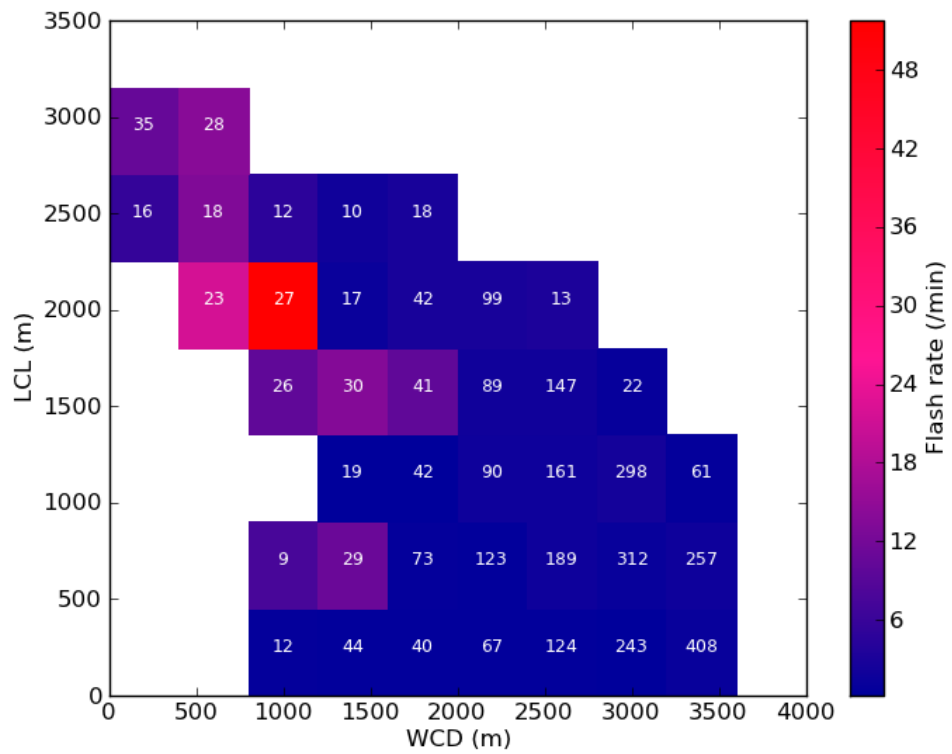


FIG. 3.46. Same as previous figure, but for WCD and LCL.

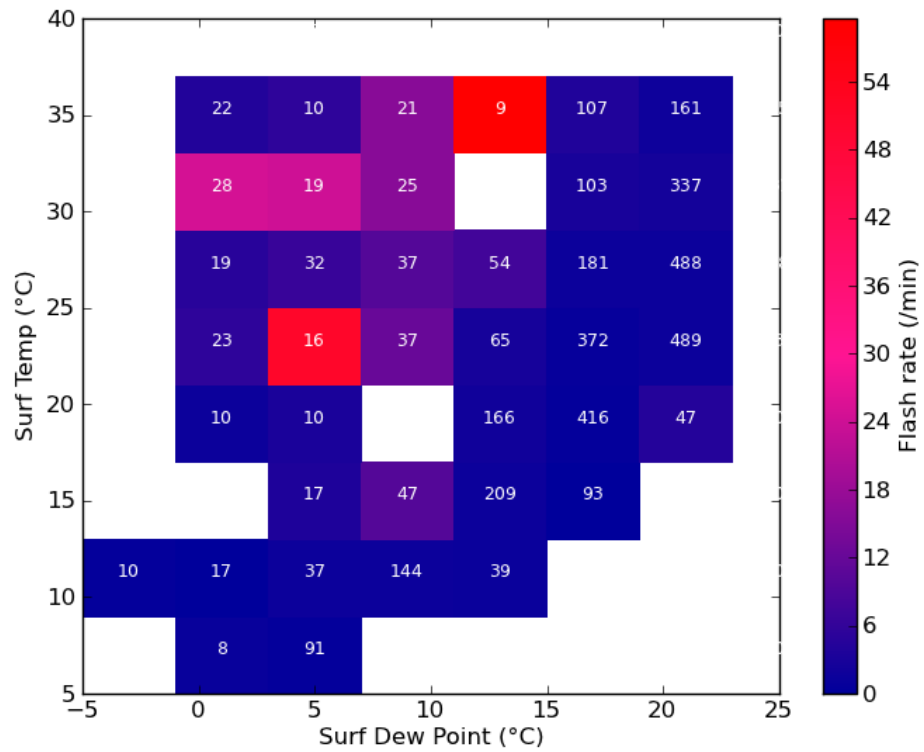


FIG. 3.47. Same as previous figure, but for surface temperature and surface dew point temperature.

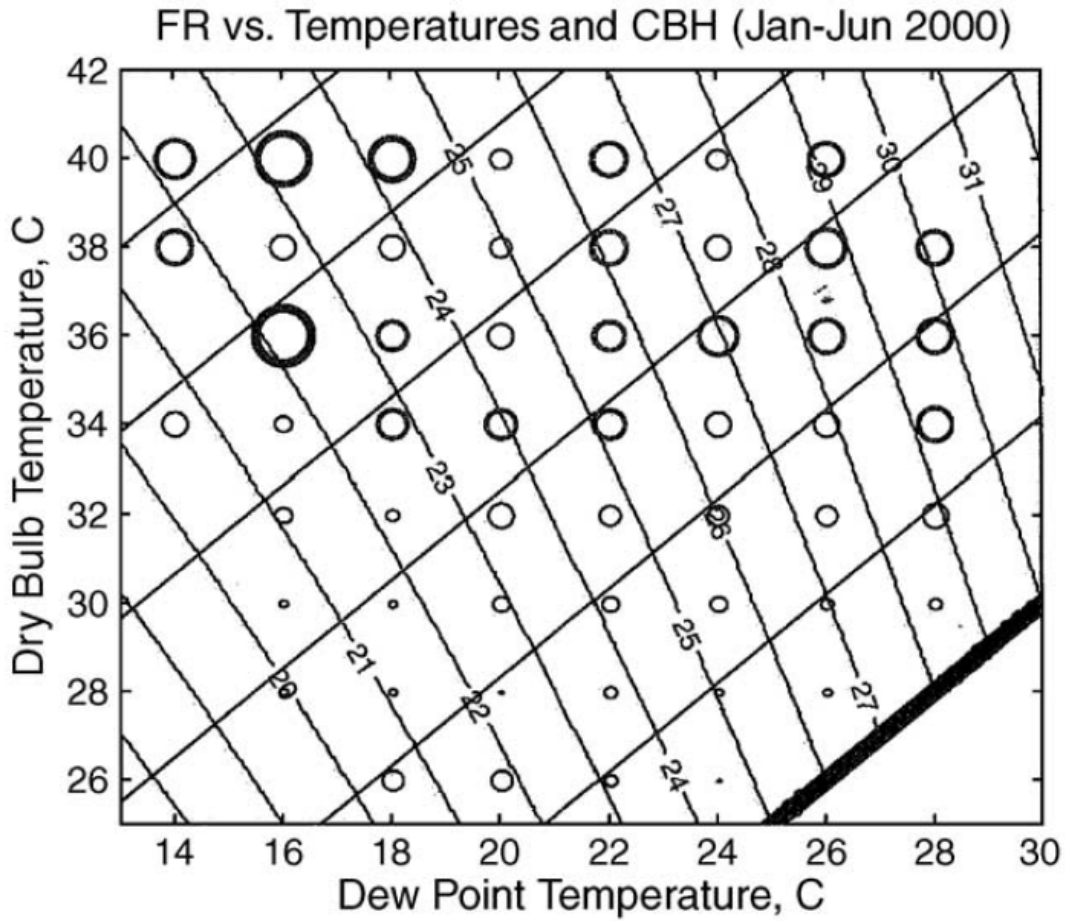


FIG. 3.48. Figure 3 from Williams et al. (2005). Sizes of the circles indicate log of total flash rate for all storms in a particular bin. Effects of surface dry bulb temperature and dew point temperature are shown for 1700 storms less than 35 degrees latitude. Figure included for comparison purposes.

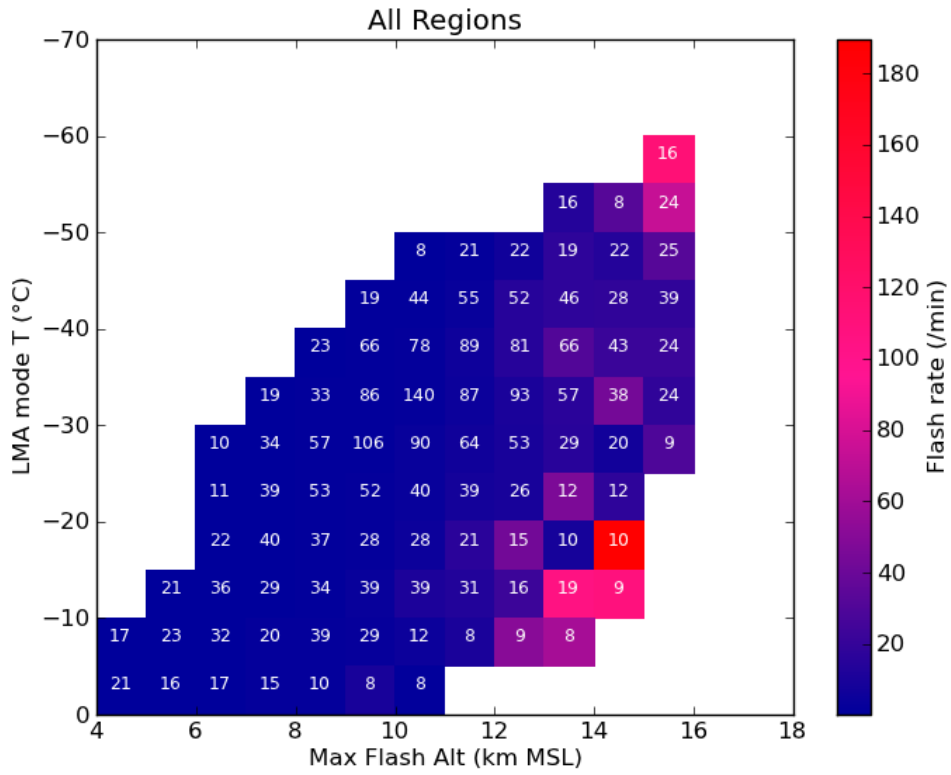


FIG. 3.49. Same as previous figure, but for maximum flash altitude and LMA mode temperature.

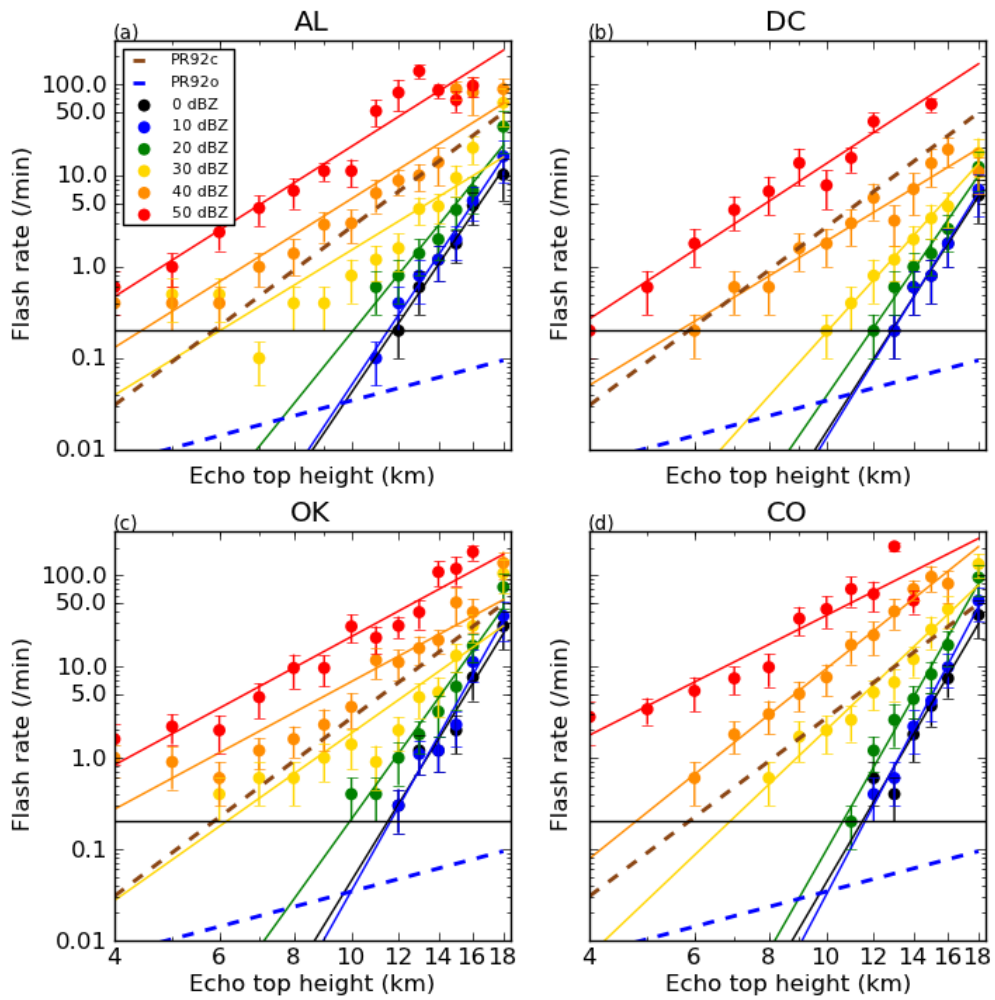


FIG. 3.50. Median flash rate dependence on echo top heights for 0 to 50 dBZ in each region. Bars represent the median absolute deviation for the flash rate distribution for each height bin.

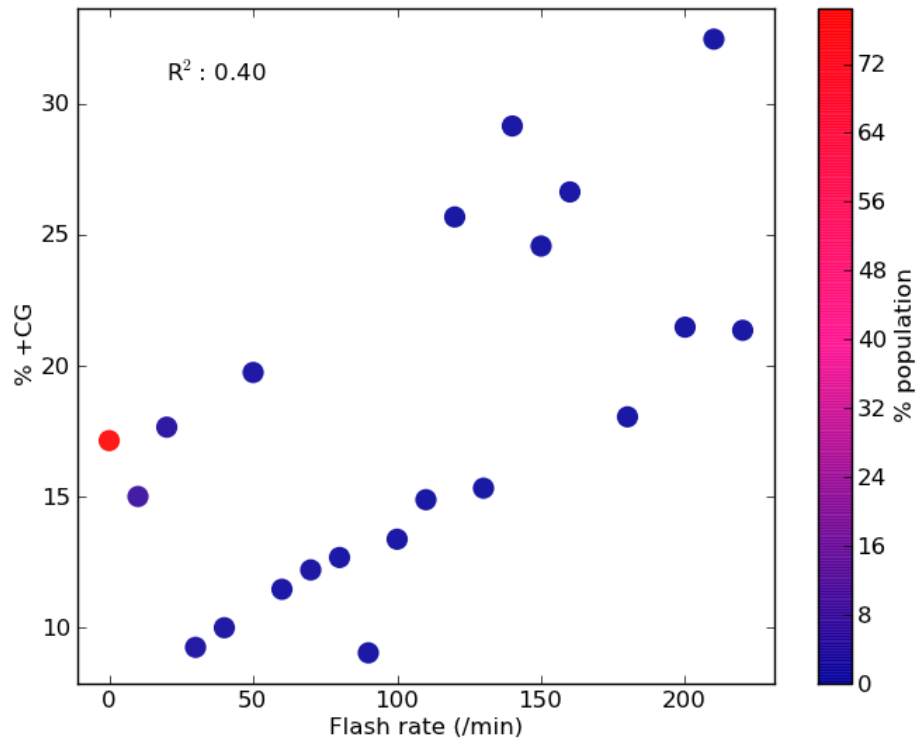


FIG. 3.51. Relationship between storm total flash rate and percentage of CG flashes that are positive polarity. Same binning and median analysis as previous plots. Points are colored by relative population of flash rates.

TABLE 3.1. Flash rate and echo top height fit parameters

	Alabama			DC			Oklahoma			Colorado		
Reflectivity	Slope	Int	R ²	Slope	Int	R ²	Slope	Int	R ²	Slope	Int	R ²
0 dBZ	10.3	-27.2	0.98	10.0	-27.1	0.96	9.7	-25.1	0.90	10.0	-25.8	0.87
10 dBZ	9.6	-25.1	0.97	10.0	-27.1	0.96	11.0	-28.6	0.91	11.6	-29.9	0.98
20 dBZ	6.6	-16.6	0.97	8.4	-22.2	0.97	8.0	-19.9	0.95	11.0	-27.5	0.96
30 dBZ	3.5	-7.7	0.71	6.7	-17.0	1.00	3.9	-8.5	0.84	5.7	-12.4	0.96
40 dBZ	4.0	-7.5	0.89	4.3	-9.1	0.96	3.2	-5.6	0.86	5.2	-9.8	0.99
50 dBZ	4.1	-6.5	0.95	4.3	-7.2	0.96	3.5	-5.1	0.94	3.3	-4.0	0.89

TABLE 3.2. Storm and environmental variables in severe and non-severe storms in Alabama

Parameter	Severe	Non-severe	p-value
Number	26	1231	
40 dBZ vol (km ³)	4381.35	212.12	1.190e-15
30 dBZ vol (km ³)	8590.54	658.39	1.651e-13
0 dBZ vol (km ³)	19691.27	2071.74	1.074e-11
40 dBZ area (km ²)	386.32	7.17	6.362e-16
30 dBZ area (km ²)	798.77	40.99	8.506e-16
0 dBZ area (km ²)	1326.00	181.38	2.884e-10
30 dBZ height (km MSL)	18.00	11.00	6.289e-15
CG rate (min ⁻¹)	13.80	0.20	3.990e-13
+CG rate (min ⁻¹)	1.10	0.00	2.726e-09
-CG rate (min ⁻¹)	12.50	0.20	2.571e-13
Total flash rate (min ⁻¹)	80.50	1.40	1.059e-14
IC flash rate (min ⁻¹)	66.10	1.00	3.746e-10
Max flash alt (m MSL)	15864.55	10197.70	1.004e-13
6 km shear (m/s)	35.93	14.62	3.700e-08
WCD (m)	3332.52	3099.31	5.078e-02
Freezing height (m AGL)	3974.13	4022.75	6.243e-01
CAPE (J/kg)	1862.67	958.67	5.201e-04
LCL (m AGL)	570.74	679.68	6.356e-01
Mixed-phase shear (m/s)	14.60	9.12	2.001e-04

TABLE 3.3. Storm and environmental variables in severe and non-severe storms in DC

Parameter	Severe	Non-severe	p-value
Number	33	1451	
40 dBZ vol (km ³)	1494.82	223.65	8.508e-17
30 dBZ vol (km ³)	4799.31	747.79	2.848e-14
0 dBZ vol (km ³)	12439.92	2556.95	1.433e-12
40 dBZ area (km ²)	127.07	2.05	1.985e-19
30 dBZ area (km ²)	362.75	32.79	1.072e-17
0 dBZ area (km ²)	836.18	222.37	1.811e-10
30 dBZ height (km MSL)	16.00	11.00	3.218e-15
CG rate (min ⁻¹)	3.20	0.00	1.357e-14
+CG rate (min ⁻¹)	0.00	0.00	1.685e-03
-CG rate (min ⁻¹)	3.20	0.00	1.771e-14
Total flash rate (min ⁻¹)	39.80	0.40	2.849e-18
IC flash rate (min ⁻¹)	32.60	0.20	2.859e-18
Max flash alt (m MSL)	13858.00	7666.30	2.341e-16
6 km shear (m/s)	14.48	14.93	6.754e-01
WCD (m)	3246.33	2975.50	9.571e-02
Freezing height (m AGL)	3969.50	3695.83	2.245e-03
CAPE (J/kg)	573.50	591.50	2.067e-01
LCL (m AGL)	780.88	516.17	6.906e-02
Mixed-phase shear (m/s)	8.18	10.42	3.554e-03

TABLE 3.4. Storm and environmental variables in severe and non-severe storms in Oklahoma

Parameter	Severe	Non-severe	p-value
Number	26	677	
40 dBZ vol (km ³)	3602.81	472.14	4.720e-10
30 dBZ vol (km ³)	7686.21	1609.59	8.874e-08
0 dBZ vol (km ³)	17223.98	5377.76	2.553e-06
40 dBZ area (km ²)	288.97	32.79	1.769e-10
30 dBZ area (km ²)	612.79	129.12	2.389e-09
0 dBZ area (km ²)	1191.76	445.76	2.776e-05
30 dBZ height (km MSL)	17.00	13.00	3.212e-10
CG rate (min ⁻¹)	0.90	0.20	7.816e-03
+CG rate (min ⁻¹)	0.30	0.00	1.732e-03
-CG rate (min ⁻¹)	0.60	0.20	3.573e-02
Total flash rate (min ⁻¹)	124.20	3.60	4.419e-11
IC flash rate (min ⁻¹)	119.70	3.20	3.538e-11
Max flash alt (m MSL)	13516.90	10113.50	4.995e-11
6 km shear (m/s)	22.84	23.80	2.396e-01
WCD (m)	3047.18	3025.82	6.558e-01
Freezing height (m AGL)	4033.63	3746.83	1.152e-04
CAPE (J/kg)	2602.50	726.67	1.462e-05
LCL (m AGL)	975.35	614.06	2.965e-02
Mixed-phase shear (m/s)	16.85	12.70	3.710e-01

TABLE 3.5. Storm and environmental variables in severe and non-severe storms in Colorado

Parameter	Severe	Non-severe	p-value
Number	20	708	
40 dBZ vol (km ³)	2702.20	363.65	4.300e-10
30 dBZ vol (km ³)	6898.33	1625.34	1.463e-08
0 dBZ vol (km ³)	22202.87	5931.50	3.333e-06
40 dBZ area (km ²)	330.47	38.43	4.112e-10
30 dBZ area (km ²)	823.88	163.96	1.491e-08
0 dBZ area (km ²)	1694.90	525.68	9.778e-05
30 dBZ height (km MSL)	16.00	13.00	5.892e-07
CG rate (min ⁻¹)	1.10	0.20	6.175e-06
+CG rate (min ⁻¹)	0.50	0.00	2.141e-05
-CG rate (min ⁻¹)	0.40	0.00	4.799e-04
Total flash rate (min ⁻¹)	105.60	7.50	1.669e-09
IC flash rate (min ⁻¹)	103.60	7.20	1.698e-09
Max flash alt (m MSL)	13618.66	10598.65	1.500e-09
6 km shear (m/s)	18.62	17.75	8.100e-01
WCD (m)	1259.11	1213.65	8.217e-01
Freezing height (m AGL)	3008.59	2995.53	7.570e-01
CAPE (J/kg)	1485.00	510.00	3.039e-04
LCL (m AGL)	1618.03	1535.57	6.063e-01
Mixed-phase shear (m/s)	8.46	9.87	2.170e-01

TABLE 3.6. Comparison of storm autocorrelation in Alabama

Parameter	5 minutes	10 minutes	p-value (%)
Number	1257	651	
Total flash rate	1.40	1.40	24
Total LMA source rate	68.20	67.00	36
CG rate	0.20	0.20	32
CAPE	986.00	960.33	1
LCL	670.13	663.70	4
30 dBZ height	11.00	11.00	26
40 dBZ height	8.00	8.00	5
30 dBZ vol	672.48	669.91	0
40 dBZ vol	216.73	212.37	15
Max flash alt	10.26	10.39	15

TABLE 3.7. Comparison of storm autocorrelation in DC

Parameter	5 minutes	10 minutes	p-value (%)
Number	1481	759	
Total flash rate	0.40	0.40	7
Total LMA source rate	6.40	7.00	13
CG rate	0.00	0.00	18
CAPE	588.00	605.00	5
LCL	516.17	536.67	21
30 dBZ height	11.00	11.00	29
40 dBZ height	7.50	7.50	7
30 dBZ vol	762.91	751.64	18
40 dBZ vol	228.26	225.70	13
Max flash alt	7.79	7.70	9

TABLE 3.8. Comparison of storm autocorrelation in Oklahoma

Parameter	5 minutes	10 minutes	p-value (%)
Number	703	351	
Total flash rate	4.20	3.60	41
Total LMA source rate	538.00	510.20	34
CG rate	0.20	0.20	0
CAPE	969.00	621.83	68
LCL	637.17	594.96	42
30 dBZ height	13.00	13.00	49
40 dBZ height	10.00	9.00	58
30 dBZ vol	1741.78	1808.39	26
40 dBZ vol	490.08	486.23	0
Max flash alt	10.24	10.09	41

TABLE 3.9. Comparison of storm autocorrelation in Colorado

Parameter	5 minutes	10 minutes	p-value (%)
Number	726	363	
Total flash rate	7.80	7.60	7
Total LMA source rate	4336.60	4202.40	25
CG rate	0.20	0.20	31
CAPE	528.33	520.00	22
LCL	1535.57	1553.23	12
30 dBZ height	13.00	13.00	7
40 dBZ height	10.00	10.00	30
30 dBZ volume	1692.08	1752.79	10
40 dBZ volume	370.69	376.84	17
Max flash alt	10.70	10.64	6

CHAPTER 4

SUMMARY

In this study we have demonstrated the use of an automated objective analysis tool to analyze a large number of storms and multiple types of storm data in distinct regions of the CONUS. This work has helped characterize the electrical behavior of thunderstorms in various regions in the context of environmental variables. The CLEAR framework was originally developed by Lang and Rutledge (2011) in an effort to take advantage of the scores of data types that exist today. This has come to fruition in this study. This is the first of its kind to combine the detailed investigation of electrical activity afforded by LMA source data and total lightning information provided by the novel flash clustering algorithm with the large sample size of storms in distinct environments in the CONUS. This study also utilizes high resolution environmental data from the RUC and RAP models to provide detailed information about storm environmental conditions. The vast amount of data included in this study comprises a complete investigation that has never been carried out before.

The novel flash clustering algorithm unveiled in this study has been shown to perform very well. Testing and improvements of this algorithm were time-consuming but the result is a valuable tool to obtain detailed electrical activity within a storm. This algorithm is based on open-source code distributed in the Python programming language which means that anyone will be able to use and modify the code as they see fit. The performance of the algorithm was tested in multiple ways. Comparisons were made with XLMA flash counts for randomly selected storms in each region, which resulted in broad agreements no worse than 15% in any region. Sensitivity studies detailed in the previous section showed that no systematic behaviors in total flash counts were present when storms were binned by distance from LMA center, even though systematic decreases

in LMA source densities were observed in all regions. The exception of this is the DC region. However, the geographic location of the DC region near the Atlantic coast may cast some doubt upon this dubious result because of the preferred location for storms and lightning in the region. Further testing will be carried out in this region to ensure that flash counts are valid. Given the significantly different VHF source detection efficiencies for each LMA network included in this study, different clustering parameters had to be used in some of the regions. Unfortunately there does not currently exist an explicit method to examine the validity of flash counting parameters on large scales short of extremely time-consuming subjective analysis. However, sensitivity studies similar to those performed in this study can provide general information on the validity of the flash counts. One of the goals of this study was to demonstrate the validity of an automated flash counting algorithm that avoids tedious GUI interfaces in order to provide efficient quantities of electrical behavior in a storm. We believe this has been accomplished and hope that future studies are able to utilize this new tool to further the field of lightning research.

Analysis performed in this study was focused on representative storms rather than outliers. The main reasoning for this was centered on the details of the framework. Because consecutive observations of the same storm were treated as separate cell observations, provided they satisfied the prescribed criteria, large amounts of scatter are unavoidable. Including all observations would yield meaningless results because of the enormous scatter in the data. However, if a median storm quantity (e.g. total flash rate) is selected out of a number of storms within a particular radar structure or environmental quantity, then physically meaningful results are obtained. For example, if a storm forms in 4000 J kg^{-1} of CAPE, each 5 minute observation of the cell captures a different period in the storms lifetime that will likely manifest in different flash rates for each observation. It is likely however, that this particular storm will have higher overall flash rates throughout its

lifecycle than a storm that forms in an environment with 1000 J kg^{-1} of CAPE, all else being equal. This will be reflected in the median flash rate for all observations and is thus the reasoning for this method. We also use the median quantities rather than means because medians are more resistant to outliers by virtue of the rank method. This method of analysis does not preclude the investigation of outlier storms however, as storms with specific characteristics can be selected based on prescribed criteria. Comparisons of storms with specific quantities can be carried out by this method. This method can also serve as a way to narrow down and subjectively select a case study, as was performed in this study.

This method of objective analysis has been shown to be effective for investigating large samples of storms. However, this does not mean that this method is without faults. These faults were particularly exposed in the Oklahoma region where transient environmental conditions and large gradients are often present. This poses problems for the objective attribution of environmental parameters because fine-scale environmental features, both spatially and temporally, may be missed. Use of model data also implies that the model can accurately represent the actual environment. This problem is yet to be totally solved as both types of inflow sounding attribution methods are subject to this problem.

The results in this study were first shown for each region individually. The relationships between total flash rates and storm parameters, both radar and lightning, were examined. The majority of storms in the Alabama region consisted of low flash rate storms. Storm variables generally exhibited monotonic relationships with total flash rates, similar to the other three study regions. Characteristic environmental quantities in Alabama such as LCL heights and CAPE values were characteristic of tropical or maritime regimes (Williams et al. 2005). Very similar environments

and storm characteristics were observed in the DC region. The Oklahoma region is more electrically active than either Alabama or DC. Median flash rates are higher and a greater number of superlative flash rates are observed in that region. Detailed analysis of these storms indicates a signal of inverted storms with a relative increase in storm intensity for LMA mode temperatures near -15°C . However, this signal was weak thereby requiring a case study approach to investigate inverted storms in this region. The Colorado region was the most electrically active region and exhibited anomalous electrical characteristics by a variety of metrics. The highest overall flash rates were observed in this region along with a very pronounced signal of inverted storms with LMA modal temperatures near -20°C , indicating that these storms are relatively common in this region. The Colorado environment is also characterized by the highest LCL heights and shallowest WCD values, but had the lowest CAPE values due in part to the high elevation of the region.

Once each region was investigated, every storm from all regions in the study were then examined simultaneously to determine if any connections could be made between regions, to explain the regional differences in lightning activity. LCL heights were found to be very well correlated with the log of total flash rates, suggesting this quantity to be a very important influence on total flash rates. Given this result, it is not surprising that WCD values were found to negatively correlate with flash rate. It is somewhat surprising that the correlation coefficient was not as strong as LCL heights. Dry bulb temperatures and CAPE values were also found to correlate with total flash rate but the correlation coefficient was not as good with LCL heights, possibly suggesting these quantities are not as influential as LCL heights in determining lightning activity. The similarity between the LCL height and flash rate relationship observed here and the Williams et al. (2005) study is striking. The data and the regime of study are markedly different between the two studies, yet the same result is observed. This suggests that these relationships may be robust. Nonetheless, these

results suggest that the relationships found here may have impacts beyond this study on global variations of flash rates.

Anomalous lightning behaviors were a central interest in this study. Quantities such as high total flash rates, IC:CG ratios, and large fractions of +CG flashes are expected to be related by virtue of the governing dynamics and microphysics within a storm. If by some means, large amounts of liquid water can be supplied to the mixed-phase region of a storm, then processes that lead to anomalous electrification are possible. These processes include graupel charge reversal, more numerous ice particle collisions and greater charge separation. These processes have the potential to produce greater storm-scale charge separation and anomalous charge structures and associated superlative total flash rates and significant +CG fractions. Very general correlations are observed between these quantities on the regional scale. The same regions that produce the highest flash rates also correspond to greatest production of +CG fractions. Fig. 3.51 also showed that the quantities are correlated throughout the regions.

Inverted charge structures, and the environments that produce them, have been the subject of many previous studies and the results shown here are generally consistent with those. It is worth noting that no inverted or +CG fraction signal was observed in either Alabama or DC. A weak signal indicating inverted charge structures was indicated in the Oklahoma study region but a much stronger signal was observed in Colorado. The reasons for the lack of inverted storms in Alabama and DC are not entirely clear. However, quantities such as LCL height and WCD undoubtedly have an influence. More puzzling is the environmental characteristics that produce anomalously electrified storms in Oklahoma and Colorado. The environmental parameters that determine the dominant CG polarity in this study behave very differently in Oklahoma and Colorado and raise questions about the interplay between environmental variables like LCL height and CAPE and

their effect on storm microphysics through updraft characteristics. Dynamical effects, especially in Colorado, may be a factor that cannot be accounted for in this study.

Future improvements will be made to this study. Most importantly, another year of observations will be added to boost the sample size and will afford an interannual comparison. This will be of particular interest because of the uncommon environments observed during the period of study. The year of 2011 was particularly severe in Alabama and DC and a large number of fires burned during the summer of 2012 in Colorado. Although unlikely to significantly affect the bulk results, valuable insight may be gained by investigating some the storms in the tails of the distribution. Given that the present aerosol data is somewhat lacking, other types of data may be added. Perhaps IMPROVE network data, which provides mass concentration values rather than AOD values and is not subject to the same cloud masking problems, will prove to be more representative of storm environments. Model data that is able to provide vertical profiles of aerosol information would be very useful to investigate aerosol effects on storm characteristics. The present results do not provide any conclusive evidence of aerosol effects on storm electrification, but perhaps better data will change that.

REFERENCES

- Ackerman, S., K. Strabala, P. Menzel, R. Frey, C. Moeller, and L. Gumley, 2010: Discriminating clear-sky from cloud with MODIS algorithm theoretical basis document. *MODIS Cloud Mask Team, Cooperative Institute for Meteorological Satellite Studies, University of Wisconsin, Citeseer*.
- Altaratz, O., I. Koren, Y. Yair, and C. Price, 2010: Lightning response to smoke from Amazonian fires. *Geophys. Res. Lett.*, **37**, 345–350.
- Andreae, M. O., D. Rosenfeld, P. Artaxo, A. A. Costa, G. P. Frank, K. M. Longo, and M. A. F. Silva-Dias, 2004: Smoking rain clouds over the Amazon. *Science*, **303**, 1337–1342.
- Baker, B., M. B. Baker, E. R. Jayaratne, J. Latham, and C. P. R. Saunders, 1987: The influence of diffusional growth rates on the charge transfer accompanying rebounding collisions between ice crystals and soft hailstones. *Q. J. R. Met. Soc.*, **113**, 1193–1215.
- Baker, M. B. and J. G. Dash, 1989: Charge transfer in thunderstorms and the surface melting of ice. *J. Cry. Grow.*, **97**, 770–776.
- Benjamin, S., D. Devenyi, and S. S. Weygandt, 2004: An hourly assimilation forecast cycle: The RUC. *Mon. Wea. Rev.*, **132**, 495–518.
- Benjamin, S. G., et al., 2006: From the 13-km RUC to the Rapid Refresh.
- Boccippio, D., K. L. Cummins, H. J. Christian, and S. J. Goodman, 2001: Combined satellite and surface-based estimation of the intracloud-cloud-to-ground lightning ratio over the continental United States. *Mon. Wea. Rev.*, **129**, 108–122.
- Boccippio, D. J., S. J. Goodman, and S. Heckman, 2000: Regional differences in tropical lightning distributions. *J. Appl. Met.*, **39**, 2231–2248.
- Bradbury, T., 2000: *Meteorology and Flight: Pilot's Guide to Weather*. AC Black London.
- Branick, M. L. and C. A. Doswell, 1992: An observation of the relationship between supercell structure and lightning ground-strike polarity. *Wea. Forecasting*, **7**, 143–149.
- Brook, M., M. Nakano, P. Krehbiel, and T. Takeuti, 1982: The electrical structure of the Hokuiriku winter thunderstorms. *J. Geophys. Res.*, **87**, 1207–1215.
- Bruning, E., S. A. Weiss, and K. M. Calhoun, 2012: Continuous variability in thunderstorm primary electrification and an evaluation of inverted-polarity terminology. *Atmos. Res.*, **135**, 274–284.
- Bruning, E. C., 2013: Streamed clustering of lightning mapping data in Python using sklearn. *Scientific Computing With Python*, Vol. 2.

- Bruning, E. C. and D. R. MacGorman, 2013: Theory and observations of controls on lightning flash rate spectra. *J. Atmos. Sci.*, **70**, 4012–4029.
- Bruning, E. C., W. D. Rust, D. R. MacGorman, M. J. Biggerstaff, and T. J. Schuur, 2010: Formation of charge structures in a supercell. *Mon. Wea. Rev.*, **138**, 3740–3760.
- Carey, L. D. and K. M. Buffalo, 2007: Environmental control of cloud-to-ground lightning polarity in severe storms. *Mon. Wea. Rev.*, **135**, 1327–1353.
- Carey, L. D. and S. A. Rutledge, 1998: Electrical and multiparameter radar observations of a severe hailstorm. *J. Geophys. Res.*, **103**, 13 979–14 000.
- Carey, L. D. and S. A. Rutledge, 2003: Characteristics of cloud to ground lightning in severe and nonsevere storms over the central United States from 1989–1998. *J. Geophys. Res.*, **108**, D15.
- Carey, L. D., S. A. Rutledge, and W. A. Petersen, 2003: The relationship between severe storm reports and cloud-to-ground lightning polarity in the contiguous United States from 1989 to 1998. *Mon. Wea. Rev.*, **131**, 1211–1228.
- Christian, H. J., R. J. Blakeslee, S. J. Goodman, D. Boccippio, and coauthors, 2003: Global frequency and distribution of lightning as observed from space by the Optical Transient Detector. *J. Geophys. Res.*, **108**, 4–15.
- Christian, H. J., R. J. Blakeslee, S. J. Goodman, D. A. Mach, and coauthors, 1999: The Lightning Imaging Sensor. *NASA conf. pub.*, **1**, 746–749.
- Corfidi, S. F., 1999: The birth and early years of the Storm Prediction Center. *Weather & Forecasting*, **14** (4).
- Crook, N. A., T. L. Clark, and M. W. Moncrieff, 1990: The Denver Cyclone. Part I: Generation in low froude number flow. *J. Atmos. Sci.*, **47**, 2725–2742.
- Cummins, K. and M. Murphy, 2009: An overview of lightning locating systems: History, techniques, and data uses, with an in-depth look at the US NLDN. *Electromagnetic Compatibility*, **51**, 499–518.
- Cummins, K., M. Murphy, E. Bardo, W. Hiscox, R. Pyle, and A. Pifer, 1998: A combined TOA/MDF technology upgrade of the U.S. National Lightning Detection Network. *Geophys. Res.*, **103**, 9035–9044.
- Curran, E. and W. Rust, 1992: Positive ground flashes produced by low-precipitation thunderstorms in Oklahoma on 26 April 1984. *Mon. Wea. Rev.*, **120**, 544–555.
- Curran, E. B., R. L. Holle, and E. L. Pez, 2000: Lightning casualties and damages in the United States from 1959 to 1994. *Journal of Climate*, **13** (19).

- Dash, J. G., B. L. Mason, and J. S. Wettlaufer, 2001: Theory of charge and mass transfer in ice-ice collisions. *J. Geophys. Res.*, **106**, 20 395–20 402.
- Deierling, W. and W. A. Petersen, 2008: Total lightning activity as an indicator of updraft characteristics. *J. Geophys. Res.*, **106**, 20 395–20 402.
- Dixon, M. and G. Weiner, 1993: TITAN: Thunderstorm identification, tracking, analysis and nowcasting - a radar-based methodology. *J. Atmos. Oceanic Technol.*, **10**, 785–797.
- Dong, Y. and J. Hallett, 1992: Charge separation by ice and water drops during growth and evaporation. *J. Geophys. Res.*, **97**, 20 361–20 371.
- Dye, J. E., J. J. Jones, W. P. Winn, and D. W. Breed, 1989: The electrification of New Mexico thunderstorms, 1. relationship between precipitation development and the onset of electrification. *J. Geophys. Res.*, **94**, 8643–8656.
- Ester, Martin, Kriegel, and coauthors, 1996: A density-based algorithm for discovering clusters in large spatial databases with noise. *KDD*, Vol. 96, 226–231.
- French, J. R., J. H. Helsdon, A. G. Detweiler, and P. Smith, 1996: Positive cloud-to-ground lightning in summer thunderstorms. *J. Geophys. Res.*, **87**, 7131–7140.
- Fuquay, D. M., 1982: Positive cloud-to-ground lightning in summer thunderstorms. *J. Geophys. Res.*, **87**, 7131–7140.
- Gatlin, P. N. and S. J. Goodman, 2010: A total lightning trending algorithm to identify severe thunderstorms. *J. Atmos. Ocean Tech.*, **27**, 3–22.
- Gauthier, M. L., W. A. Petersen, and L. D. Carey, 2010: Cell mergers and their impact on cloud-to-ground lightning over the Houston area. *Atmos. Res.*, **96**, 626–632.
- Gilmore, M. S. and L. J. Wicker, 2002: Influences of the local environment on supercell cloud-to-ground lightning, radar characteristics, and severe weather on 2 June 1995. *Mon. Wea. Rev.*, **130**, 2349–2372.
- Goodman, S. J., D. E. Buechler, P. D. Wright, and W. D. Rust, 1988: Lightning and precipitation history of a microburst-producing storm. *Geophys. Res. Lett.*, **15**, 1185–1188.
- Goodman, S. J., et al., 2005: The North Alabama Lighting Mapping Array: Recent severe storm observations and future prospects. *Atmos. Res.*, **76**, 423–437.
- Heckman, S., E. Williams, and B. Boldi, 1998: Total global lightning inferred from Schumann Resonance measurements. *Journal of Geophysical Research: Atmospheres (1984–2012)*, **103 (D24)**, 31 775–31 779.

- Holben, B., et al., 1998: AERONET – a federated instrument network and data archive for aerosol characterization. *Remote sensing of environment*, **66** (1), 1–16.
- Jacobson, E. A. and E. P. Krider, 1976: Electrostatic field changes produced by Florida lightning. *J. Atmos. Sci.*, **33**, 103–117.
- Jayarathne, E. R., C. P. R. Saunders, and J. Hallett, 1983: Laboratory studies of the charging of soft-hail during ice crystal interactions. *Q. Jour. of the Roy. Met. Soc.*, **109**, 609–630.
- Johnson, J. T., P. L. MacKeen, A. Witt, E. Mitchell, G. J. Stumpf, M. D. Eilts, and K. W. Thomas, 1998: The storm cell identification and tracking algorithm: An enhanced WSR-88D algorithm. *Wea. Forecasting*, **13**, 263–276.
- King, M. D., Y. J. Kaufman, D. Tanré, and T. Nakajima, 1999: Remote sensing of tropospheric aerosols from space: Past, present, and future.
- King, M. D., et al., 2003: Cloud and aerosol properties, precipitable water, and profiles of temperature and water vapor from MODIS. *Geoscience and Remote Sensing, IEEE Transactions on*, **41** (2), 442–458.
- Klemp, J. B. and R. B. Wilhelmson, 1978: The simulation of three-dimensional convective storm dynamics. *J. Atmos. Sci.*, **35**, 1070–1096.
- Koren, I., Y. Kaufman, D. Rosenfeld, L. Remer, and Y. Rudich, 2005: Aerosol invigoration and restructuring of Atlantic convective clouds. *Geophys. Res. Lett.*, **32**, 14 828.
- Krehbiel, P., 1986: *The Electrical Structure of Thunderstorms*. National Academies Press.
- Krehbiel, P., 2008: The DC Lightning Mapping Array. *Preprints, 3rd Conf. on Meteorological Applications of Lightning Data, New Orleans, LA, Amer. Meteor. Soc.*, Vol. 3.
- Krehbiel, P., R. J. Thomas, W. Rison, T. Hamlin, M. Davis, and J. Harlin, 2000: Lightning mapping observations in central Oklahoma. *Eos*, **81** (3), 21–25.
- Kyle, T. G., W. R. Sand, and D. J. Musil, 1976: Fitting measurements to thunderstorm updraft profiles to model profiles. *Mon. Wea. Rev.*, **104**, 611–617.
- Lang, T. J. and S. A. Rutledge, 2002: Relationships between convective storm kinematics, precipitation and lightning. *Mon. Wea. Rev.*, **130**, 2492–2506.
- Lang, T. J. and S. A. Rutledge, 2006: Cloud-to-ground lightning downwind of the 2002 Hayman forest fire in Colorado. *Geo. Res. Lett.*, **33**.
- Lang, T. J. and S. A. Rutledge, 2008: Kinematic, microphysical and electrical aspects of an asymmetric bow-echo mesoscale convective system observed during STEPS 2000. *J. Geophys. Res.*, **113**, D08 213.

- Lang, T. J. and S. A. Rutledge, 2011: A framework for the statistical analysis of large radar and lightning datasets: Results from STEPS 2000. *Mon. Wea. Rev.*, **139**, 2536–2551.
- Lang, T. J., S. A. Rutledge, J. E. Dye, M. Venticinque, P. Laroche, and E. Defer, 2000: Anomalous low negative cloud-to-ground lightning flash rates in intense convective storms observed during STERAO-A. *Mon. Wea. Rev.*, **128**, 160–173.
- Lang, T. J., S. A. Rutledge, and K. C. Wiens, 2004a: Origins of positive cloud-to-ground lightning flashes in the stratiform region of a mesoscale convective system. *Geophys. Res. Lett.*, **31** (10).
- Lang, T. J., et al., 2004b: The severe thunderstorm electrification and precipitation study. *Bull. Amer. Meteor. Soc.*, **85**, 1107–1125.
- LeMone, M. A. and E. J. Zipser, 1980: Cumulonimbus vertical velocity events in GATE. Part I: Diameter, intensity and mass flux. *J. Atmos. Sci.*, **37**, 2444–2457.
- Livingston, J. and P. Krider, 1978: Electric fields produced by Florida thunderstorms. *Jour. Geophys. Res.*, **83**, 385–401.
- Lyons, W. A., T. E. Nelson, E. R. Williams, J. A. Cramer, and T. R. Turner, 1998: Enhanced positive cloud-to-ground lightning in thunderstorms ingesting smoke from fires. *Science*, **282**, 77–80.
- MacGorman, D. R. and D. W. Burgess, 1994: Positive cloud-to-ground lightning in tornadic storms and hailstorms. *Mon. Wea. Rev.*, **122**, 1671–1697.
- MacGorman, D. R., W. D. Rust, T. J. Schuur, M. J. Biggerstaff, J. M. Straka, and coauthors, 2008: TELEX the thunderstorm electrification and lightning experiment. *Bull. Amer. Met. Soc.*, **89**, 997–1013.
- MacGorman, D. R., J. M. Straka, and C. L. Ziegler, 2001: A lightning parameterization for numerical cloud models. *J. Appl. Meteor.*, **40**, 459–478.
- Markowski, P. and Y. Richardson, 2010: *Mesoscale Meteorology in Midlatitudes*. Wiley-Blackwell.
- McCaul, E. W., S. J. Goodman, K. M. LaCasse, and D. J. Cecil, 2009: Forecasting lightning threat using cloud-resolving model simulations. *Wea. and Fore.*, **24**, 709–729.
- Moore, C. B. and B. Vonnegut, 1977: *The Thundercloud*. Academic Press.
- Morton, B. R., G. Taylor, and J. S. Turner, 1956: Turbulent gravitational convection from maintained and instantaneous sources. *Proc. R. Soc. Lond.*, **234**, 1–23.

- Orville, R. E., 1994: Cloud-to-ground lightning flash characteristics in the contiguous United States: 1989–1991. *Journal of Geophysical Research: Atmospheres (1984–2012)*, **99 (D5)**, 10 833–10 841.
- Orville, R. E., R. W. Henderson, and L. F. Bosart, 1988: Bipole patterns revealed by lightning locations in mesoscale storms. *Geophys. Res. Lett.*, **15**, 129–132.
- Orville, R. E. and G. R. Huffines, 2001: Cloud-to-ground lightning in the united states: NLDN results in the first decade. *Mon. Wea. Rev.*, **125**, 631–638.
- Orville, R. E. and A. C. Silver, 1997: Lightning ground flash density in the contiguous United States: 1992–95. *Mon. Wea. Rev.*, **125**, 631–638.
- Orville, R. E. and D. W. Spencer, 1979: Global lightning flash frequency. *Mon. Wea. Rev.*, **107**, 934–943.
- Pawar, S. D. and A. K. Kamra, 2007: End-of-storm oscillation in tropical air mass thunderstorms. *Jour. Geophys. Res.*, **112**.
- Potvin, C. K., K. L. Elmore, and S. J. Weiss, 2010: Assessing the impacts of proximity sounding criteria on the climatology of significant tornado environments. *Wea. and Forecasting*, **25**, 921–930.
- Price, C., 1993: Global surface temperatures and the atmospheric electric circuit. *Geophys. Res. Lett.*, **20**, 1363–1366.
- Price, C. and D. Rind, 1992: A simple lightning parameterization for calculating global lightning distributions. *J. Geophys. Res.*, **97**, 9919–9933.
- Price, C. and D. Rind, 1994: The impact of a 2 x CO₂ climate on lightning-caused fires. *J. Climate*, **7**, 1484–1494.
- Reap, R. M. and D. R. MacGorman, 1989: Cloud-to-ground lightning: Climatological characteristics and relationships to model fields, radar observations and severe local storms. *Mon. Wea. Rev.*, **117**, 518–535.
- Reeve, N. and R. Toumi, 1999: Lightning activity as an indicator of climate change. *Q. J. R. Met. Soc.*, **125**, 893–903.
- Remer, L. A., et al., 2008: Global aerosol climatology from the MODIS satellite sensors. *Journal of Geophysical Research: Atmospheres (1984–2012)*, **113 (D14)**.
- Reynolds, S. E., M. Brook, and M. F. Gourley, 1957: Thunderstorm charge separation. *J. Meteor.*, **14**, 426–436.

- Rison, W., R. Thomas, P. Krehbiel, T. Hamlin, and J. Harlin, 1999: A GPS-based three-dimensional lightning mapping system: Initial observations in central New Mexico. *Geophys. Res. Lett.*, **26**, 3573–3576.
- Rorig, M. L. and S. A. Ferguson, 1999: Characteristics of lightning and wildland fire ignition in the Pacific Northwest. *J. Appl. Meteor.*, **38**, 1565–1575.
- Rosenfeld, D., U. Lohmann, G. B. Raga, C. D. O’Dowd, M. Kulmala, S. Fuzzi, A. Reissell, and M. O. Andreae, 2008: Flood or drought: How do aerosols affect precipitation? *Science*, **321**, 1309–1313.
- Rowe, A. K., S. A. Rutledge, and T. J. Lang, 2011: Investigation of microphysical processes in isolated convection in NAME. *Mon. Wea. Rev.*, **139**, 424–443.
- Rudlosky, S. D. and H. E. Fuelberg, 2013: Documenting storm severity in the Mid-Atlantic region using lightning and radar information. *Mon. Wea. Rev.*, **141**, 3186–3202.
- Rust, W. D., et al., 2005: Inverted-polarity electrical structures in thunderstorms in the severe thunderstorm electrification and precipitation study (STEPS). *Atmos. Res.*, **76**, 247–271.
- Rutledge, S. A., C. Lu, and D. R. MacGorman, 1990: Positive cloud-to-ground lightning in mesoscale convective systems. *J. Atmos. Sci.*, **47**, 2085–2100.
- Rutledge, S. A. and D. R. MacGorman, 1988: Cloud-to-ground lightning activity in the 10-11 June 1985 mesoscale convective system observed during the Oklahoma-Kansas PRE-STORM project. *Mon. Wea. Rev.*, **116**, 1393–1408.
- Rutledge, S. A., E. R. Williams, and T. D. Keenan, 1992: The down under doppler and electricity experiment (DUNDEE): Overview and preliminary results. *Bull. Amer. Met. Soc.*, **73**, 3–16.
- Saba, M. M., K. L. Cummins, T. A. Warner, E. P. Krider, L. Z. Campos, M. G. Ballarotti, O. Pinto, and S. A. Fleenor, 2008: Positive leader characteristics from high-speed video observations. *Geophysical Research Letters*, **35** (7).
- Saunders, C. P. R., 2008: Charge separation mechanisms in clouds. *Space Sci. Rev.*, **137**, 335–353.
- Saunders, C. P. R., H. Bax-Norman, C. Emersic, E. E. Avila, and N. E. Castellano, 2006: Laboratory studies on the effect of cloud conditions on the graupel/crystal charge transfer in thunderstorm electrification. *Quar. J. of the Royal Met. Soc.*, **132**, 2653–2673.
- Saunders, C. P. R., W. D. Keith, and R. P. Mitzeva, 1991: The effect of liquid water on thunderstorm charging. *J. Geophys. Res.*, **96**, 11 007–11 017.
- Saunders, C. P. R. and S. L. Peck, 1998: Laboratory studies of the influence of the rime accretion rate on charge transfer during graupel/crystal collisions. *J. Geophys. Res.*, **103**, 13 949–13 956.

- Schultz, D. M., C. C. Weiss, and P. M. Hoffman, 2007: The synoptic regulation of dryline intensity. *Mon. Wea. Rev.*, **135**, 1699–1709.
- Seimon, A., 1993: Anomalous cloud-to-ground lightning in an F5-tornado-producing supercell thunderstorm on 28 August 1990. *Bull. Amer. Met. Soc.*, **74**, 189–203.
- Shackford, C. R., 1960: Radar indications of a precipitation-lightning relationship in New England thunderstorms. *J. Meteor.*, **17**, 15–19.
- Smith, S. B., J. G. LaDue, and D. R. MacGorman, 2000: The relationship between cloud-to-ground lightning polarity and surface equivalent potential temperature during three tornadic outbreaks. *Mon. Wea. Rev.*, **128**, 3320–3328.
- Stolzenburg, M., 1994: Observations of high ground flash densities of positive lightning in summertime thunderstorms. *Mon. Wea. Rev.*, **122**, 1740–1750.
- Takahashi, T., 1978: Riming electrification as a charge generation mechanism in thunderstorms. *Atmos. Sci.*, **35**, 1536–1548.
- Tessendorf, S. A., S. A. Rutledge, and K. C. Wiens, 2007: Radar and lightning observations of normal and inverted multicellular storms from STEPS. *Mon. Wea. Rev.*, **135**, 3682–3706.
- Thomas, R. J., P. R. Krehbiel, W. Rison, S. J. Hunyady, W. P. Winn, T. Hamlin, and J. Harlin, 2004: Accuracy of the lightning mapping array. *Jour. Geophys. Res.*, **109**, 14 207–14 216.
- Thompson, R. L., R. Edwards, J. A. Hart, K. L. Elmore, and P. Markowski, 2003: Close proximity soundings within the supercell environments obtained from the Rapid Update Cycle. *Wea. and Fore.*, **18**, 1243–1261.
- van den Heever, S. C., G. G. Carrio, W. R. Cotton, P. J. DeMott, and A. J. Prenni, 2006: Impacts of nucleating aerosol on Florida storms. Part I: Mesoscale simulations. *J. Atmos. Sci.*, **63**, 1752–1775.
- Vonnegut, B., 1963: Some facts and speculations concerning the origin and role of thunderstorm electricity. *Meteor. Monogr.*, **5**, 224–241.
- Weisman, M. L. and J. B. Klemp, 1982: The dependence of numerically simulated convective storms on vertical wind shear and buoyancy. *Mon. Wea. Rev.*, **110**, 504–520.
- Whipple, F., 1929: On the association of the diurnal variation of electric potential gradient in fine weather with the distribution of thunderstorms over the globe. *Quarterly Journal of the Royal Meteorological Society*, **55 (229)**, 1–18.
- Wiens, K. C., S. A. Rutledge, and S. A. Tessendorf, 2005: The 29 June 2000 supercell observed during STEPS. Part II: Lightning and charge structure. *J. Atmos. Res.*, **62**, 4151–4177.

- Wilcoxon, F. and R. A. Wilcoxon, 1964: *Some rapid approximate statistical procedures*. Lederle Laboratories.
- Wilks, D., 2006: *Statistical Methods in the Atmospheric Sciences*. Academic Press.
- Williams, E., 2005: Lightning and climate: A review. *Atmospheric research*, **76** (1), 272–287.
- Williams, E. R., 1985: Large-scale separation in thunderclouds. *J. Geophys. Res.*, **90**, 6013–6025.
- Williams, E. R., 1989: The tripole structure of thunderstorms. *J. Geophys. Res.*, **94**, 13 151–13 167.
- Williams, E. R., 1992: *The Schumann resonance: A global tropical thermometer*. 14, Center for Global Change Science, Massachusetts Institute of Technology.
- Williams, E. R., 1994: Global circuit response to seasonal variations in global surface air temperature. *Mon. Wea. Rev.*, **122**, 1917–1929.
- Williams, E. R., 2001: The electrification of severe storms. *Meteor. Monogr.*, **50**, 527–561.
- Williams, E. R., 2009: The global electric circuit: A review. *Atmos. Res.*, **91**, 140–152.
- Williams, E. R., B. Boldi, A. Matlin, M. Weber, S. Hodanish, D. Sharp, and D. Buechler, 1999: The behavior of total lightning activity in severe Florida thunderstorms. *Atmos. Res.*, **51**, 245–265.
- Williams, E. R. and S. J. Heckman, 1993: The local diurnal variation of cloud electrification and the global diurnal variation of negative charge on the Earth. *J. Geophys. Res.*, **98**, 5221–5234.
- Williams, E. R., V. Mushtak, D. Rosenfeld, S. Goodman, and D. Boccippio, 2005: Thermodynamic conditions that lead to superlative updrafts and mixed-phase microphysics. *Atmos. Res.*, **76**, 288–306.
- Williams, E. R. and N. Renno, 1993: An analysis of the conditional instability of the tropical atmosphere. *Mon. Wea. Rev.*, **121**, 21–36.
- Williams, E. R., D. Rosenfeld, N. Madden, J. Gerlach, and coauthors, 2002: Contrasting convective regimes over the Amazon: Implications for cloud electrification. *J. Geophys. Res.*, **107**, 501–520.
- Williams, E. R. and S. Stanfill, 2002: The physical origin of the land-ocean contrast in lightning activity. *Comp. Rend. Phys.*, **3**, 1277–1292.
- Williams, E. R., M. E. Weber, and R. E. Orville, 1989: The relationship between lightning type and convective state of thunderclouds. *J. Geophys. Res.*, **94**, 13 213–13 220.

- Wilson, C. T. R., 1916: On some determinations of the sign and magnitude of electric discharges in lightning flashes. *Phil. Trans. Roy. Soc. London*, 555–574.
- Wilson, C. T. R., 1920: Investigations on lightning discharges and on the electric field of thunderstorms. *Phil. Trans. Roy. Soc. London*, 73–115.
- Workman, E. J. and S. E. Reynolds, 1950: Electrical phenomena occurring during the freezing of dilute aqueous solutions and their possible relationship to thunderstorm electricity. *Phys. Rev.*, **78**, 254–259.
- Yuan, T., L. Remer, K. Pickering, and H. Yu, 2011: Observational evidence of aerosol enhancement of lightning activity and convective invigoration. *Geophys. Res. Lett.*, **38**, 4071.
- Yuter, S. E. and R. A. Houze, 1998: The natural variability of precipitating clouds over the Western Pacific warm pool. *Q. J. R. Meteor. Soc.*, **124**, 53–99.
- Zajac, B. and S. A. Rutledge, 2001: Cloud-to-ground lightning activity in the contiguous United States from 1995 to 1999. *Mon. Wea. Rev.*, **129**, 999–1019.
- Zhang, J., K. Howard, C. Langston, and coauthors, 2011: National Mosaic and Multi-Sensor QPE (NMQ) System: Description, results, and future plans. *Bull. Amer. Meteor. Soc.*, **92**, 1321–1338.
- Zipser, E. J., 1994: Deep cumulonimbus cloud system in the tropics with and without lightning. *Mon. Wea. Rev.*, **122**, 1837–1851.
- Zipser, E. J., D. J. Cecil, C. Liu, S. W. Nesbitt, and D. P. Yorty, 2006: Where are the most intense thunderstorms on Earth? *Bull. Amer. Met. Soc.*, **87**, 1057–1071.

APPENDIX A

LMA DETECTION AND FLASH COUNTING PERFORMANCE

The different sensitivities and detection efficiencies of the various LMA networks pose a problem when trying to perform interregional comparisons. Comparisons of total source rates between regions are not physically meaningful as evidenced by the orders of magnitude differences in source rates, but total flash rates comparisons should be valid in theory if proper flash counting is performed. For all regions source detection decreased rapidly with distance from the center of the LMA, consistent with Thomas et al. (2004). This is shown in Fig. A.1 which shows 2D source density histogram of detected source in the Alabama LMA for the study period, normalized by bin annulus area. This compensates for the lower number of detected sources near the center of the network by virtue of the area between smaller radius bins and allows for an appropriate comparison. The maximum in detected sources is near the center of the LMA and around 10 km MSL, this shows the decreasing detection efficiency and the typical upper-level positive charge present in normal polarity tripole storms common in this region. The lack of sources near the ground at any radius is evidence that LMA networks struggle to detect CG flashes (P. Krehbiel, personal communication). The Earth curvature effect is also present in the upward curvature of the lower altitude source detection limit, where no sources are detected at low altitudes past 200 km. The combined effects of the Earth curvature and the decreased source detection efficiency dictated that the LMA radius threshold was set at 125 km. This was the best choice as it included a large number of storms but did not include storms with large range and azimuth errors, which increase rapidly with radius outside the network (Thomas et al. 2004). Also note the upward curvature of the 10 km local maximum outside of 150 km, this is evidence of the height errors at long distances outside

of the LMA network. Qualitatively similar results are observed in other regions. Although the Alabama network is older and lacks detection efficiency compared to other regions, similar patterns are observed in the newer Oklahoma and Colorado networks, albeit at longer distances from the respective LMA centers. Fig. A.2 shows the plan view of LMA source densities for the Alabama LMA for the period of study in an effort to provide another perspective on the detection efficiencies. The center of the network is located near Huntsville, AL in extreme northern Alabama. Not coincidentally, the maximum of sources is located over the network, as the highest detection efficiencies are inside the network (Thomas et al. 2004). Similar to the previous figure, the number of detected sources falls off rapidly from the network location to roughly half of the maximum value around 100 km from the network center. As one would expect, inclusion of cells far from the LMA center should result in a decrease in overall source rates as it is likely that sources may be missed as the distance from the network increases. However, flash counts should remain stable out to a sufficient distance if the clustering algorithm is performing well. This issue is addressed later where flash and source rate characteristics are examined as a function of distance from LMA center.

The different LMA networks included in this study have very different source detection sensitivities by virtue of the different installation times, involved technologies, ambient radio frequency (RF) noise and the number of station in each network. This is the main reason for the large discrepancies of total source rates for storms between regions. Detection efficiencies are much lower in Alabama and DC than Oklahoma and Colorado. Overall the Colorado network is vastly superior to the other networks due to its superior technology, high number of stations and desolate station locations. To compensate for the various detection efficiencies, different parameter values for filtering sources were used in different regions. More restrictive parameters were used in the

Oklahoma and Colorado regions, which have high sensitivities. These restrictive values cut down on noisy sources. The Alabama and DC regions are not as sensitive and less restrictive values had to be used in these regions. The minimum number of stations required to contribute to a solution was set to 7 in the Oklahoma and Colorado regions while the minimum stations were set to 6 in Alabama and DC regions. While the less restrictive value of 6 did slightly increase the number of noisy points, it also allowed 20-50% more sources which made flash counting much more successful, as measured by subjective analysis. This selection is justified because of the fewer active stations in the Alabama (≤ 10) and DC (≤ 8) networks. The chi-squared solution fit error was also less restrictive in Alabama and DC where a maximum in this value was allowed to be 2. The better networks in Colorado and Oklahoma were only allowed a maximum fit error of 1 (McCaul et al. 2009).

The sensitivity to the radius choice was tested by investigating storm characteristics as function of distance from the LMA center. Any systematic behaviors in lightning data will appear from this analysis and effects on presented results can be put in context of other choices of radii. Systematic behaviors in source detection and flash clustering algorithm performance will also be presented, assuming a random distribution of storms relative to each LMA network for the period of study, which will be more valid with another year of data.

Fig. A.3 shows various storm parameters and the variations as a function of distance from LMA center for the Alabama region. Fig. A.3a shows the LMA source rate density normalized by 30 dBZ area. The overall behavior of source rate density follows the previous figure. Dramatic decreases in source rate density are observed as distance from the LMA increases, this is mainly due to the decrease in detection efficiency at long distances, particularly for weaker VHF sources. Note the larger spreads at smaller radii and the smaller spreads at large radii, mainly due to the lack

of any large source densities at large distances. Fig. A.3b shows that although a systematic drop in source densities occurs with increasing distance from the LMA, total flash rate densities do not show any systematic behaviors. The maximum in flash density is actually located near 80 km and the difference between the ends of the data is only a factor of 2 versus a factor of 5 for source rate densities. The large spread in all flash density values shows that the flash rate variations are similar for most radii. The 80 km maximum is coincident with a maximum in flash altitude and 30 dBZ echo top height indicating that some strong storms must have been located there. These results provide strong evidence that the flash counts produced by the clustering algorithm are accurate and fairly resistant to decreasing source detection efficiencies as LMA distance increases.

Fig. A.4 shows the same storm parameters for the DC region. Similar to the Alabama region, a sharp decrease in source densities is observed for increasing distance from the LMA. However, in the DC region the flash rates exhibit a similar behavior to the source rate densities. The range of these quantities is also very similar. The smaller spreads for flash rate densities at large radii mean these differences are likely significant. Unfortunately, this flash density decrease cannot be attributed to inhomogeneities of storm intensities. Figs. A.4c and A.4d do not show any systematic relationships that can explain the behaviors in flash rates, unlike the Alabama region. Thus, future work should be invested to examine the performance of the flash counting algorithm with DC LMA data.

Fig. A.5 shows the same storm parameters presented earlier for the previous regions. The familiar decrease in source rates with increasing distance is observed here like the other regions. Storms in Oklahoma do not show any systematic behavior in flash rate density, similar to the Alabama region. Also, no systematic behaviors are observed in storm intensity that could be masking biases in flash rate densities. These results provide confidence in the performance of

the flash counting algorithm in the Oklahoma region. Recall that the Oklahoma LMA network has more stations and better overall detection efficiencies than either the Alabama or DC regions. Therefore it is not surprising that the flash counts in Oklahoma are fairly well-behaved.

The storm parameters in Colorado are a little more complicated given the location of the network in relation to local topography. The Palmer Lake Divide and the Cheyenne Ridge are both located 70-100 km from the center of the Colorado LMA. These ridges are preferred areas for convection and initiation. An overall decrease in source rate densities similar to other regions is evident in panel (a) of Fig. A.6. Notice however that the flash rate densities in panel (b) follow the same distinct pattern observed in the source densities. The high source and flash rate densities can be explained by the abnormally strong storms that occurred there during the study and also the smaller number of observations due to the smaller areas at shorter distances from LMA center. The local maximum in flash and source densities around 80 km is a little more nebulous because nothing obvious is evident in the maximum flash altitude or 30 dBZ echo top height. This may be the effect of the local ridges. Given all of the information here, confidence is given to the flash rates in the Colorado region. This is not surprising given the newest technologies, most stations and lowest RF noise floors are in this region (P. Krehbiel, personal communication). This sensitivity study has shown that flash rates can be trusted with confidence in all regions except DC, where flash rates systematically decrease with increasing distance from LMA center. The performance of the Alabama flash counts gives credence to the choices of source and flash counting criteria in that region. The strict choices imposed in the Oklahoma and Colorado regions are also deemed valid on the account of the flash count validity. While all regions have very different source detection characteristics, the reliable flash counts shown here give physical meaning to inter-regional flash count comparisons.

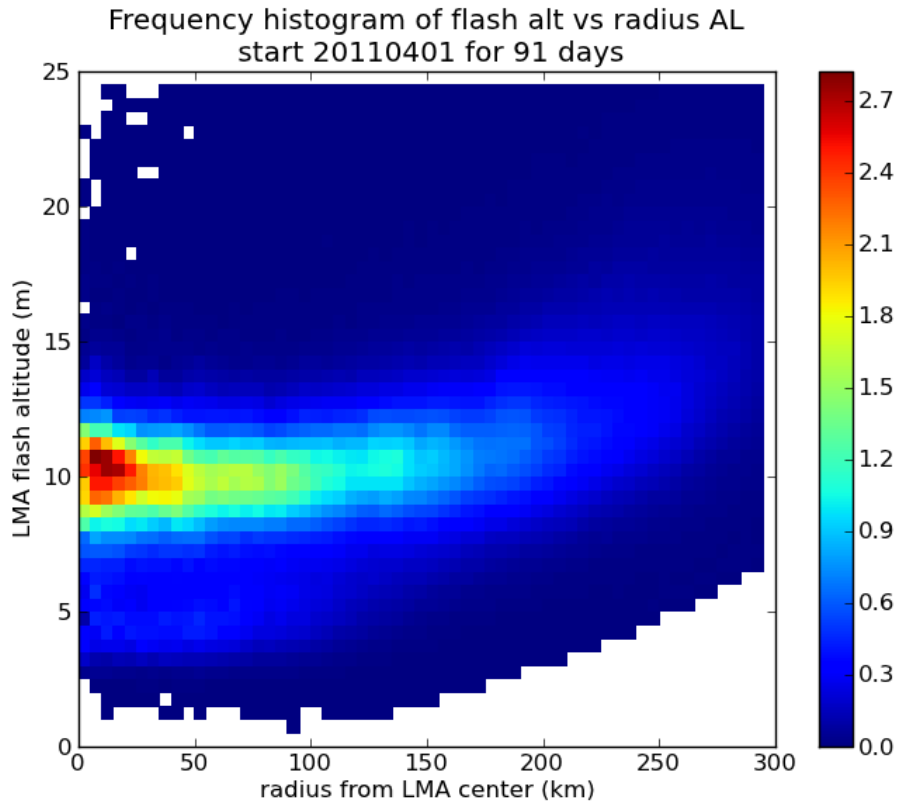


FIG. A.1. 2D frequency of flash altitude and distance from LMA center for the Alabama LMA network. Other networks have similar behaviors.

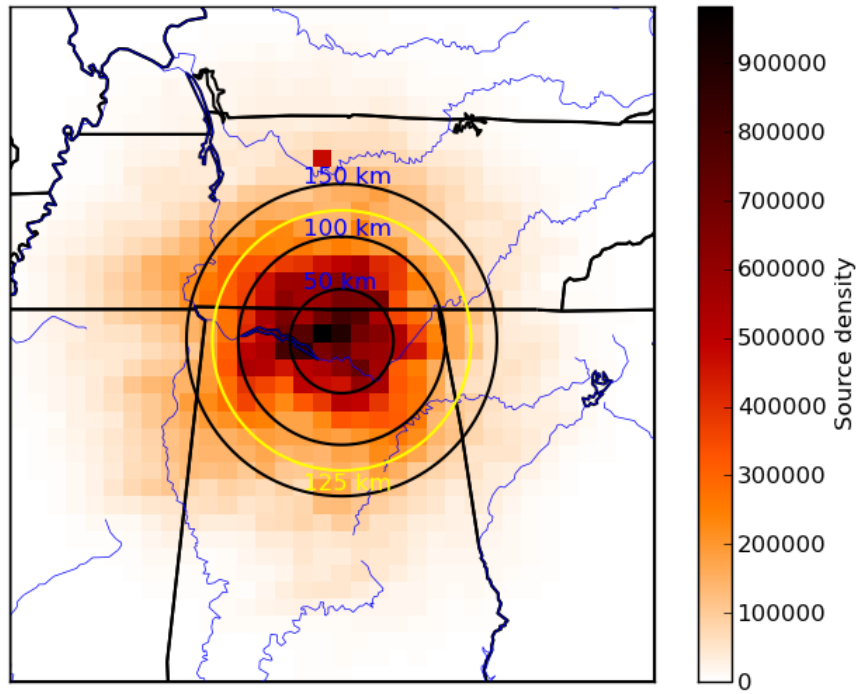


FIG. A.2. 2D plan view of source density for the Alabama LMA network for the 3 months of study.

AL

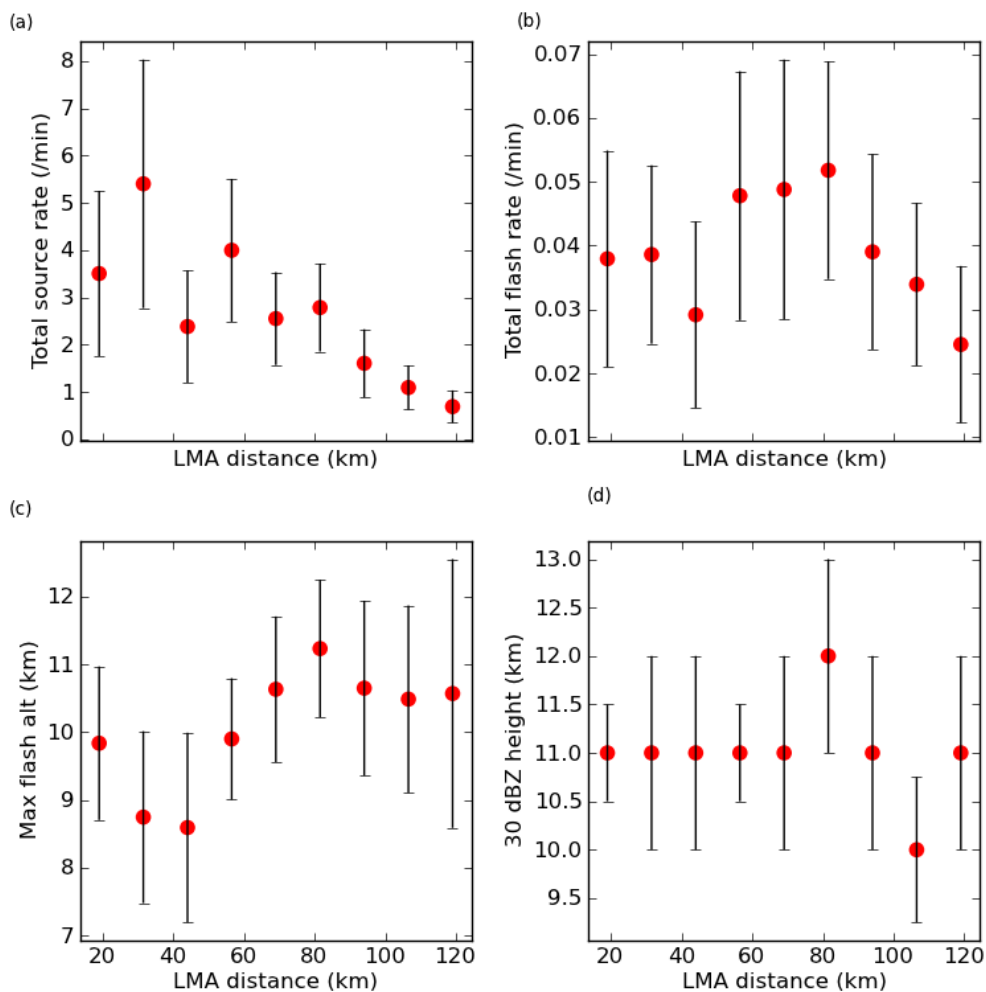


FIG. A.3. Sensitivity plots of various storm lightning and radar quantities for storms in the Alabama region. Points denote the median quantity for each bin following the horizontal axis. Error bars indicate the median absolute deviation of flash rates for each bin.

DC

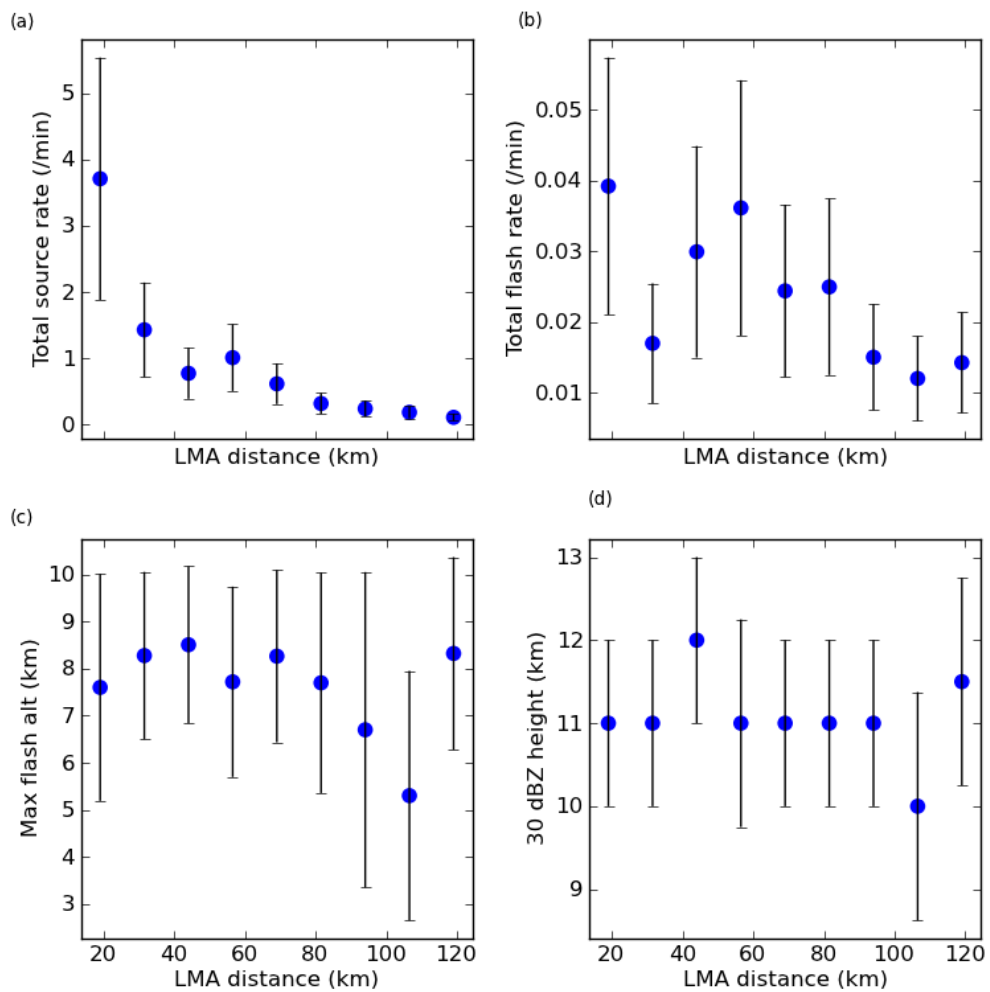


FIG. A.4. Same as previous plot for DC.

OK

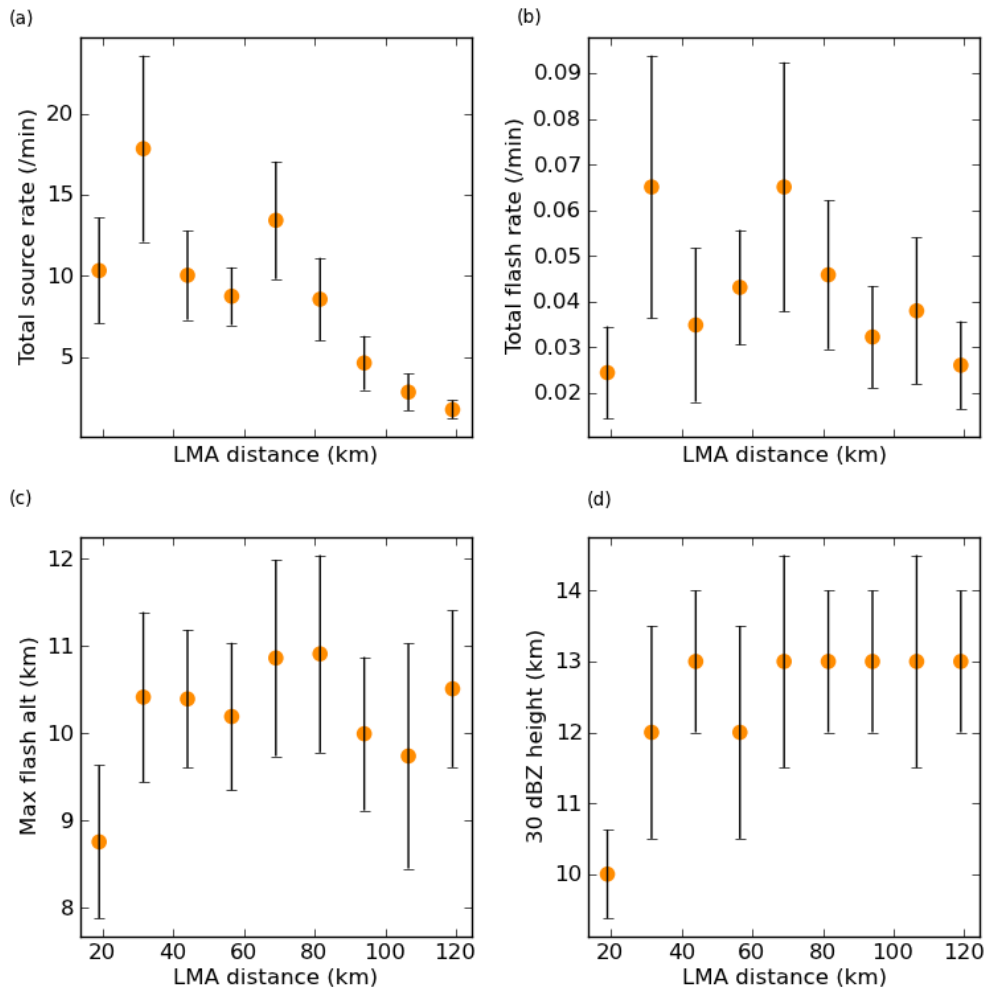


FIG. A.5. Same as previous plot for Oklahoma.

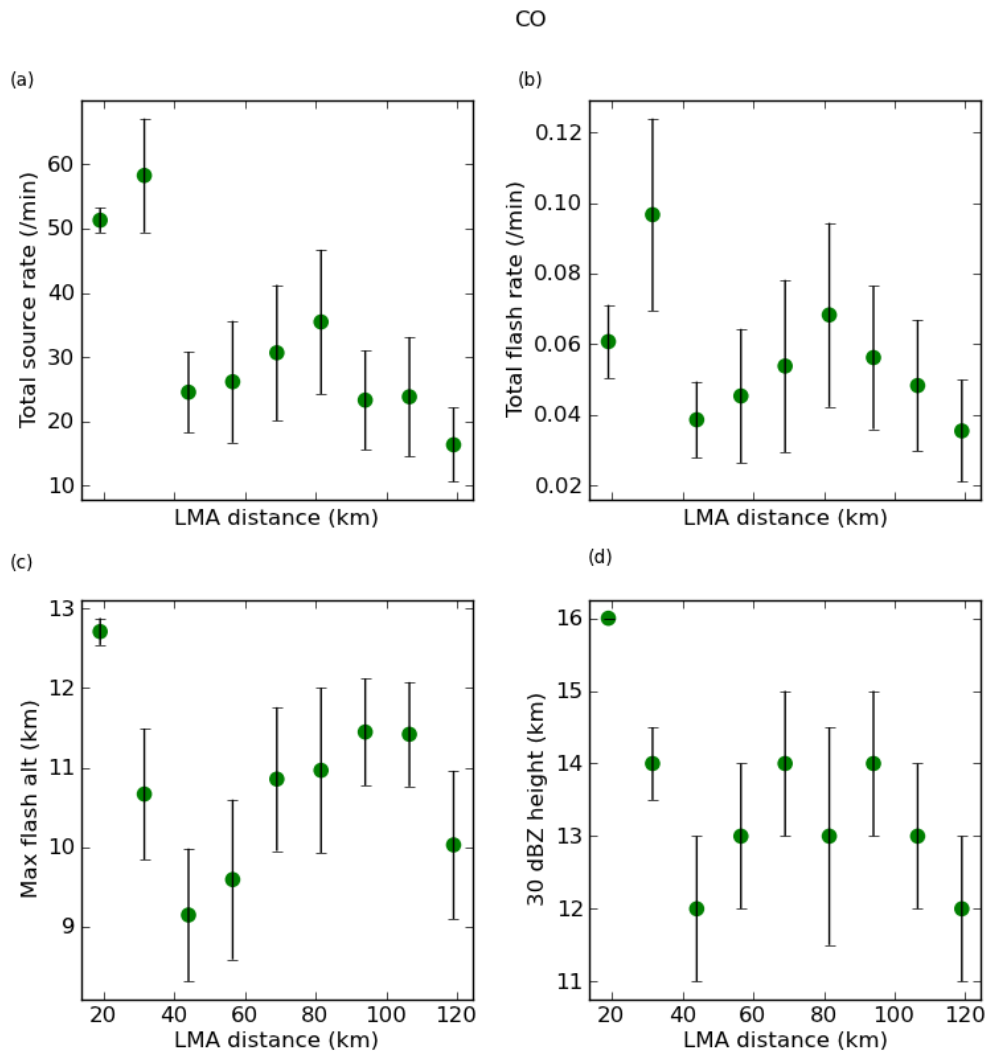


FIG. A.6. Same as previous plot for Colorado.